Reconstructing possible causes for the darkening of Skagerrak coastal water in the Hvaler estuary during the past century

A geochemical and micropalaeontological study

Amund Bråten Rian

Thesis submitted for the degree of Master in Environmental Geoscience 60 credits

Department of Geology

Faculty of mathematics and natural sciences

UNIVERSITY OF OSLO

June 2022

Reconstructing possible causes for the darkening of Skagerrak coastal water in the Hvaler estuary during the past century

A geochemical and micropalaeontological study

Amund Bråten Rian

Reconstructing possible causes for the darkening of Skagerrak coastal water in the Hvaler estuary during the past century

http://www.duo.uio.no/

Printed: Reprosentralen, University of Oslo

Abstract

Geochemical and micropalaeontological analyses conducted on two dated sediment cores from the Hvaler estuary (SE Norway) indicate a relationship between the darkening phenomenon of Skagerrak coastal waters and an increase of riverine discharge to estuarial waters. The sediments cores are collected from different stations in the Hvaler estuary, and demonstrate varying influences of terrestrially derived organic matter, primarily determined by their proximity to the coastland and the Glomma River. The sediment cores represent a time series from the early 1930s to the present. Increased riverine discharge, accompanied by bottom trawling, and dredging in the area, are suggested to promote the darkening of the Skagerrak coastal water. This is reflected in the majority of analyses performed on the sediment cores; grain size distribution, heavy metal concentrations, TC, TN, TOC, $\delta^{13}C$, $\delta^{15}N$ and changes of the benthic foraminiferal assemblages. The heavy metal concentrations show distinct increasing trends to 1963, which partially reflects the previously documented pollution development in the estuary. Organic material present in the sediments is predominantly marine of origin but becomes more terrestrial over the years. The benthic foraminiferal assemblage reflects the increasing TOC and TIC accumulation with a distinct shift in the late 1990s/early 2000s with an increasing abundance of agglutinated foraminifera species (primarily *Textularia earlandi* and *Liebusella goesi*). *Stainforthia fusiformis*, a species tolerant to organic matter enrichment, increases simultaneously as the TOC accumulation rates increase.

Forord

Flere veiledere, støttespillere og motivatorer fortjener en stor takk for deres innspill og påvirkning på denne oppgaven. Jeg vil først takke mine veiledere Elisabeth Alve og Silvia Hess for uvurderlige bidrag med tolkningsforslag, artsbestemmelse av foraminiferer, litteraturopplysning og konstruktive tilbakemeldinger. Thaise Ricardo de Freitas har bistått med tolkning og tilbakemeldinger, og hun har vært en stor motivator under hele denne prosessen.

Jeg ønsker å takke Mufak Said Naoroz for hans engasjement, imøtekommenhet og hjelp med laboratorieresultatene. Magnus Kristoffersen fortjener en takk for hans arbeid med tungmetall-analysene og William Martin Hagopian for isotop-resultatene. Jeg takker Aleksandr Berezovski for bidrag til diverse tolkninger og Trine Fjeldstad for tilgang til hydrologiske data.

Mine foreldre og søsken fortjener en stor takk for deres forståelse og støtte gjennom hele prosessen. Jeg ønsker avslutningsvis å takke samboeren min for hennes oppmuntringer og hjelpsomhet.

Prosessen med å skrive denne masteroppgaven har vært interessant, utfordrende og givende. I tillegg har denne prosessen lært meg en god del om meg selv, som jeg tar med meg videre.

Contents

1 **Introduction** **1**

1.1 Background and aims 1

1.2 Study area: The Hvaler estuary 5

1.3 Pollution history 7

1.3.1 Glomma River 8

1.3.2 Halden area 8

1.3.3 Fredrikstad and Sarpsborg area 8

1.3.4 Hvaler area 8

1.3.5 Sources of nitrogen and phosphorus in the Hvaler area 9

2 Materials and methods **10**

2.1 Material collection and treatment 10

2.1.1 Sample acquisition 10

2.2 Analyzed core intervals 10

2.3 Freeze drying and water content calculation 11

2.4 Radiometric dating and sediment accumulation rate 11

2.5 Grain size distribution analysis 11

2.6 Carbon and nitrogen analysis 12

2.6.1 Sample handling of TC, TOC and TIC 12

2.6.2 TOC analysis 12

2.6.3 TC, TN analysis 13

2.7 Stable isotope analysis 13

2.8 Mixing equation 13

2.9 Heavy metal analyses 14

2.10 Micropalaeontological analyses 14

3 Results **17**

3.1 Core description 17

3.2 Sediment accumulation rate (SAR) and dating 18

3.3 Grain size analysis 20

3.4 Heavy metal analysis 21

3.5 Carbon, nitrogen, and stable isotopes 24

3.5.1 Total Carbon 24

3.5.2 Total Nitrogen 24

3.5.3 TOC_{63} 25

3.5.4 Total inorganic carbon 25

3.5.5 Stable isotopes 26
3.5.5.1 $\delta^{13}C$ 26
3.5.5.2 $\delta^{15}N$ 26
3.6 TOC/TN ratio and mixing equation 27
3.6.1 TOC/TN 27
3.6.2 Mixing equation 28
3.7 Accumulation rates 29
3.8 Foraminiferal analyses 30
3.8.1 Absolute abundance of foraminifera 30
3.8.2 Relative abundance of foraminifera 32
3.8.3 Agglutinated vs calcareous foraminifera 34
3.8.4 Ecological quality indices, diversity and sensitivity 35
4 Discussion 39
4.1 Heavy metal pollution history 39
4.2 Heavy metal accumulation rates 43
4.3 Sources and accumulation rates of organic carbon over time 44
4.4 Determining the sources of organic carbon over time 44
4.5 Mixing equation 46
4.6 Ecological parameters 48
4.6.1 The use of foraminifera as environmental proxies 48
4.6.2 Foraminifera influenced by heavy metal pollution 48
4.6.3 Ecological changes 49
4.7 Implications and evidence of coastal darkening 53
4.8 Reference conditions 56
6 Conclusion 57
7 References 58
8 **Appendix 65**
9 Taxonomic refrence list 88

List of Figures

Figure 1: Map with the locations of the sampling sites....5
Figure 2: Simplified illustration of the major coastal currents in the Skagerrak/Kattegat area....6
Figure 3: Mean annual discharge of the river Glomma from 1964 to 2021 measured at Solbergfoss....7
Figure 4: Pictures of the northern and southern sediment cores....17
Figure 5: Water content (%) of the analyzed sediment cores....18
Figure 6: Sediment accumulation rate estimated for the sediment cores....18
Figure 7A: Mean grain size at the northern and southern cores. 20
Figure 7B: Clay, silt and sand content. Northern core....20
Figure 7C: Clay, silt and sand content. Southern core....20
Figure 8: Heavy metal concentrations at the northern core....21
Figure 9: Heavy metal concentrations at the southern core 22
Figure 10: Heavy metal accumulation rates for the northern and southern core....23
Figure 11: TC-concentrations....24
Figure 12: TN-concentrations....24
Figure 13: TOC_{63} concentrations....25
Figure 14: TIC concentrations....25
Figure 15: $\delta^{13}C$ (‰) northern and southern core....26
Figure 16: $\delta^{15}N$ (‰) northern and southern core....26
Figure 17: TOC/TN-ratio of northern and southern core....27
Figure 18: Percentage of terrestrial organic carbon in the northern and southern core 28
Figure 19: Accumulation rate of TIC and TOC in northern and southern core....29
Figure 20: Absolute abundance of selected species. Northern core 31
Figure 21: Absolute abundance of selected species. Southern core....31
Figure 22: Relative abundance of selected species in the northern core....33
Figure 23: Relative abundance of selected species in the southern core....33
Figure 24: Percentage of agglutinated foraminifera 34
Figure 25: Benthic foraminifera accumulation rate....35
Figure 26: Foram-AMBI at the northern and southern stations....36
Figure 27: Relative abundance of ecological groups. Northern core....37
Figure 28: Relative abundance of ecological groups. Southern core....37
Figure 29A: H'(log2). 38
Figure 29B: ES(100)....38
Figure 29C: NQI_f....38
Figure 30: Location of station 2,5,8 and 9 41
Figure 31: Relative distribution of particles in surface waters from Glomma River....42
Figure 32: Surface circulation patterns 42
Figure 33: Location of sediment core KSK-12-01C/D from the Kosterfjord 49
Figure 34: Foram-AMBI, ecological groups, primary production & NQI_f results....50
Figure 35: TOC and TIC-AR compared to the absolute abundance of benthic foraminifera 52
Figure 36: Salinity result from the northern and southern stations....54
Figure 37: Annual air temperature deviations....55
Figure 38: Dumping sites and dredging in the Hvaler estuary 56

List of Tables

Table 1: Sediment accumulation rates and age of the analyzed sediment cores (GL2 and GL3).....19
Table 2: Difference in average heavy metal concentrations between the stations (GL2 and GL3).....41
Table 3: Ecological Status classification.....65
Table 4: Mean annual discharge of the river Glomma from 1964 to 2021 measured at Solbergfoss ...66
Table 5: Selected core intervals for subsampling (GL2).....67
Table 6: Selected core intervals for subsampling (GL3).....68
Table 7: Water content (%) in the northern (GL2) and southern (GL3) sediment cores.....76
Table 8: Grain size distribution at GL2-21A.....77
Table 9: Grain size distribution at GL3-21A.....78
Table 10: Heavy metal concentrations and environmental status classification (GL2) 79
Table 11: Heavy metal concentrations and environmental status classification (GL3) 80
Table 12: TC, TOC and TN results for GL2 81
Table 13: TC, TOC and TN results for GL3. 82
Table 14: Carbon-isotope results for GL2 and GL3 83
Table 15: Nitrogen-isotope results for GL2 and GL3. 84
Table 16: Foraminifera count (500-63µm) of GL2 and GL3. 85
Table 17: Foraminifera species assigned to ecological groups and AMBI 87

List of Appendixes

A Ecological status classification: 65
B Mean annual discharge measured at Solbergfoss:.....66
C Overview of selected intervals for subsampling: 67
D Radiometric dating and SAR report: 69
E Water content: 76
F Grain size distrubution: 77
G Heavy metal concentrations: 79
H TC, TOC, TN results: 81
I Isotope results: 83
J Foraminifera counts: 85
K AMBI-groups: 87

1 Introduction

1.1 Background and aims

Since the beginning of the 20th century, organic material originating from terrestrial sources has increased in the coastal Skagerrak. Which is affected by a complex interaction between increased precipitation and riverine discharge, changes in land cultivation, elevated temperatures on land and in oceans, that in turn sustain an increase of dissolved organic matter (DOM) to the coastal area (*Monteith et al., 2007; de Wit et al., 2016*). An extensive influx of DOM to coastal areas can potentially lead to increased greenhouse gas emissions to the atmosphere and higher light attenuation. As well as hinder the productivity of marine organisms, increase bacterial productivity, and negatively influence the structure of the food web (*Lapierre et al., 2013; Deininger et al., 2016; Deininger & Frigstad, 2019; Frigstad et al., 2020a*). This increasing trend of suspended particulate material in the Skagerrak coastal waters has been related to the increased riverine discharge and detected darkening in the coastal area (*Aksnes et al., 2009; Dupont & Aksnes, 2013; Frigstad et al., 2018*).

The term "darkening" is used to describe the decrease of water clarity due to eutrophication and increased turbidity (*Blain et al., 2021*). This process occurs when a body of water becomes excessively enriched with DOM (dissolved organic material), and consequently nutrients, that increase turbidity and reduces water transparency. Eutrophication can naturally occur due to climate change, air temperature fluctuations, and increased precipitation (*The research council of Norway, 2019*). However, when the increased input of nutrients is caused by anthropogenic activity, it is called cultural eutrophication. Cultural eutrophication can aggravate the effects of natural eutrophication (*Malone & Newton, 2020*). The sources of nutrients are primarily agricultural practices and sewage emissions (*The research council of Norway, 2019*), whereas terrestrially derived organic matter is transported to the Skagerrak coastal waters by precipitation and runoff. Algae blooms can be stimulated by the excessive input of nutrients, which contain nitrogen and phosphorous (*Sterner, 2013*). In that case, as too much organic matter decomposes at the seabed, the oxygen consumption exceeds the resupply of oxygen-rich water. This decomposition process can ultimately lead to hypoxia or anoxia. The term hypoxia means that low oxygen levels are prevalent (bellow 2.0 ml^{-1}), while the term anoxia refers to oxygen depletion (0.0 ml^{-1}) (*Veileder, 2018; Diaz & Rosenberg, 1995*).

Darkening of the Hvaler coastal areas (Outer Oslofjord, SE Norway) is still increasing despite a decrease in nutrient discharge from sewage and agriculture (*Guerrero & Sample, 2021*). Discharge of terrestrially derived nutrients, sediments and organic matter has contrarily increased from ~1990 (*Frigstad et al., 2020b*). The darkening itself adverse the living conditions for marine biota (plankton, kelp, fish), as it absorbs or blocks the sunlight from penetrating down in the water column (*Frigstad et al., 2020b*). Identifying the sources and the spatiotemporal nutrient flux to the Hvaler estuary is important to improve and understand the development of the darkening phenomenon.

The Hvaler coastal area represent a type of estuary. Estuaries are generally coastal areas influenced by river discharge. A high fresh-water input to the marine water masses can result in an assorted combination of marine and terrestrial material contained in the estuarine sediments *(Thornton & McManus, 1994)*. Furthermore, estuaries can be naturally stressed due to strong increase in turbidity caused by stratified water masses, tidal flow, and water circulation. Additionally, estuarine areas are commonly predisposed to anthropogenic–influence due to the high urbanization density in coastal areas. Estuaries are commonly associated with high biological activity which results from a high influx of nutrients into the coastal areas (*Alve, 1995*).

Environmental studies using foraminifera were initially introduced in the late 1950s to assess environmental health and marine ecology (e.g., *Martins et al., 2019; Zalesny, 1959*). Foraminifera are eucaryotic unicellular microorganisms which inhabit all marine environments (*WoRMS, 2022; Martins et al., 2019)*. The benthic foraminifera live on the seafloor with their single cell protected by an agglutinated or calcareous test. The tests can be preserved in the sediment record and used as a proxy of environmental changes. The distribution of various species depends on their tolerance and adaption to different environmental conditions. Foraminifera are sensitive and respond quickly to physiochemical changes in the environment, which can be driven by nutrient discharge, temperature, substrate characteristics, pH-values, water depth, salinity, accumulation rate, distribution of subsistence and oxygen concentration (*Martins et al., 2019; Zalezny, 1959*). This environmental sensitivity makes benthic foraminifera an appropriate parameter for environmental monitoring (*Bouchet et al., 2012*). Hence, the abundance and distribution of benthic foraminiferal tests in dated sediment cores are used to characterize endemic environmental conditions of past environments. Several studies have been conducted in the Oslofjord using foraminiferal assemblages as proxies and environmental monitoring tools (e.g., *Dolven et al., 2013; Hess et al., 2014; Alve et al., 2019; Aasgaard, 2020*), which propose that foraminifera may assess past ecological status classes in coastal waters and assist in the establishment of reference conditions. Analyzed foraminiferal assemblages from the area have seemingly shown a direct correlation to increasing rates of TOC accumulation (*Alve et al., 2018; Aassgaard. 2020*).

The Norwegian Pollution Control Authority was commissioned in 1995 to determine the eutrophication effects in the Outer Oslofjord, and therein the Hvaler coastal area (*Staalstrøm et al., 2022*). Their report concluded that eutrophication occurred in the outer part of the fjord and negatively affected the lower growth limit for macroalgae. In the following years, increasing amounts of nitrogen and DOM (dissolved organic matter) were detected in the fjord from 1995 to 2021 (*Staalstrøm et al., 2022*). The increasing eutrophication effects and extents are seen as acute and concerning in the Outer Oslofjord and Hvaler area (*Staalstrøm et al., 2022*).

The Norwegian environmental agency (Miljødirektoratet) states that acute measures are needed to reduce the influx of nitrogen to the Outer Oslofjord and locate the primary nitrogen sources *(Hambro, 2021*). An Oslofjord with high biodiversity and low pollution is important for human health, life quality, and economy (*Miljødirektoratet et al., 2019*). In contrast to earlier beliefs, the coastal currents from neighboring countries are not the primary nitrogen contributor to the Outer Oslofjord. The sources of nitrogen are mainly from Norwegian agriculture activities and sewage outlets. Water masses flowing northwards from the Skagerrak coastal areas cause a dilution of said nutrients (*Staalstrøm et al., 2022*). Since the early 1990s, agricultural emissions of nitrogen have increased by 19% and sewage emissions by 30% (*Hambro, 2021*). Since pre-industrial times, the nitrogen concentrations are elevated, and are fivefold as high at present day (*Hambro, 2021*). Nitrogen and phosphorous is processed by treatment plants in the inner part of the Oslofjord, while the outer part is only refined for phosphorus emissions (*Hambro, 2021*).

The Water Framework Directive (WFD) commits all membering countries to achieve "good" or higher ecological quality status for all coastal marine and freshwater bodies (*European Environmental Agency, 2021*). Their main objective is to prevent deterioration and enhance the status of aquatic ecosystems (*Water Framework Directive*, 2022). Whilst some water bodies naturally have a “moderate” to “bad” status, anthropogenic activities can exacerbate the environments condition (*Dolven et al., 2013*). The ecological status classification used in this study is presented in the Appendix (A). Analysis of sediment cores can help to distinguish areas with naturally and anthropogenically induced poor environmental conditions. This is done by establishing reference conditions. Reference conditions are a range of attainable ecological parameters in a water body that are minimally disturbed by human activities (*Vermont Water Quality Standards, 2014*). These reference conditions can accordingly enable correlation of a location’s modern conditions to past environments, whereas the initiation and evolution of anthropogenic influence and impact is present in the sedimentary record (*Dolven et al., 2013*). This concept is used to construct a timeline of different environmental events of an area. If an area currently has a status worse than “good”, actions are needed to improve and enhance the conditions in accordance with the reference conditions (*European Environmental Agency, 2021*).

This thesis is a part of the NFR-founded project “A green-blue link made browner: how terrestrial climate change affects marine ecology” (*The research council of Norway, 2019*). The project aims to unravel the linkage of atmospheric processes to terrestrial greening, consequent darkening of water basins and its impact on coastal ecology (*Opdal et al., 2019*). Of these aims, the latter linkage-point “*darkening of water basins and its impact on coastal ecology*” is considered. As such, the objective of this thesis was to further increase the understanding of the reported darkening of coastal Skagerrak during the past century (*Aksnes et al., 2009; Dupont & Aksnes, 2013; Frigstad et al., 2018*). The knowledge of how specific coastal environments are affected by the darkening phenomenon is still limited, especially in relation to the impact on ecosystems along the Norwegian coastline (*Frigstad et*

al., 2020a). To achieve this objective, two sediment cores from the Hvaler estuary, (Outer Oslofjord, SE Norway), was studied to investigate the development and influence of coastal darkening. The Hvaler estuary was selected for this review as it represents the northern part of the coastal Skagerrak and is extensively influenced by river outflow from the largest river in Norway, Glomma (Figure 1). This thesis includes an evaluation of the change in organic carbon accumulation rate, ecological quality, pollution development and the variability of riverine influence at the two sampling stations in the estuary. It is suspected that the influx of organic carbon varies between the stations. If this is the case, the nutrient focusing at the two locations can describe a spatial, as well as temporal, evolution in the study area. These implications will be used to address how and if the benthic foraminiferal assemblages are affected by these changes.

1.2 Study area: The Hvaler estuary

The Hvaler estuary is located in the Outer Oslofjord. In general, the Outer Oslofjord comprises the coastal areas south of the Drøbak sill to the skerries of Hvaler and Vestfold County in Norway. The Outer Oslofjord consists of several basins whereas the Hvaler basin is the deepest at approximately 450 meters (*Miljødirektoratet et al., 2019*, Figure 1).

The sampling sites of the sediment cores analyzed in this study are located in the outer Hvaler estuary, close to the Swedish maritime boarder, near the Hvaler skerries (Figure 1). The distance between the sites is approximately 8.5 kilometers. The northern station (GL2) is situated south of the Akerøy Island, and the southern station (GL3) south of Herføl Island (Figure 1).

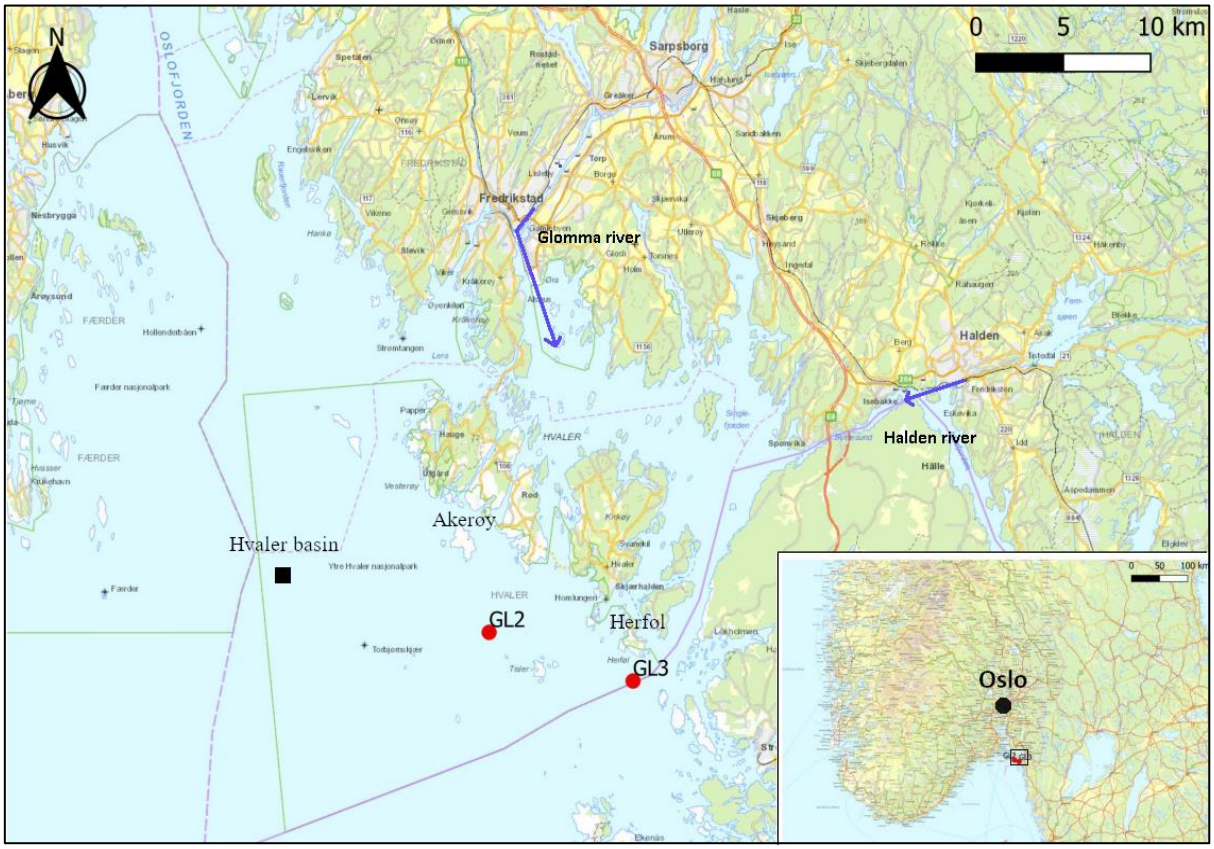

Figure 1: *Map with the locations of the sampling sites GL2 and GL3. The Glomma and Halden rivers are marked with blue arrows and the Hvaler basin is marked with a black square.*

Main inflow of marine water derives from the Jutland current (JWS) from the Danish west coast, the Atlantic current (AW), the Norwegian coastal current (NCC), and the Baltic Sea current (BW) that flows from the sounds in the south *(Christensen et al., 2018*) (Figure 2). The primary driving force of these circulations is the wind patterns of the inner Skagerrak area (*Gade, 1968*). The Norwegian coastal current can affect the fjord by estuarine circulations, freshwater inflow and riverine discharge, as well as wind and tide forcing (*Frigstad et al., 2020a*). These marine water currents mix with freshwater from river outlets. The main freshwater sources in the Outer Oslofjord are the Glomma, Drammen, Halden, Skien rivers and Numedalslågen *(Stenseth et al., 2019; Miljødirektoratet, 2019*). Together, they

represent 90% of all freshwater influx to the Outer Oslofjord (*Miljødirektoratet et al., 2019*). The Glomma River is Norway's largest river, and it has the highest contribution of freshwater to the Outer Oslofjord (*Engesmo et al., 2021*). The river is ~621 km long with a catchment area of 41 967 km² *(NVE, 2022b*). This river feeds the Hvaler estuary with approximately 700 $m^3 s^{-1}$ freshwater each year *(Walday & Moy, 1996*). Spring floods from the Glomma occur during the months of May and June (*Frigstad et al., 2020a*).

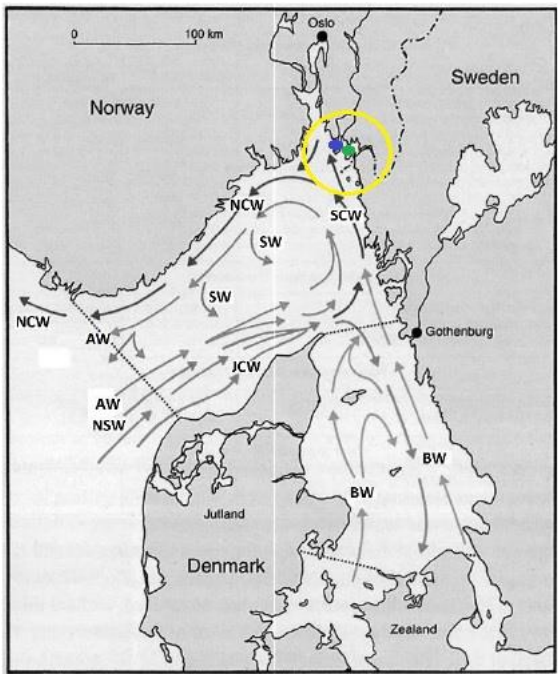

Figure 2: *Simplified illustration of the major coastal currents in the Skagerrak/Kattegat area. BW is the Baltic coastal current and JWS is the Jutland coastal current which mix in the Outer Oslofjord. (Modified from Anon, 1993). Stations are denoted inside the yellow circle with blue (northern) and green (southern) dots.*

Strong estuarine water circulations are characteristic of the areas proximal to the river mouths. This results in the stratification of fresh- and marine salt-water masses. Freshwater, being lighter, flows over the marine water and becomes thinner as it progresses out in the estuary. The mixing of freshwater and saltwater in an estuary can lead to variable chemical conditions, especially concerning salinity (*NOAA, 2021*). The thickness and salinity of the surface waters depend on the magnitude of river discharge and seasonal changes in precipitation in the area. The upper 0-25 meters of the water masses in the Outer Oslofjord are affected by the freshwater draining (*Dahl & Naustvoll, 2018*).

Throughout the last decade, precipitation has increased in the southern part of Norway, and the mean annual temperature has risen (~1°C from 1990-2014) (*Meteorologisk institutt, 2021; Hanssen-Bauer et al., 2017*). A warmer and wetter climate is associated with an increase in river runoff, which can affect coastal circulations (*Miljødirektoratet et al., 2019*). In addition, the increased precipitation enhances

erosional processes and consequently, the sediment discharge into the river systems *(Walday et al., 2019*).

The draining rivers (Glomma and Halden river) displayed a significant increase in discharge to the Outer Oslofjord during the period 2014 to 2018 (*Naustvoll et al., 2017*). Mean annual discharge from 1964 to 2021 measured at Solbergfoss (~60 km north of Fredrikstad**)** demonstrates the increased discharge from the river Glomma to the estuary (Figure 3, Appendix: B) (*NVE, 2022a*).

The bottom waters of the Hvaler estuary have experienced moderate replacements throughout the last decades (*Walday et al., 2014*). This replacement resulted in improved conditions of oxygenated bottom waters, which was measured all the way to the Idde fjord, during the years 2013 and 2016 (*Naustvoll et al., 2017*). The oxygen conditions are seemingly better in the distal parts of the estuary and become progressively worse towards the outer part of the Idde fjord (*Naustvoll et al., 2017*). Temperatures are stable at 6-7°C in the bottom waters with varying salinities of 25-35 ‰ *(Walday et al., 2006*).

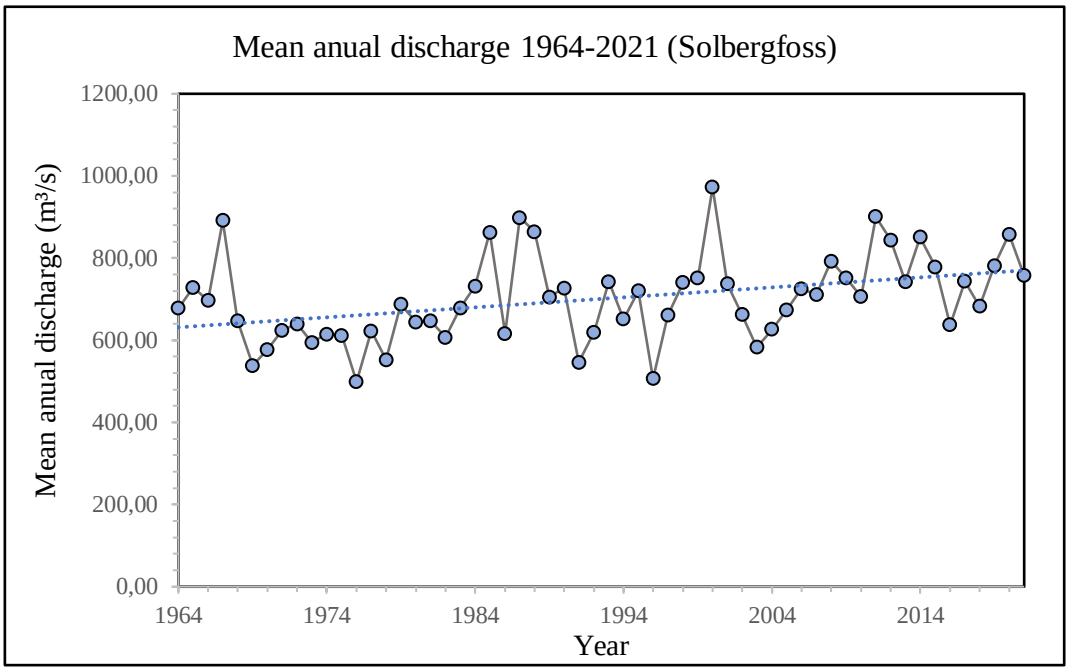

Figure 3: *Mean annual discharge of the Glomma River from 1964 to 2021 measured at Solbergfoss: Norwegian Water Resources and Energy Directorate station 2.605.0 (NVE, 2022a).*

1.3 Pollution history

In the vicinity of the Hvaler estuary, industrial pollution became evident during the first part of the 20th century (*Arnesen, 2001*). The Hvaler estuary effectively functions as a sink for the draining of several rivers and runoff from proximal cities. The Glomma River followed by the Halden river, and other smaller creeks have transported contaminants and extensive organic matter to the estuary, while the wastewater treatment, industries, and surrounding agriculture from the largest cities, (Fredrikstad, Sarpsborg, Halden), and the local cabin society at Hvaler, are viewed as the main pollutant sources (*The research council of Norway. 2019*).

1.3.1 Glomma River

The wood processing industry along the Glomma River first appeared in the late 1500s. The intensity was greatest in the early 1950s before the activity ended in 1985 *(Bækkelund, 2021; SSB, 2020*). The river was used to transport driftwood, operate sawmills, and later (from 1922) hydropower plants (*Akershus energi, 2022*). By the second part of the 1890s, 14 cellulose fabrics, 7000 sawmills and several paper factories concentrated in the Oslo area were operated in the country (*Faugli, 2022*). This resulted in extensive accumulation of sawdust, wood fiber, and pulp in the Hvaler estuary.

1.3.2 Halden area

The Hvaler estuary was the recipient of wood industry activities and associated chemical plants from the Halden area. Founded in 1859, Saugbrugsforeningen was a union of 30 sawmills along the Halden river. An accompanying sulfide plant was established in 1908. The area was gradually modernized and expanded by a cellulose factory in 1908 *(Anno Norsk skogmuseum, 2020*), which closed in 1991 (*Berge et al., 1996*). Further strain on the estuary occurred in 1915 as paper mills were initiated in the area (*Polovodova Asteman et al., 2015*). Suspended material consisting of wood material, pulp and heavy metals from the respective industries accumulated in the estuary. However, the emissions have seemingly improved since the 1970s due to discharge regulations (*Polovodova Asteman et al., 2015*).

1.3.3 Fredrikstad and Sarpsborg area

Since the first part of the 1900s, pernicious wastes from industries of the Fredrikstad and Sarpsborg-area have influenced the environmental conditions of the Hvaler estuary (*Berge et al., 1996*). Kronos Titan A/S manufactured titan-dioxide pigmentation which was used as a coloring agent in paper, paint, and rubber (*Brekke, 2021*). The practice, which started in 1918, did evidently lead to a decline in the biodiversity of the tidal zone in the Hvaler estuary (*Berge et al., 1996*). In addition, the Borregaard industries ltd. and Greaker A/S operated paper mills, cellulose factories, and a sulfite plant in the Fredrikstad and Sarpsborg area. This contributed to elevated accumulation of organic material and heavy metals in the Hvaler estuary (*Berge et al., 1996; Brekke, 2021; Fosseng, 2000*).

Emission regulations from Kronos Titan A/S in the late 1980s, and the closedown of the sulfite plant in 1980, did seemingly decline the heavy metal concentrations (*Brekke, 2021*; *Berge et al., 1996*). Communal sewage treatment plants for Fredrikstad and Sarpsborg were established in 1989 which reduced the liability to the estuary (*Berge et al., 1996*). By the second half of the 1980s, the inflow of acid waste was reduced to 7%, and phosphorous down to 5% of the discharge of the previous decade (*Bokn et al., 1996*).

1.3.4 Hvaler area

Six locations in the Hvaler estuary, two of them in conservation areas, were previously used as dumping sites for dredged marine sediments (*Walday et al., 2006; Helland, 1995; Miljødirektoratet, 2021*). These sediments were primarily collected from the Hvaler skerries and its vicinity (*Helland, 1995*). Sediment

dumping in coastal waters can lead to increased turbidity and sludge accumulation which can aggravate the ecological conditions. At Jylterenna and Angroetrenna -two of the dumping sites, approximately 48 000 m^3 and 3 300 m^3 of sediments had been deposited between 1990 and 1995 (*Helland, 1995*). Jylterenna is located 3 km northwest of the southern station (GL3), and Angroetrenna 4 km northwest of the northern station (GL2). The areas were regularly used until 2000 (*Walday et al., 2006*).

The Hvaler-area is populated with approximately 4310 cabins, which are connected to the local sewer network (*SSB, 2022*). Sewage treatment plants for the area were established in the first half of the 1970s, which decreased the phosphorus emissions from sewage during the 1980s (*Berge et al., 1996*).

1.3.5 Sources of nitrogen and phosphorus in the Hvaler area

The supply of total nitrogen to the Outer Oslofjord has increased by approx. 19% from agricultural runoff, and approx. 30% from treated wastewater, since the beginning of the 1990s (*Hambro, 2021*). The strain on the treatment plants is expected to increase as the population grows. Nitrogen removal from agriculture and sewage emissions were introduced in the Oslo area in the late 1990s (*Arnesen, 2001*).

The combined discharge of nitrogen from aquaculture, agriculture, urbanization, industry, and diffuse emissions to the Glomma and Hvaler coastal area was estimated by the Norwegian Institute for Water Research (NIVA) to be 18 003 tonnes/year in 2019. Of the total nitrogen, 63.3% was of anthropogenic origin. During the same year, the discharge of phosphorus to the estuary was estimated to be 352 tonnes/year whereas 78.7% was from anthropogenic sources (*Guerrero & Sample, 2021*). The discharge of total nitrogen and phosphorus has decreased since the early 1990s. In 1990, the total amount of nitrogen was 19 574 tonnes/year and 467 tonnes/year phosphorous. This is approximately a decline of 8% total nitrogen and 25% total phosphorus discharge to the estuary (*Guerrero & Sample, 2021*).

2 Materials and methods

2.1 Material collection and treatment

2.1.1 Sample acquisition

The samples analyzed in this study were collected in the Hvaler estuary, Outer Oslofjord, in August 2021 onboard the RV Trygve Braarud. Sediment cores from two stations were sampled with a Gemini corer; the core liners are 79 cm long and have an 8 cm inner diameter. One sediment core from each station was selected for further sub-sampling (GL2-21A: N 59° 00.092, E 10° 54.401, 209 m water depth and GL3-21A: N 58° 58.481, E 11° 02.913, 212 m water depth; Figure.1). The sediment cores were selected by their apparent undisturbed sediment-water interface, minor visible bioturbation, and appropriate length.

For sub-sampling onboard, the cores were placed on a sediment core-stand integrated with a piston mechanism that could gradually push the core out of the core liner. As the sediment cores were gradually pushed out, intervals were horizontally sliced using a thin metal-plate, and an acrylic cylinder. Both utensils were rinsed between each interval as to avoid cross-contamination. However, some smearing may have occurred inside the core liner. This means that some cross-contamination between the intervals may have occurred. The slicing was performed in 1 cm intervals for the upper 20 cm, while the remaining sediment was sliced in 2 cm intervals. All sub-samples were placed in pre-weight labelled containers and immediately frozen.

A CTD-instrument was used to measure temperature, salinity and oxygen saturation in the water column. The instrument was lowered to about 4 meters above seabed at each location as to avoid contamination from the sediments at seafloor.

2.2 Analyzed core intervals

After the cruise, the following parameters were analyzed for the sediment cores GL2-21A and GL3-21A: water content, radiometric dating and sediment accumulation rate, grain size distribution, total carbon (TC), total nitrogen (TN), total inorganic carbon, total organic carbon (TOC), heavy metals (Cu, Zn, Pb, Hg, Cr, Ni, Cd), stable isotopes ((C^{13}/C^{12}) and (N^{15}/N^{14})) and benthic foraminiferal analysis. Each core interval was analyzed to achieve the water content. For the radiometric dating and sediment accumulation rate, every other interval in the shallowest 5 cm of the cores, and every fourth from 5-19 cm, were analyzed by the researchers at the Environmental Radioactivity Research Centre (ERRC-University of Liverpool - UK). The core intervals selected for grain size analysis, carbon and nitrogen parameters, heavy metal analysis and stable isotopes were the shallowest 10, and deepest 20 cm, as well as every-other interval in between. Selected intervals for subsampling are presented in the Appendix (C).

2.3 Freeze drying and water content calculation

In order to calculate the water content, the frozen sediment samples were weighed before they were freeze dried. The dry sample weights were used in conjunction with the wet sample weights to calculate the water content (Equation 1). M_w represents the weight of the wet sediment weight, and M_d represents the dry sample weight.

$$\%\, Water\ content\ = \frac{Mw - Md}{Mw} * 100 \qquad (1)$$

2.4 Radiometric dating and sediment accumulation rate

The freeze-dried sediment samples from GL2-21A and GL3-21A were carefully homogenized and approximately 3.5 g (±0.2 g) from each sediment interval were sent to the Environmental Radioactivity Research Centre (ERRC) at the University of Liverpool for radiometric dating and sediment accumulation rate determination.

The ^{210}Pb and ^{137}Cs radioactive isotopes were used to date the sediment cores. The ^{210}Pb dates were calculated using the CRS model. ^{210}Pb naturally occurs as a radionuclide with a half-life of 22.3 years (*Arias-Ortiz et al., 2018*). In marine sediments, the ^{210}Pb has two components: supported and unsupported ^{210}Pb. Supported ^{210}Pb is the fraction that derives from ^{226}Ra decay found in sediments, while unsupported ^{210}Pb derives from atmospheric deposition. This unsupported fraction decays over time and is used to determine the age of sediments (*Heldal et al., 2021*). ^{137}Cs is an artificial radionuclide and is used to determine specific historical events. The beginning of the 1960s has the greatest concentration of ^{137}Cs as extensive atmospheric nuclear weapon testing occurred during the beginning of this decade. Therefore, ^{137}C peaks are used as an identifier of the early 1960s (*Heldal et al., 2021*). It is also used to determine the record marker of fallout from the 1986 Chernobyl accident. Further analytical details can be read in the ERRC report in the Appendix (D). The dating results were interpolated using an Excel-spreadsheet to determine the dates of the unanalyzed intervals. The report estimates that the deepest core interval at the northern core (GL2) represents sediment deposits from early 1940s, while the deepest interval at the southern core (GL3) represents the mid of the 1930s. The dated lower and upper boundaries of the core intervals were used to determine the sediment accumulation rate. As such, the accumulation rate, AR, is defined as a quantity, W, of solid matter taken place over a time span, t, on a unite area, A (*Einsele, 1992*) (Equation 2).

$$\mathrm{AR} = \mathrm{W}\ /\mathrm{A}\ /\mathrm{t} \qquad (2)$$

2.5 Grain size distribution analysis

The grain size distribution of the sediment samples was determined using a Beckman Coulter LS12 320. The instrument uses diffracted light intensity to determine particle size. As the sample is loaded into the culvert of the instrument, obscurity is detected. The sample is then pumped through the instrument where

a laser is pointing at a sensor. Sediments passing by the laser diffract light at different angles onto the sensor, corresponding to distinct particle sizes. To achieve reliable results, the optimal degree of obscurity detected by the instrument was tested in advance of the analysis. Therefore, 0.07 g sediments were used as the sample amount. As to achieve a representative grain size distribution analysis, the 0.07 g from each interval was sampled at random from different parts of the main sample. However, larger particles (shell fragments) were intentionally avoided to not cause a blockage in the instrument. The samples were placed in a beaker and treated with approx. 10 ml of 5% Calgon and placed in an ultrasonic bath over a duration of 3 minutes to disintegrate aggregates, fecal pellets, and sediments clumps.

At the minimum, two replicas from the same core interval were analyzed. If the grain size distribution curves deviated too much, an additional sample was analyzed. This ensured the validity of the analysis. The results from the analysis were averaged. The background obscurity in the culvert was re-measured and the instrument was completely rinsed between each sample to avoid cross contamination.

2.6 Carbon and nitrogen analysis

Total carbon (TC) is the total amount of carbon detected in the sediments. The total amount is further divided as total organic carbon (TOC), and total inorganic carbon (TIC). TN is the total amount of nitrogen found in the sediments.

2.6.1 Sample handling of TC, TOC and TIC

A subsample of the homogenized freeze-dried samples (~ 2.0 g) was pulverized with an agate mortar. To limit the potential of cross-contamination between the samples, all the utensils were cleaned with ethanol between each individual sample. The pulverized sample was then placed in pre-labeled glass vials. Approximately 0.5 g of the pulverized samples were transferred from the glass vials to 15 ml centrifugal tubes and weighed with 0.001 mg readability.

2.6.2 TOC analysis

A small amount (3 mg) of 1 M HCl was initially added to the centrifugal tubes which contained the pulverized sediments. The acid and the sediments were thoroughly mixed with a glass rod. This glass rod was rinsed free of sediment particles inside the tubes with more HCl to ensure that no sediments were lost. Between each mixing the glass rod was cleaned with distilled water and dried. The tubes were filled up with a total of 8 ml HCl to then be placed under a fume hood on shaking racks. Under the fume hood, the added acid dissolved the inorganic carbon in the sediments. The samples were left under the fume hood over night to ensure a complete dissolvement.

The acid treated samples were centrifuged at 3000 rpm for 10 minutes and then the supernatant was gently decanted. The samples were then rinsed with distilled water to remove the remaining acid, centrifuged again and subsequently oven dried at 40 °C. The dry, acid treated samples were weighed in the tubes to ensure that all material was accounted for. Subsequently, the sediments were emptied from

the tubes and re-pulverized using an agate mortar. The pulverized sediments were then stored in pre-labeled glass vials. This method is following the guidelines of NS-EN 13137, 2001: Determination of total organic carbon (TOC) in waste, sludges and sediments. The total organic carbon (TOC) was analyzed with a Thermo scientific FlashSmart CHNS/O Analyzer with Multi-Valve Control (MVC), at the Geoscience department of the University of Oslo. Approximately 12 mg (±1.0 mg) re-pulverized acid treated sediments were transferred from the glass vials to tin capsules (8 x 5 mm) and sealed prior to TOC measures. All measured values were adjusted for the weight loss of TIC (total inorganic carbon) due to acid treatment.

The TOC values were corrected for the sand content (>63µm) using Equation 3 (*Veileder, 2018*) (*Equation 3*).

$$\mathrm{TOC}_{63} = \mathrm{TOC}_{\mathrm{mg/g}} + 18 * (1 - \mathrm{p} < 63\mu\mathrm{m}) \qquad (3)$$

The TOC and TIC-accumulation rates were calculated by Equation 4:

$$\mathrm{TOC\ or\ TIC} - \mathrm{AR} = \mathrm{TOC_g\ or\ TIC_g} * \mathrm{SAR} \qquad (4)$$

2.6.3 TC, TN analysis

Pulverized, non-acid treated sediments were used to obtain the TC and TN content in the sediments. Approx. 0.5 g dry, pulverized sediment was transferred into tin capsules, sealed, and analyzed in a Thermo scientific FlashSmart CHNS/O Analyzer with Multi-Valve Control (MVC), at the Geoscience department of the University of Oslo.

2.7 Stable isotope analysis

The stable carbon and nitrogen isotope analysis was conducted using a Thermo Fisher Scientific EA IsoLink IRMS System. $\delta^{13}C$ and $\delta^{15}N$ are the ratios of the respective stable isotopes: C^{13}/C^{12} and N^{15}/N^{14}. These measures were compared to reference samples with documented isotope signatures. Equation 5 was used to calculate the different ratios (*Equation 5*).

$$\delta^{15}\mathrm{N\ or\ } \delta^{13}\mathrm{C}(\%) = \left(\frac{R_{\mathrm{Sample}}}{R_{\mathrm{Standard}}} - 1\right) X\ 1000 \qquad (5)$$

For $\delta^{13}C$ analysis, pulverized, HCl-treated sediment samples were used, while the $\delta^{15}N$ analysis used, dried, untreated pulverized material.

2.8 Mixing equation

Using the calculated values of $\delta^{13}C$ and C/N-ratio, the fractions of terrestrial vs. marine organic material in the sediments were determined (*Shultz & Calder, 1976; Thornton & McManus, 1994)*. This was done by using the mixing equation (*Equation 6 and 7*), where the sample values are compared to end member values representing values of terrestrial and marine organic material in an area. The $\delta^{13}C$ end members used in this study are obtained from Helland et al. (*2002*), whereas the marine end member used is -

21.2‰ and -27‰ for the terrestrial end member. Terrestrial C/N- ratio used is 7.84 and 11.45 for the marine end member (*Helland et al., 2002*).

$$X = F_t X_t + F_m X_m \qquad (6)$$

The equation is further rearranged to:

$$F_t = \frac{X - X_m}{X_{t-} X_m} \qquad (7)$$

F_t in this equation is the terrestrial organic matter fraction, while F_m represents the marine organic matter fraction. These factors combined equals 1. X is the selected sample that is analyzed and compared to the terrestrial and marine end member. X_t is the terrestrial end member, and X_m is the marine end member.

2.9 Heavy metal analyses

The sediments of the northern (GL2-21A) and southern core (GL3-21A) were analyzed for metal concentrations of Cr, Cd, Hg, Cu, Zn, Pb and Ni. These metals were selected for analysis because they are some of the most common pollutants in aquatic environments, and they don't require complex analytical techniques (*Kristoffersen, pers. comm., March 2022).*

Approximately 0.5 g of dried sediment from representative core intervals was pulverized using an agate mortar. The samples were then transferred to pre-labeled 15 ml centrifuge tubes. The centrifuge tubes were filled with 10 ml 7.22 M HNO_3. Thereafter, the tubes were set in an autoclave (~ 30 min) at 120°C with constant pressure of 1.2 bar. This sample treatment extracts the bioavailable metals in the sediments. Subsequently, the tubes were centrifuged at 4000 rpm for 10 minutes before approximately 2 ml of the extraction was transferred into 15 ml pre-labeled centrifuge tubes. The fluid was then diluted 50 times with 1 % HNO_3 and analyzed at the Department of Geoscience at the University of Oslo using an ICP-MS (Inductively Coupled Plasma Mass-Spectrometry). The method follows the NS 47700:1994 guidelines about determination of metals by atomic absorption spectrophotometry, atomization in flame.

The heavy metal accumulation rates were calculated by Equation 8, where C stands for the heavy metal concentrations and SAR is the sediment accumulation rates.

$$\text{Heavy metal AR} = \text{C} * \text{SAR} \qquad (8)$$

2.10 Micropalaeontological analyses

For micropalaeontological analyses approximately 2 g of dried sediment were washed through 500µm and 63µm sieves and dried in a heating cabinet at 45 °C. The sieved samples were portioned into two fractions: 63µm-500µm and >500µm. All fractions were weighed. The core intervals selected for micropalaeontological analysis were the topmost 2 cm, about every tenth cm down to 35 cm core depth.

A portion of the 63-500µm fraction was placed on a picking tray and all benthic foraminifera were handpicked with a damp brush. The load of sediments analyzed varied as the desirable number of foraminiferal species picked required different amounts of sediment. The desired number of individuals picked in each interval was between 300-350. For picking and identifying the species a binocular microscope (Nikon C-DSS230) was used. All picked individuals were glued in a microfossil slide, identified, and counted. The absolute abundance of individuals was normalized to the dry weight of the sediments and expressed as foraminiferal tests g^{-1} dry sediment.

Foram-AMBI

The Foram-AMBI is a marine biotic index used to assess ecological quality statuses for benthic foraminifera assemblages. Different foraminiferal species are assigned to one of five ecological groups (EG) –depending on their sensitivity/tolerance to organic carbon supply and resulting decrease in oxygen concentration at the seabed (*Alve et al., 2016*). Species which are assigned to group IV and V represents opportunistic species that displays a strong, positive, response to organic carbon enrichment. These groups characterize environments with moderate to poor ecological status classes (*Alve et al., 2016*). Group III are represented by species which are tolerant to enrichment. Those in group II are indifferent to the loading and as such appear under several concentrations of organic carbon. Species that are assigned to group I are sensitive to organic carbon enrichment. Equation 9 was used to calculate the foram-AMBI (*Alve et al., 2016*).

$$\mathrm{AMBI} = \frac{\{(0 \times \%\mathrm{G\,I}) + (1.5 \times \%\mathrm{G\,II}) + (3 \times \%\mathrm{G\,III}) + (4.5 \times \%\mathrm{G\,IV}) + (6 \times \%\mathrm{G\,V})\}}{100} \qquad (9)$$

Diversity indices

The software PRIMER (Plymouth Routines In Multivariate Ecological Research) version 6.1.13 (*Clarke & Gorley, 2006*) was used to calculate the Hurbert's diversity (ES100) and Shannon-Wiener diversity index (H'log2). The ES100 measures the expected number of species among 100 randomly chosen individuals in a sample (*Hurlbert, 1971*). In Equation 10, *S* is the total number of species, *N* is the number of individuals, N_i represents the number of individuals which corresponds to the species *i*.

$$\mathrm{ES100} = \sum_i^S \left(1 - \frac{\frac{N-N_i}{100}}{\frac{N}{100}}\right) \qquad (10)$$

The Shannon-Wiener index measures the species richness and gives information about how evenly distributed the individuals are between species (*Spellerberg, 2008*). The H'log2 is given by Equation 11, where *S* represents the total number of species, *N* is the number of individuals, while N_i represents the number of individuals of species *i*.

$$H'\log 2 = \sum_{i=1}^{S} \left(\frac{N_i}{N}\, x - log_2 \frac{N_i}{N}\right) \qquad (11)$$

NQI_f

NQI_f (Norwegian Quality Index based on foraminifera) is used as an ecological index. The index combines the diversity ES100 and the sensitivity index AMBI (*Alve et al., 2019*). A spreadsheet was used to calculate the NQI_f. The NQI_f is given by Equation 12:

$$NQI_f = 0.5\left(1 - \frac{AMBI_f}{7}\right) + 0.5\left(-\frac{ES100_{\_f}}{35}\right) \qquad (12)$$

3 Results

3.1 Core description

Sediments of the northern (GL2-21A) and southern (GL3-21A) cores were overall homogenous and fine grained. At the northern station (GL2), sediments were gray from the bottom up to 8 cm core depth, brown-greyish in the consecutive 6 cm and brown in the topmost 2 cm. The deepest 34-67 cm transitioned from grey to dark grey as the sediments became stiffer and more homogenous down-core. In this stiffer sediment, black sulfide spots were detected. Traces of bioturbation occurred down from 3 to 34 cm core depth (Figure 4, left).

In the southern core (GL3), the sediment at the bottom of the core up to 7 cm core depth was grey and homogenous with specks of sulfide spots. Between 7-2 cm core depth, the sediments had an intermediate brown-greyish color. This was followed by surface sediments (2-0 cm) being soft and brown. Polychaete tubes were detected in the core top 3 cm. Additional traces of bioturbation occurred between 3 to 22 cm (Figure 4).

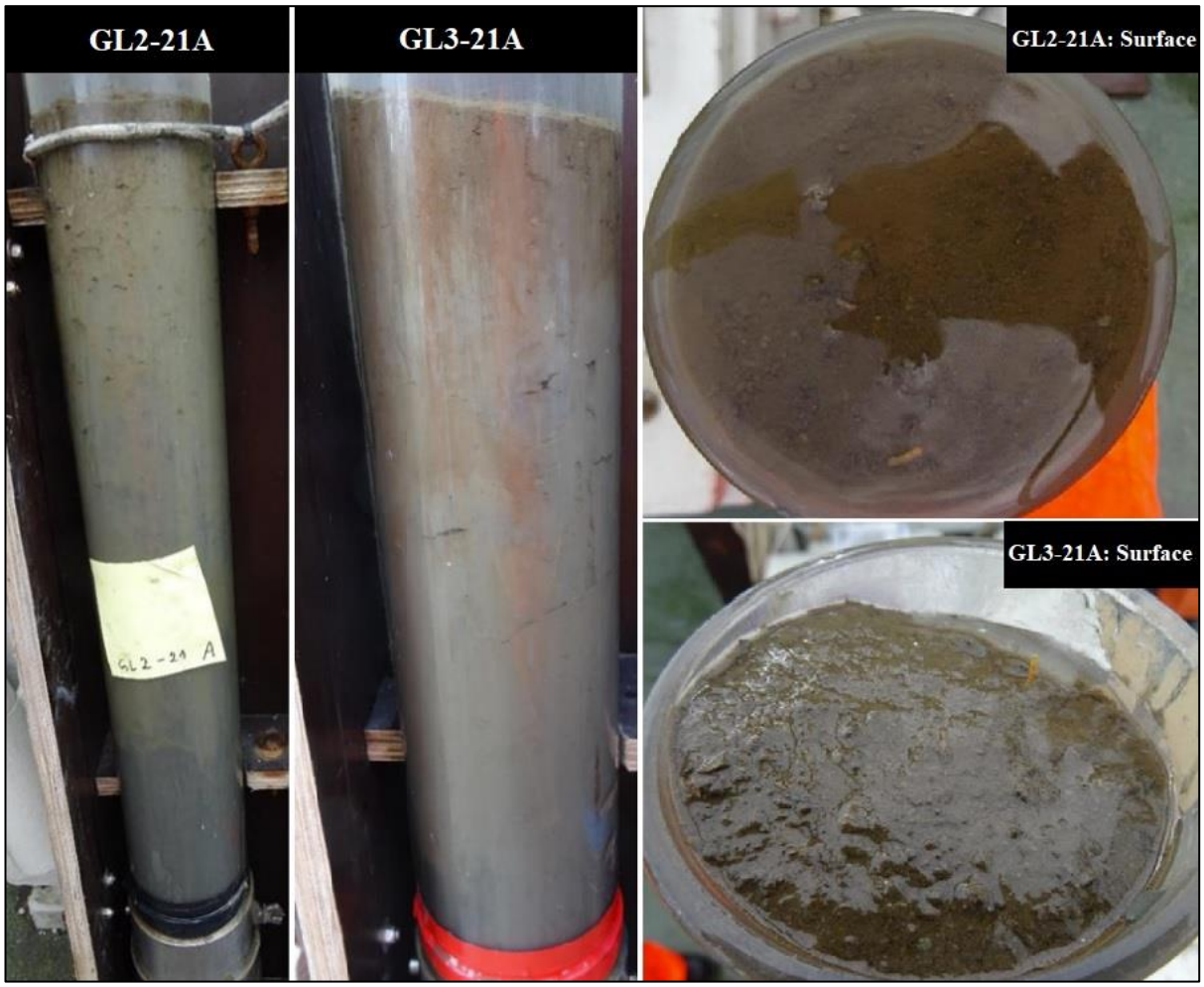

Figure 4: *Pictures of the northern (Gl2-21A) and southern (Gl3-21A) cores collected from the Hvaler estuary (Photos: Hess, 2021).*

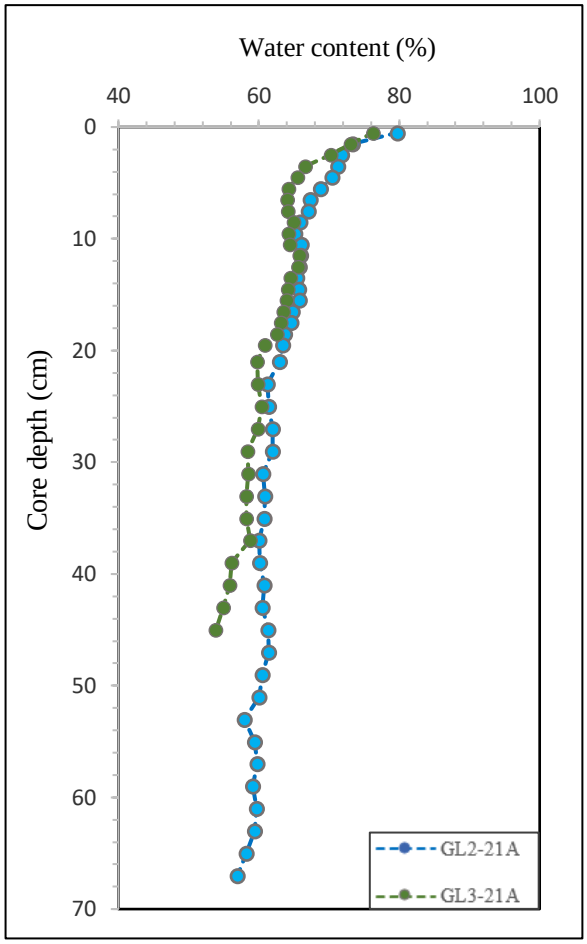

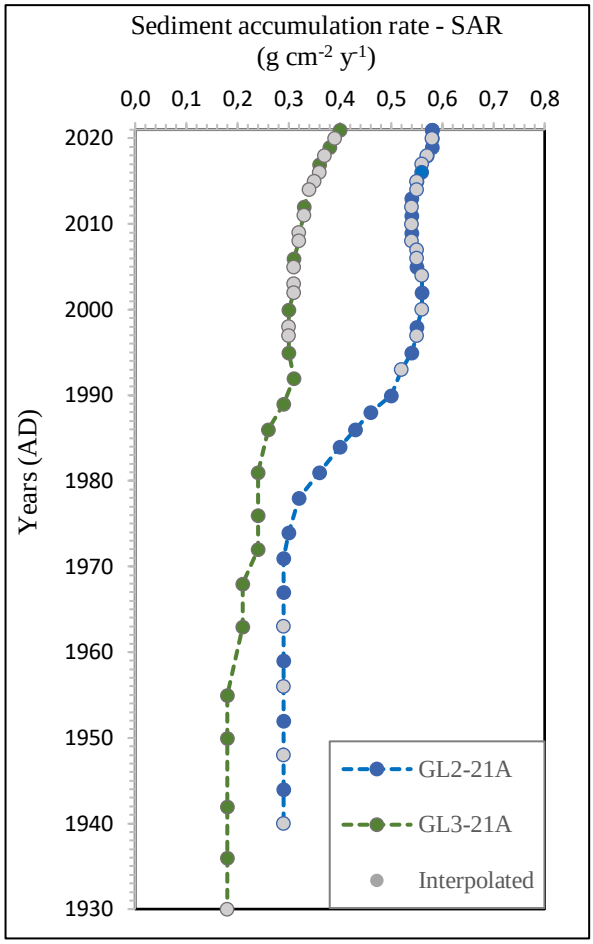

Figure 5 *(left): Water content of the two analyzed sediment cores.* **Figure 6** *(right)**:** Sediment accumulation rate estimated for the two sediment cores. Grey spots indicate interpolated values.*

Figure 5 shows the percentage of water content in the northern and southern sediment cores. The figure displays a relatively consistent decline in water content from top to bottom of the cores (Appendix: E). The tendency is conventional, as water content usually decline downwards in sediments due to burial and consequently compaction. A minor anomaly, (a drop), is detected at 53 cm core depth in the northern core (GL2). Irregularities are detected between 8-18 cm core depth, in the southern core (GL3) (Figure 5). These inconsistencies can indicate bioturbated sediments and, thereby, a reworked stratigraphy.

3.2 Sediment accumulation rate (SAR) and dating

Sedimentation accumulation is the combined result of sediment deposition and transportation that leads to preservation of strata (*Szmytkiewicz & Zalewska, 2014*). The sediment accumulation rate (SAR) increased, up-core, at both stations (Figure 6). Overall, the SAR was higher at the northern station (GL2) compared to the southern (GL3). The elevated SAR at the northern station (GL2) results in it covering a shorter time period. Prior to the mid-1970s, the rate at the northern station is consistent at 0.29 g cm^{-2} y^{-1}, while the southern station has experienced a gradual increase from 0.18 to 0.24 g cm^{-2} y^{-1}. From the mid-1970s to the late 1990s, the accumulation rate accelerates. The rate at the northern station stabilizes between 2000-2002 at ~0.56 g cm^{-2} y^{-1} and the southern between 2000-2014 at ~0.3 g cm^{-2} y^{-1} (Table 1, Figure 6). The dating report from ERRC is presented in the Appendix (D).

Table 1: Sediment accumulation rates and age of the two analyzed sediment cores (GL2 and GL3). The double-black line separates the two cores, the northern highlighted in blue and southern in green.

Core	Core depth (cm)	SAR ($g\ cm^{-2}\ y^{-1}$)	Year (AD)	Core	Core depth (cm)	SAR ($g\ cm^{-2}\ y^{-1}$)	Year (AD)
GL2-21 A	0.5	**0.58**	**2021**	GL2-21 A	59	0.29	1956
GL2-21 A	1.5	0.58	2021	GL2-21 A	61	**0.29**	**1952**
GL2-21 A	2.5	**0.58**	**2020**	GL2-21 A	63	0.29	1948
GL2-21 A	3.5	0.58	2020	GL2-21 A	65	**0.29**	**1944**
GL2-21 A	4.5	**0.58**	**2019**	GL2-21 A	67	0.29	1940
GL2-21 A	5.5	0.57	2018	GL3-21 A	0.5	**0.4**	**2021**
GL2-21 A	6.5	0.57	2018	GL3-21 A	1.5	0.39	2020
GL2-21 A	7.5	0.56	2017	GL3-21 A	2.5	**0.38**	**2019**
GL2-21 A	8.5	**0.56**	**2016**	GL3-21 A	3.5	0.37	2018
GL2-21 A	9.5	0.55	2015	GL3-21 A	4.5	**0.36**	**2017**
GL2-21 A	10.5	0.55	2015	GL3-21 A	5.5	0.36	2016
GL2-21 A	11.5	0.55	2014	GL3-21 A	6.5	0.35	2015
GL2-21 A	12.5	**0.54**	**2013**	GL3-21 A	7.5	0.34	2014
GL2-21 A	13.5	0.54	2012	GL3-21 A	8.5	**0.33**	**2012**
GL2-21 A	14.5	0.54	2011	GL3-21 A	9.5	0.33	2011
GL2-21 A	15.5	0.54	2010	GL3-21 A	10.5	0.32	2009
GL2-21 A	16.5	**0.54**	**2009**	GL3-21 A	11.5	0.32	2008
GL2-21 A	17.5	0.54	2008	GL3-21 A	12.5	**0.31**	**2006**
GL2-21 A	18.5	0.55	2007	GL3-21 A	13.5	0.31	2005
GL2-21 A	19.5	0.55	2006	GL3-21 A	14.5	0.31	2003
GL2-21 A	21	**0.55**	**2005**	GL3-21 A	15.5	0.31	2002
GL2-21 A	23	0.56	2004	GL3-21 A	16.5	**0.3**	**2000**
GL2-21 A	25	**0.56**	**2002**	GL3-21 A	17.5	0.3	1998
GL2-21 A	27	0.56	2000	GL3-21 A	18.5	0.3	1997
GL2-21 A	29	**0.55**	**1998**	GL3-21 A	19.5	**0.3**	**1995**
GL2-21 A	31	0.55	1997	GL3-21 A	21	**0.31**	**1992**
GL2-21 A	33	**0.54**	**1995**	GL3-21 A	23	**0.29**	**1989**
GL2-21 A	35	0.52	1993	GL3-21 A	25	**0.26**	**1986**
GL2-21 A	37	**0.5**	**1990**	GL3-21 A	27	**0.24**	**1981**
GL2-21 A	39	**0.46**	**1988**	GL3-21 A	29	**0.24**	**1976**
GL2-21 A	41	**0.43**	**1986**	GL3-21 A	31	**0.24**	**1972**
GL2-21 A	43	**0.4**	**1984**	GL3-21 A	33	**0.21**	**1968**
GL2-21 A	45	**0.36**	**1981**	GL3-21 A	35	**0.21**	**1963**
GL2-21 A	47	**0.32**	**1978**	GL3-21 A	37	**0.18**	**1955**
GL2-21 A	49	**0.3**	**1974**	GL3-21 A	39	**0.18**	**1950**
GL2-21 A	51	**0.29**	**1971**	GL3-21 A	41	**0.18**	**1942**
GL2-21 A	53	**0.29**	**1967**	GL3-21 A	43	**0.18**	**1936**
GL2-21 A	55	0.29	1963	GL3-21 A	45	0.18	1930
GL2-21 A	57	**0.29**	**1959**				

3.3 Grain size analysis

A stable trend up-core of the mean grain size can be observed in the northern sediment core (GL2) (Figure 7A). The mean particle size ranges from ~9.9 µm at 55 cm (~1963) core depth to ~16.1 µm in the surface sediments. Overall, the mean grain size is relatively stable at 12-13 µm. Clay, silt and sand percentage illustrate the distribution of particle sizes in the sediment core (Figure 7B, Figure 7C, Appendix: F).

The mean grain size in the southern core (GL3) has remained quite stable from the bottom of the core to the surface sediments. The largest mean grain size is detected in the surface sediments at ~18.9 µm, while the smallest grain size is ~10.9 µm at 7.5 cm (~2014) core depth. There is little variation in clay, silt and sand content in the core, and silt dominates (Figure 7A, Figure 7C, Appendix: F).

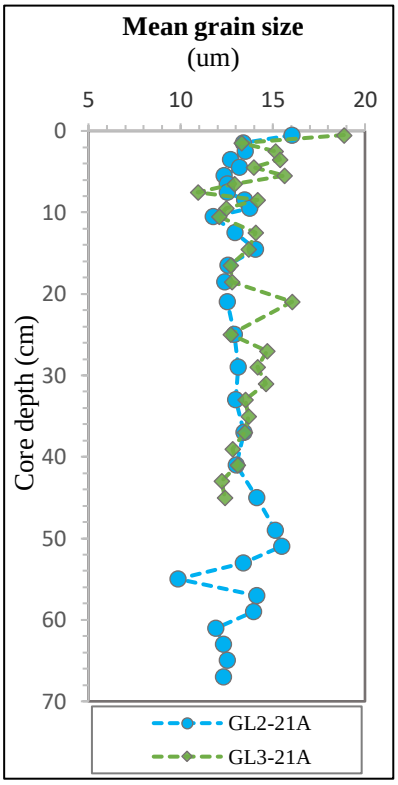

Figure 7A: *Mean grain size in northern (GL2) and southern (GL3) cores.*

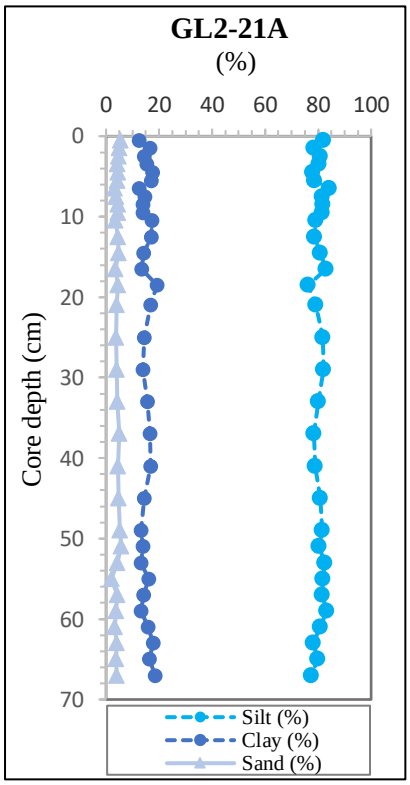

Figure 7B: *Clay, silt and sand content. Northern core (GL2).*

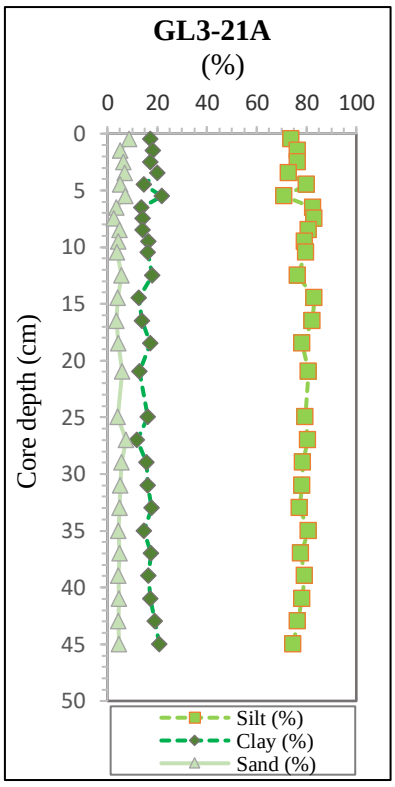

Figure 7C: *Clay, silt and sand content. Southern core (GL3).*

3.4 Heavy metal analysis

All heavy metal concentrations (except Cd) at the northern station (GL2) show an increasing trend up to the early 1960s (1963). After that, concentrations display an irregular but decreasing trend from the mid-1960s (Figure 8, Appendix: G). The concentrations of Cd are much lower than other heavy metals analyzed – less than 20% and is represented by the smaller secondary x-axis in the figure. The fluctuations of Cd are comparatively negligible and, therefore, considered stable. Concentrations of Hg display a similar declining trend as Pb and Zn except from a distinct spike in ~2015. However, in this study, Hg concentrations are semiquantitative and should be interpreted with caution. It is difficult to ionize the Hg concentrations in its entirety, due to large amounts of energy required, whereas the ICP-MS instrument used in this study solely measure ions. The relationship between Hg concentration can however indicate the change in magnitude to itself.

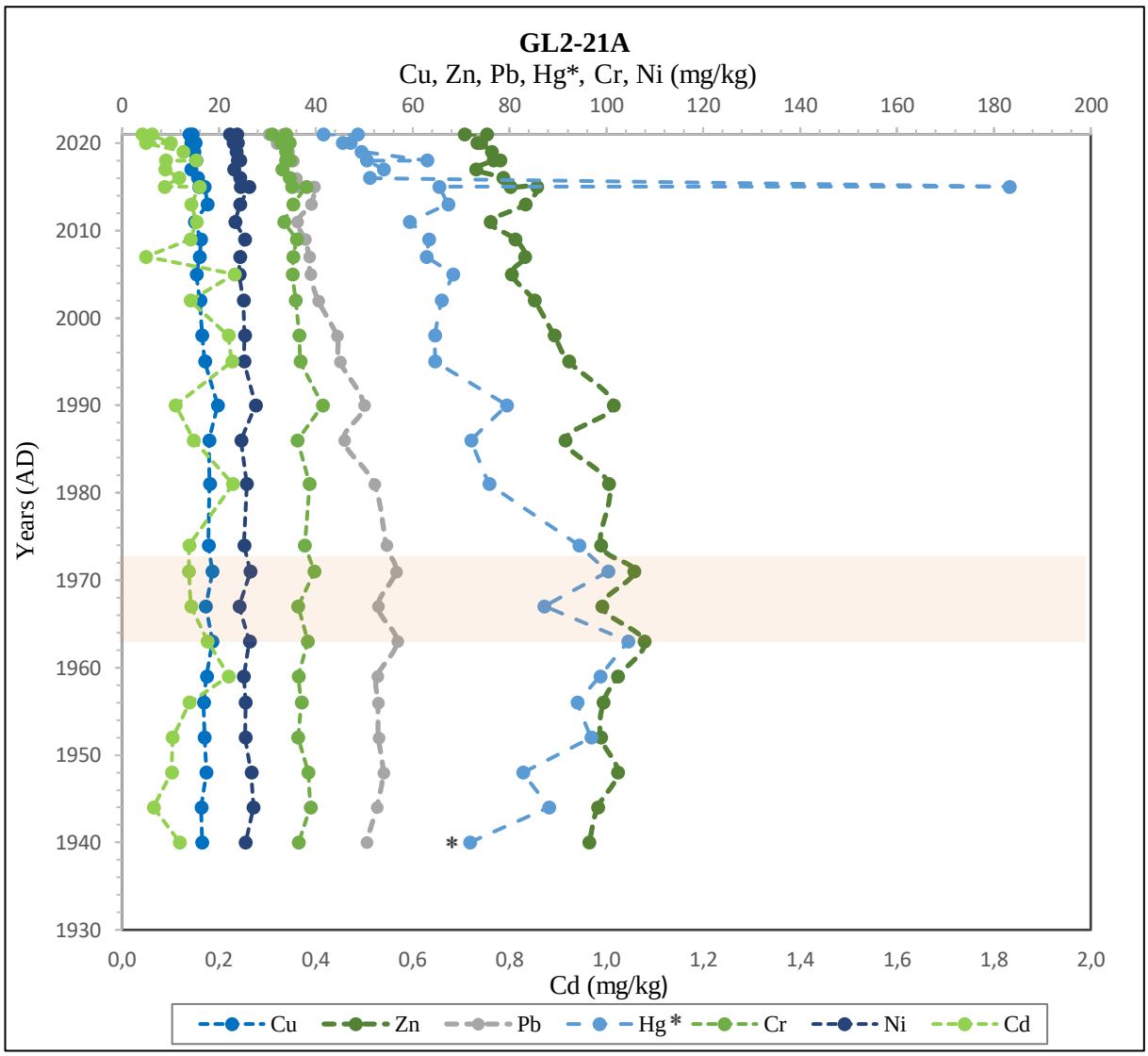

Figure 8: *Heavy metal concentrations of the northern core (GL2). Note the secondary scale for Cd-concentrations. The horizontal orange box show observable decreasing trends of heavy metals from ~1963.* Hg is only semiquantitiative and should be viewed with caution.*

Heavy metal concentrations of the southern core (GL3) begins to decline from the early 1960s (Figure 9). This decline corresponds to the initial decline at the northern station (GL2) (Figure 8). Elevated concentrations are found in the early 2010s (2012) followed by a distinct decreasing trend from 2017. Overall, the heavy metal concentrations have declined from ~1930 to 2021 (Figure 9, Appendix: G).

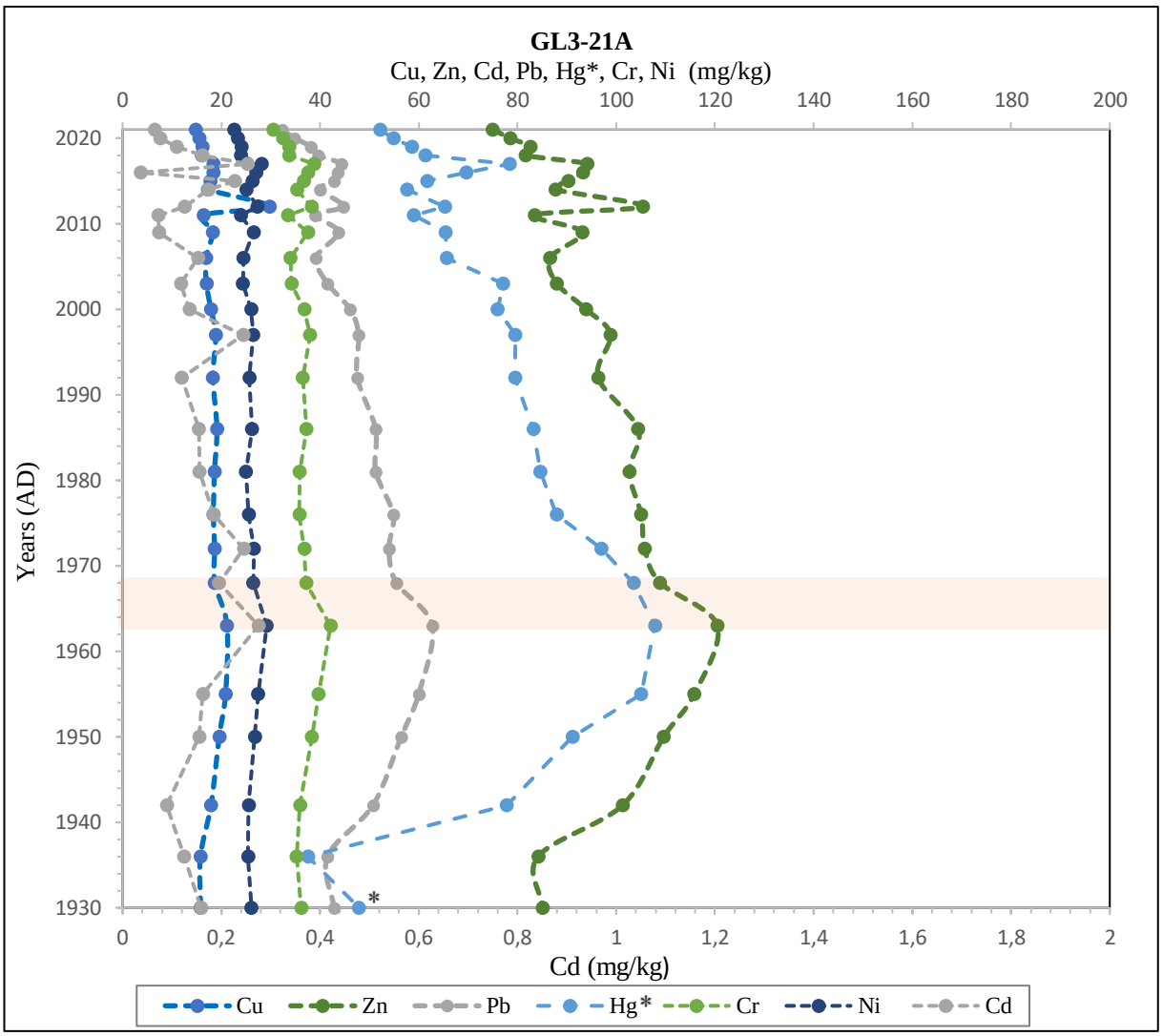

Figure 9: *Heavy metal concentrations of the southern core (GL3). Note the secondary scale for Cd-concentrations. The horizontal* orange box *show an observable decreasing trend of heavy metal concentrations from ~1963. * Hg is only semiquantitiative and should be viewed with caution.*

The heavy metal concentrations are classified in accordance with the Norwegian guidelines for classification of environmental status classes in sediments (*Veileder, 2018*). The classification of the temporal changes in the sediment cores is presented in the Appendix (A).

The heavy metal accumulation rates at the northern station (GL2) show an increase trend to the late 1980s/early 1990s. Thereafter, the rates decline towards the present (Figure 10). At the southern station (GL3), the heavy metal accumulation rate increased from the early 1930s to the late 2010s (2017), before the rates show a minor decline towards 2021.

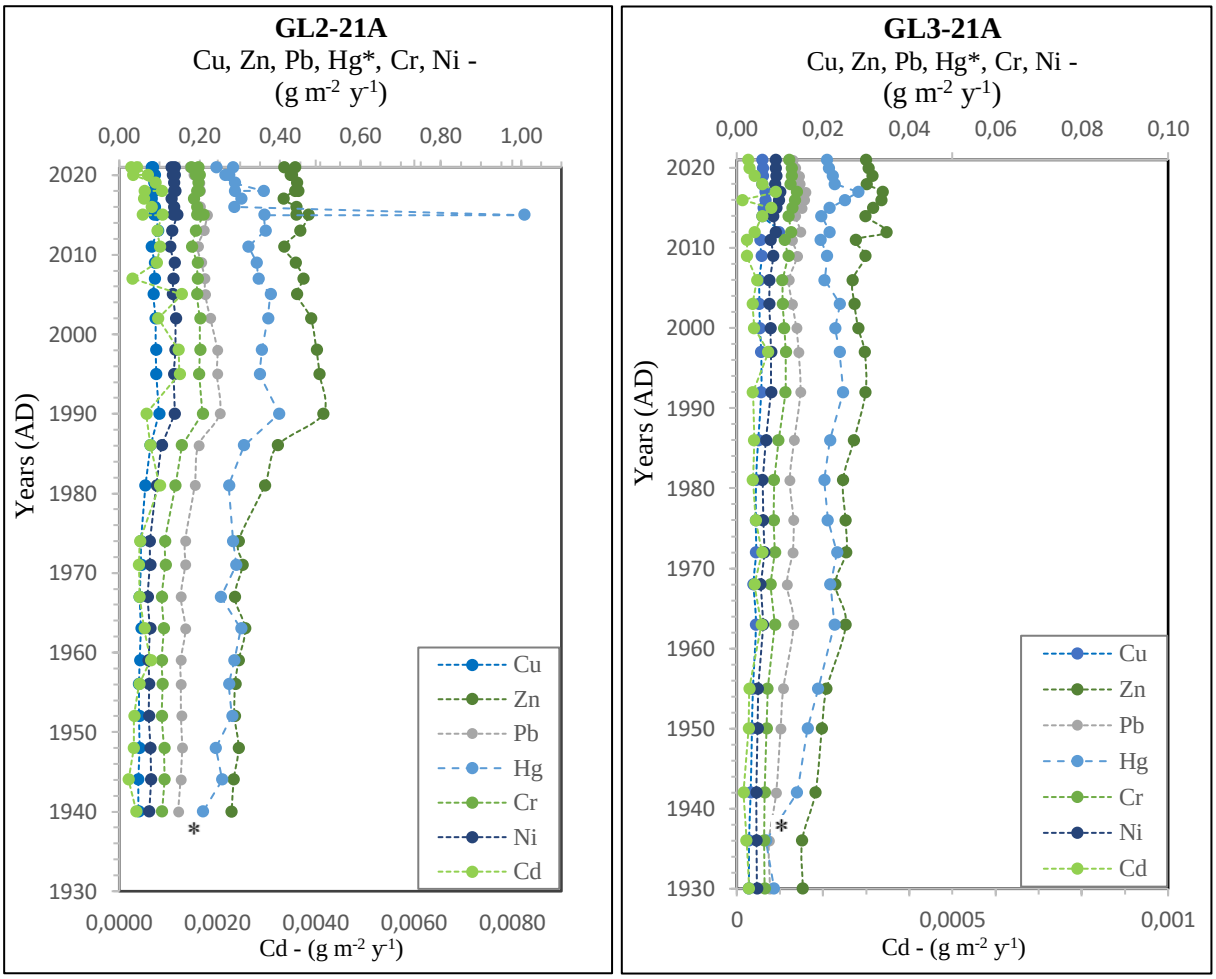

Figure 10*: Heavy metal accumulation rates for the northern core (GL2) (left) and southern core (GL3) (right). Note that the scales used for the GL3-heavy metal-AR (right) are ten times as large as that of the northern station (GL2).* * Hg is only *semiquantitative and should be viewed with caution.*

3.5 Carbon, nitrogen, and stable isotopes

3.5.1 Total Carbon

The total carbon (TC) concentrations in the northern (GL2) and southern cores (GL3) are presented in Figure 11. The TC concentrations in the northern core range from 27.47 mg/g to 35.89 mg/g. The deeper part of the sediment core has the greatest variability with the most distinct drop in concentrations found in the mid-1970s, and the highest concentration in the mid-1960s. TC stabilizes in the early 1980s with values around 35 mg/g. At the core surface, there is another abrupt decrease in TC (32.61 mg/g, Figure 11). Altogether, concentrations have been mostly stable at the northern station. The concentrations at the southern core have increased and are higher than the northern station in the younger sediments. The increase has slowed down from the mid-1980s to recent years. In the early 1930s, concentrations were 32.48 mg/g and have increased to 37.06 mg/g by 2021 (Figure 11).

3.5.2 Total Nitrogen

The TN (total nitrogen) concentrations have steadily increased throughout the years at the northern station (GL2). The concentration peaks in the mid-1970s (1974) and increased from 2.89 mg/g to the top of the core with values around 3.21 mg/g (Figure 12). In the southern core (GL3), TN increased from the early 1930s to the 2021. The values are generally higher compared to the northern station with a range from 2.94 mg/g to 3.77 mg/g (Figure 12, Appendix; H).

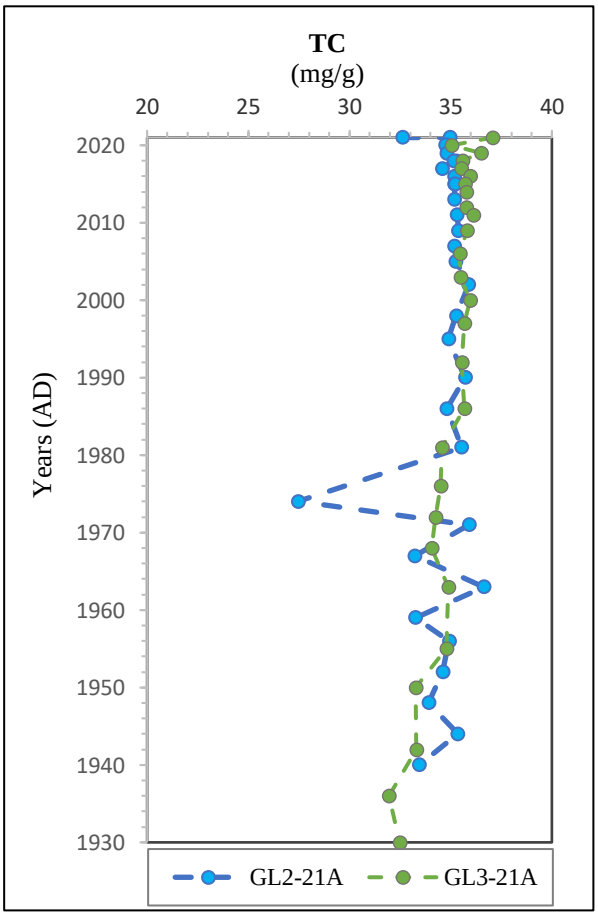

Figure 11: *TC- concentrations.*

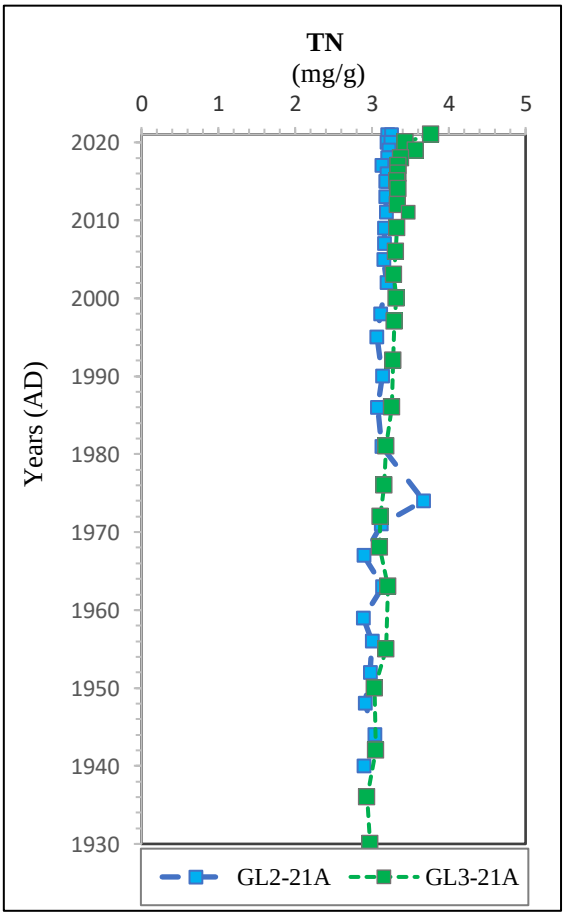

Figure 12: *TN-concentration.*

3.5.3 TOC_{63}

The sand corrected TOC (TOC_{63}) is stable in the northern core apart from smaller peaks in the late 1950s and early 1990s (Figure 13). Concentrations have a narrow range from 22.02 mg/g to 23.96 mg/g. In the southern core, the TOC_{63} has increased and is elevated in contrast to the northern core. Smaller peaks are detected in the late 1990s and mid-2010s. The values range from 20.86 mg/g to 25.73 mg/g (Figure 13).

3.5.4 Total inorganic carbon

The TIC fluctuates in the older part of the northern core (GL2) and stabilizes in the early 1980s, ranging from 6.27 mg/g to 14.99 mg/g. In younger segments of the core, the concentrations are about 14 mg/g. There is a prominent drop in the mid-1970s (1974) with values of 6.27 mg/g. The concentrations in the southern core (GL3) are generally more consistent and lower than in the northern core, with a range from 11.65 mg/g to the youngest interval at 18.02 mg/g (Figure 14).

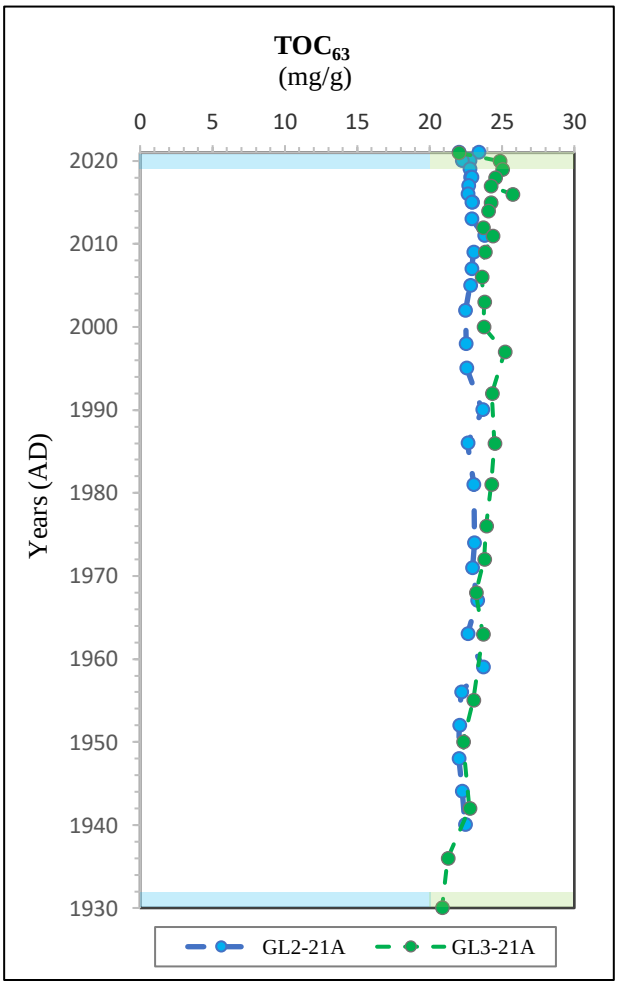

Figure 13: *TOC_{63} (mg/g) concentrations. The coloration at the top and bottom of the graph represents the status classes defined in Veileder, 2018. See, Appendix (A).*

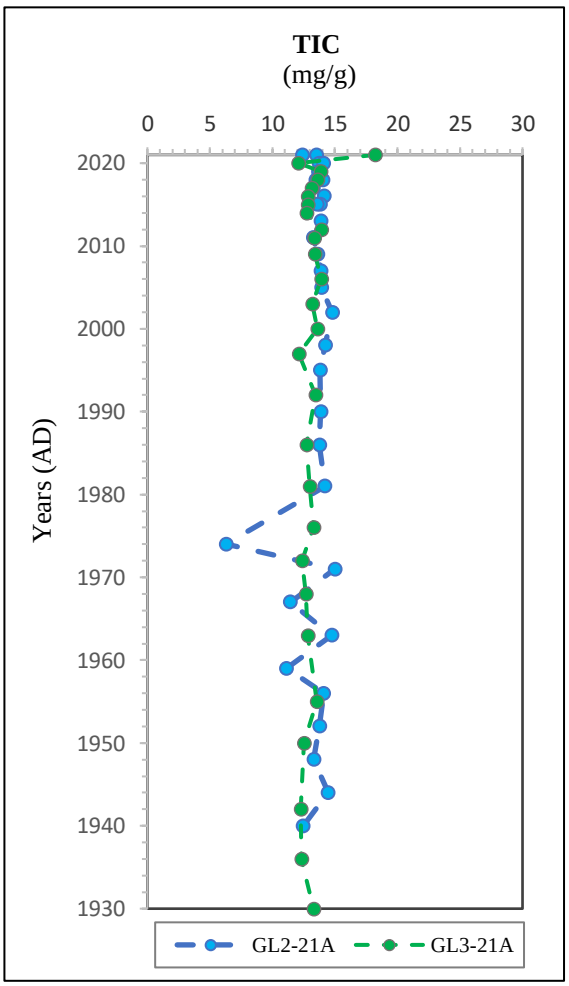

Figure 14*: TIC (mg/g) concentrations.*

3.5.5 Stable isotopes

3.5.5.1 $\delta^{13}C$

At the northern station (GL2), $\delta^{13}C$ values have a small increasing trend from the early 1960s (-22.85‰) to the early 2000s (2002, -22.53‰) (Figure 15). The trend revers and decline up to 2021 (-23.02‰). In the southern station (GL3), values decrease from -22.34‰ in the early 1930s up to -22.96‰ in the mid-2010s. In younger sediments, $\delta^{13}C$ fluctuate towards the surface as it approaches -22.75‰. $\delta^{13}C$ values are generally enriched in the southern station in comparison to the northern (Appendix: I).

3.5.5.2 $\delta^{15}N$

The $\delta^{15}N$ values are moderately consistent throughout the northern sediment core. The highest value is a peak of 7.07‰ in ~1967, while the lowest is 6.70‰ in 2018. Surface sediments reaches 6.99‰ (Figure 16). In the southern station, $\delta^{15}N$ have increased from the early 1930s to 2021, with more consistent values from the mid-1970s to the early 2010s and increases in the younger sediments. The values are generally lower compared to the northern station. Maximal value is detected in ~2020 of 6.80‰, and lowest in the mid-1930s of 6.38‰ (Figure 16, Appendix: I).

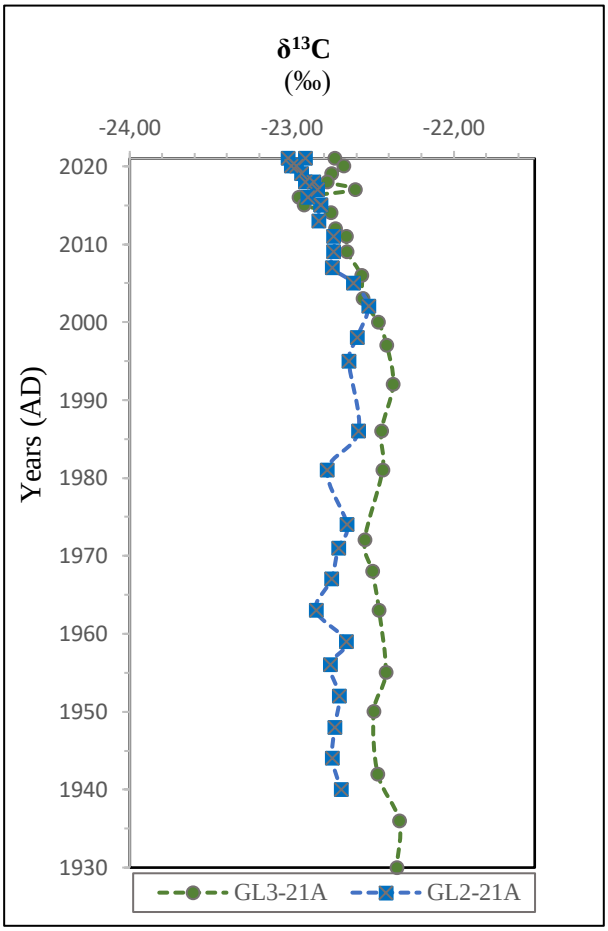

Figure 15: *$\delta^{13}C$ (‰) northern (GL2) and southern core (GL3).*

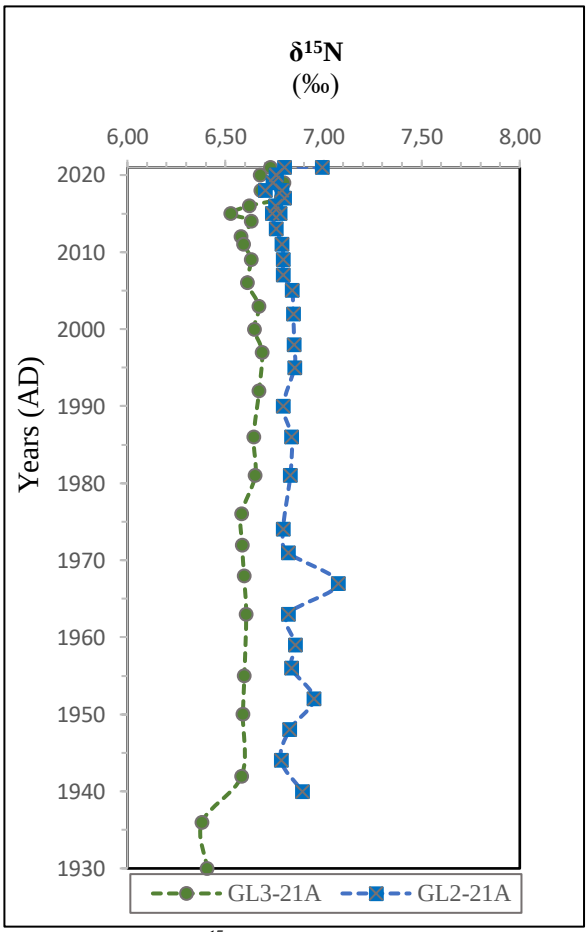

Figure 16: *$\delta^{15}N$ (‰) northern (GL2) and southern core (GL3).*

3.6. TOC/TN ratio and mixing equation

3.6.1 TOC/TN

The TOC/TN ratio is the method to characterize the source of organic matter (OM) in marine sediments. Helland et al. (2002) presents TOC/TN values with representative end-members of marine and terrestrial origin. The marine end-member represents values in the basin of the outer Glomma estuary (7.8) and the terrestrial end-member values from the estuary river mouth (11.5) (*Helland et al., 2002*). The OM from the northern (GL2) and southern (GL3) stations are predominantly from marine sources (Figure 17). There are two exceptions, ~1963 and 1956 in the northern station, where the organic carbon has a higher contribution of terrestrial sources. The ratio at the northern station (GL2) range from 7.93 (1959) to 6.03 (1974) and between 7.39 (1997) and 5.41 (2021) at the southern station (GL3). In 1974, the OM influx to the northern station (GL2) is predominantly marine.

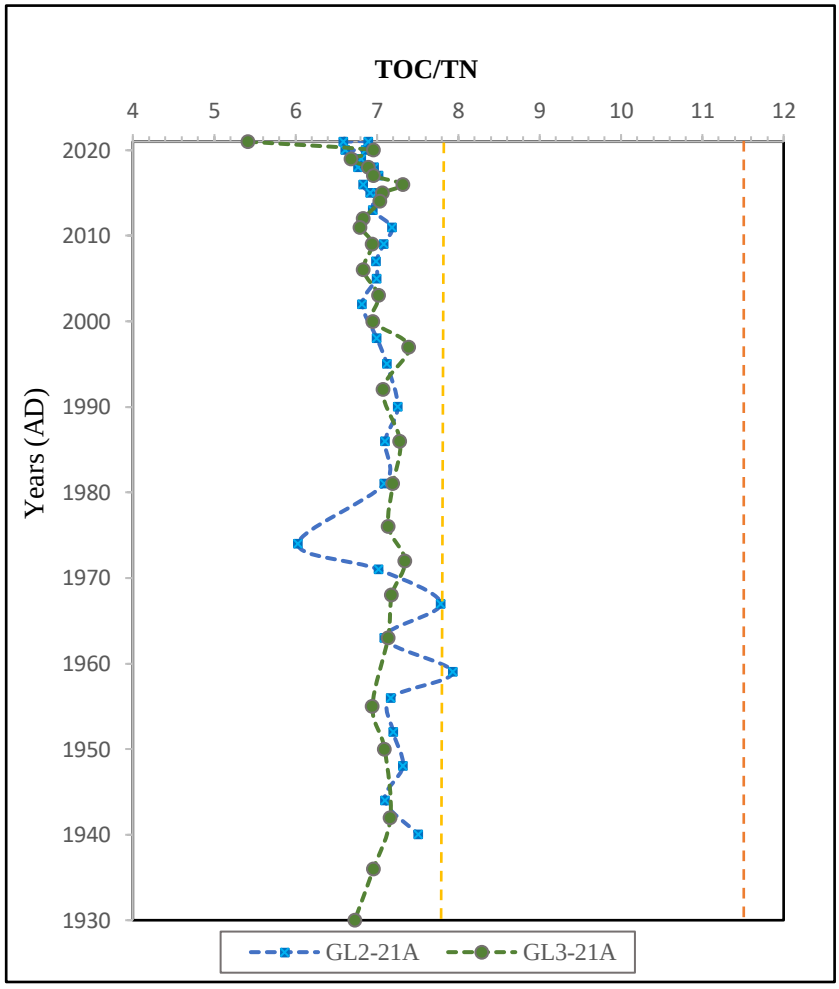

Figure 17*: TOC/TN-ratio of northern (GL2) and southern core (GL3). The yellow vertical dotted line represents the marine end-member and orange the terrestrial end-member.*

3.6.2 Mixing equation

The end-members described by Helland et al. (2002) combined with the isotope analysis results were used to determine the proportion of terrestrial organic carbon (T-TOC) in the sediment cores. Terrestrial $\delta^{13}C$ end-member used in this study is -21,2‰ and -27‰ for the $\delta^{13}C$ marine end-member. The results show that the T-TOC increases from the bottom to the top of both sediment cores (Figure 18), yet T-TOC is elevated in the northern core (GL2), with the highest value of 31.4% in 2021, and lowest of 22.9% in 2002. In the southern core (GL3), the highest value was observed in ~2016 (30.3%), and lowest in 1936 (19.6%). From the 1990s on percentage of terrestrial organic carbon has increased at the stations.

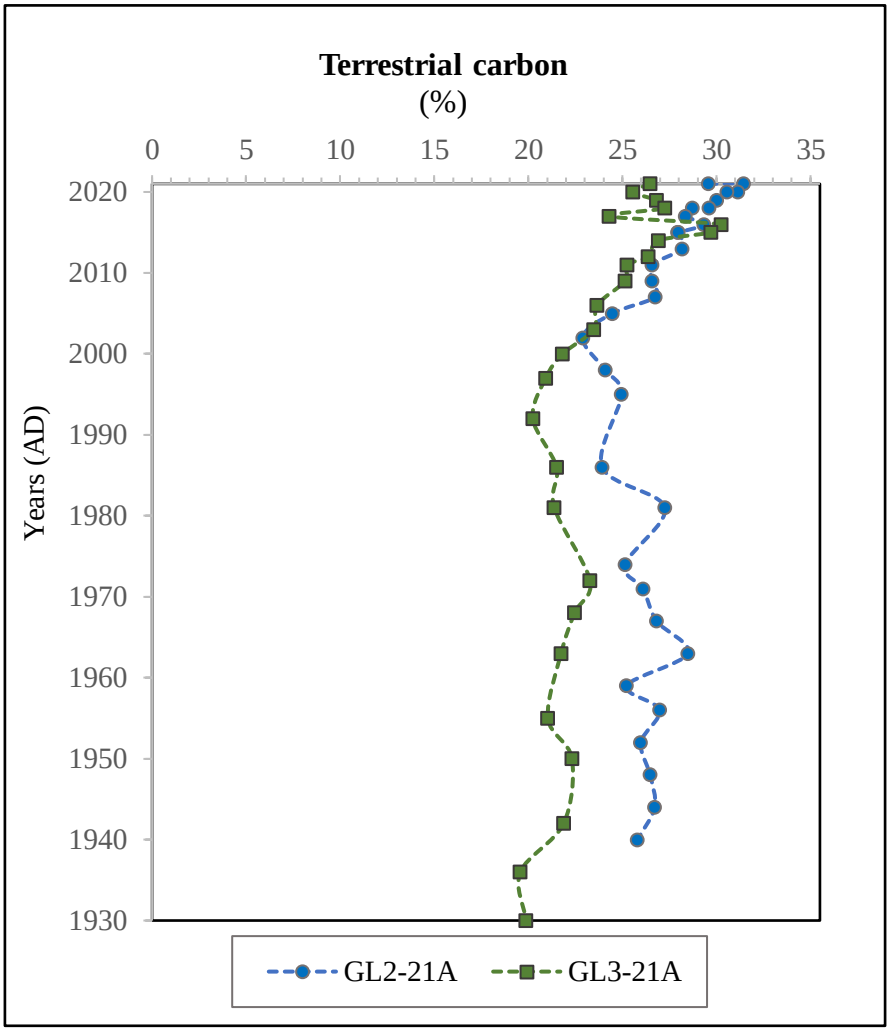

Figure 18: *Percentage of terrestrial organic carbon in the northern (GL2) and southern (GL3) sediment core.*

3.7 Accumulation rates

The inorganic carbon (AR-TIC) and organic carbon accumulation rates (AR-TOC_{63}) have increased in both the northern (GL2) and southern core (GL3) towards the surface. The rates are increasing in the northern core (GL2) from the early 1940s to the mid-1970s where a drop in AR-TIC occurs (Figure 19). Accumulation rates (AR-TIC and AR-TOC_{63}) at the northern station (GL2) increase up to the early 1990s before the rates stabilize towards 2021 (Figure 19). The accumulation rates in the southern core have gradually risen (Figure 19). Overall, the northern station (GL2-21A) has experienced higher organic and inorganic carbon accumulation rates than the southern station (GL3-21A).

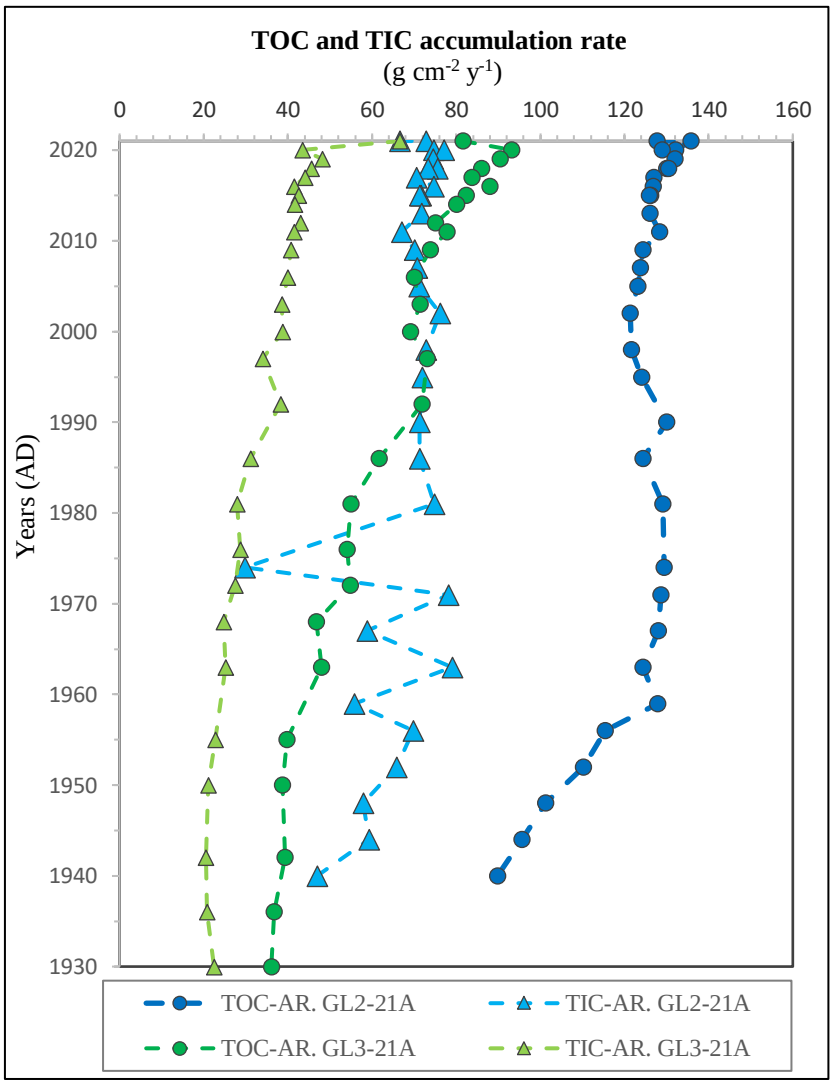

Figure 19: *Accumulation rate of TOC and TIC in the northern (GL2) and southern core (GL3).*

3.8 Foraminiferal analyses

3.8.1 Absolute abundance of foraminifera

The figures 20 and 21 represent the absolute abundance (tests/g of dry sediment) of the foraminifera species which dominates in the one of the sediment cores (GL2 and GL3) (>4% - Appendix: J). At the oldest core interval (1944) in the northern core (GL2), *Hyalinea balthica (~26* tests/g dry sed.) and *Pullenia osloensis* (~25 tests/g dry sed.) are the most abundant foraminifera. The absolute abundance of the selected species is quite stable from 1944 up to 1995, except from a gradual increase of *Stainforthia fusiformis* that reaches ~35 tests/g dry sed. in 1995. In the beginning of the 2010s (~2011), *S. fusiformis* rises to 55 tests/g dry sed. In recent years (~2020), *Stainforthia fusiformis, Cassidulina neoteretis* and *Textularia earlandi* peak at respectively ~68, ~38 and ~92 tests/g dry sed. The highest absolute abundance of all species is found in recent years, where *Liebusella goesi* is the most abundant (~149 tests/g dry sed. - Figure 20, Appendix: J).

The oldest core interval at the southern core (GL3) (~1930) has the highest absolute abundance of *Hyalinea balthica, Melonis barleanum* and *Pullenia osloensis* (68, ~53 and ~32 tests/g dry sed, respectively - Figure 20). This abundance decreases in the consecutive interval (1972) to ~54, ~28 and ~24 tests/g dry sed. *Brizalina spathulata, Cibicides lobatulus* and *Liebusella goesi* peaks in 2012 while *Textularia earlandi* and *Eggerelloides medius* increase towards the surface. The other foraminifera continue their consistent trends with low fluctuations. Further up in the core (2018), *Hyalinea balthica* has a peak at ~52 tests/g dry sed. as well as the highest abundance of *Stainforthia fusiformis* with ~25 tests/g dry sed. A relatively low abundance of foraminifera is observed around 2020. The surface interval is dominated by *Textularia earlandi, Eggerelloides medius* and *Hyalinea balthica* with ~70, ~50 and ~30 tests/g dry sed. respectively (Figure 21, Appendix: J).

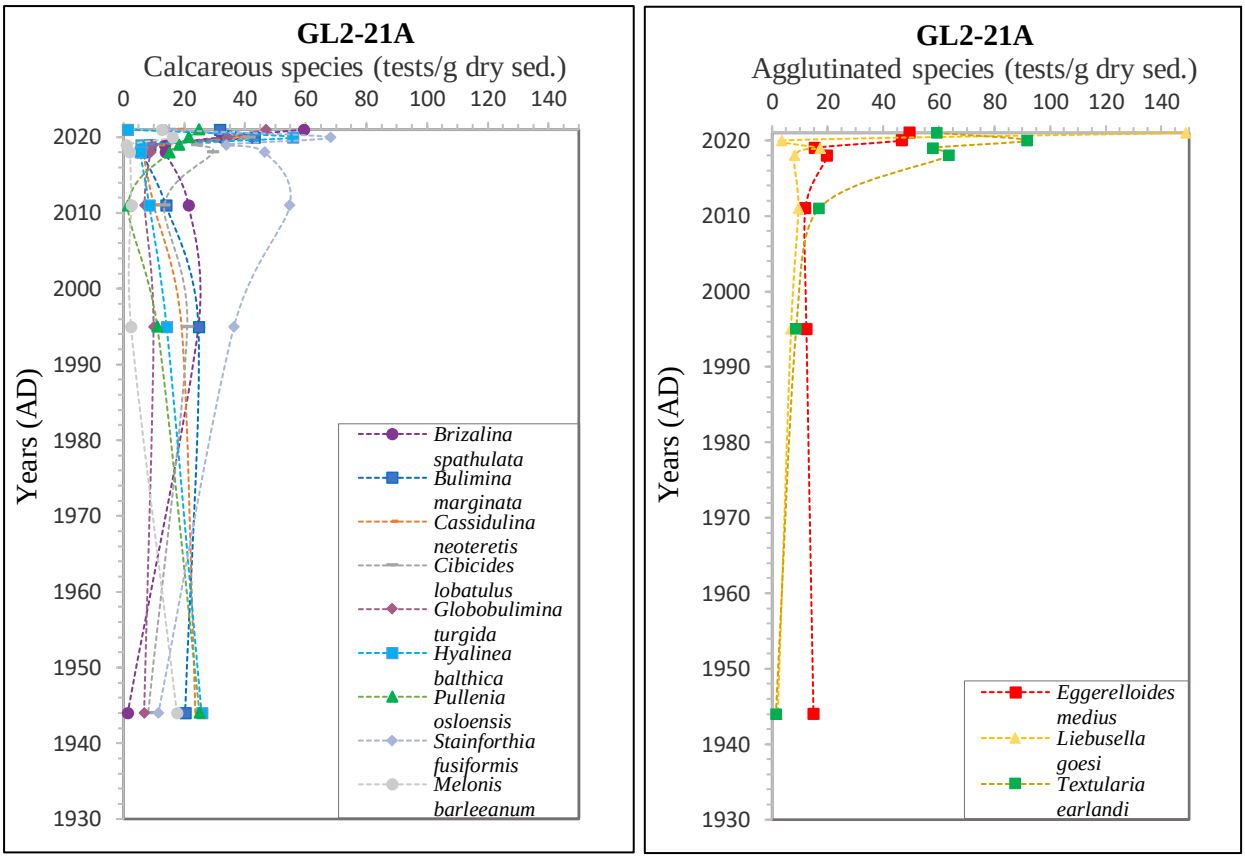

Figure 20: *Absolute abundance of selected species. Northern core (GL2). Calcerous species are presented on the left and agglutinated on the right*

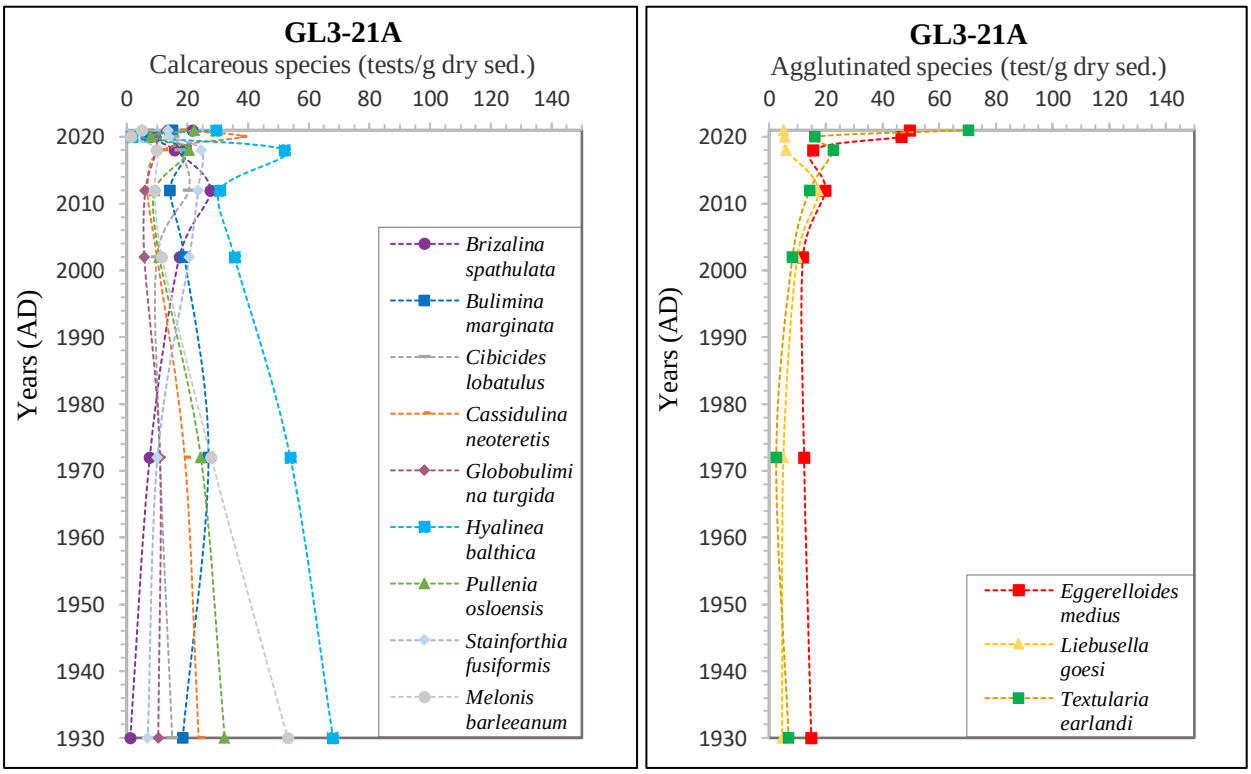

Figure 21: *Absolute abundance of selected species. Southern core (GL3). Calcerous species are presented on the left and agglutinated on the right*

3.8.2 Relative abundance of foraminifera

The figures 22 and 23 illustrate the relative abundance of selected species in the northern (GL2) and southern (GL3) sediment core. These are species with >4 % in at least one core sample. In general, the relative abundances show the same trends observed in the absolute abundances (Figure 20 and 21). At the northern station (GL2), the trends are consistent between the mid-1940s (1944) to mid-1990s (1995) as the relative abundance of; *S. fusiformis, B. marginata, B. spathulata, C. lobatulus, G. turgida, T. earlandi* and *L. goesi* increase (Figure 22). The rest of the selected species decline during this period. Another distinct trend occurs from the mid-1990s to 2011; *S. fusiformis, T earlandi* and *C. lobatulus* continue to increase, while all the other species decline. From the mid-1940s to the early 2010s, *S. fusiformis* has reached ~21%, *T. earlandi* ~6%, and *C. lobatulus* ~5% relative abundance. From the early to late 2010s (2011-2018), all species, except from *T. earlandi, C. lobatulus, E. medius* and *G. turgida* decline. The relative abundance in the period between 2018 to 2021 are fluctuating but it shows a distinct increasing trend of agglutinated foraminifera. *L. goesi*, *T. earlandi* and *E. medius*, (all agglutinated species), makes up 39.6% of the relative abundance in 2021. In 1944, these species only constituted ~7% (Figure 22).

At the southern station (GL3), the trends are consistent from the early1930s to the early 2000s. *S. fusiformis, B. marginata, B. spathulata, L. goesi* and *T. earlandi* all increase up to ~8%, ~7%, ~6%, ~4% and ~3%, respectively, while the remaining species decline during this period. These increasing trends prolongs to the early 2010s with the addition of *E. medius* and *T. earlandi which* increases to ~6% and ~7% respectively. From the early 2010s to 2020, the calcareous species *H. balthica* and *S. fusiformis* have the highest relative abundances at ~15% and ~7%. *T. earlandi* has the greatest relative abundance in 2021 at the southern station as it constitutes ~19% (Figure 23).

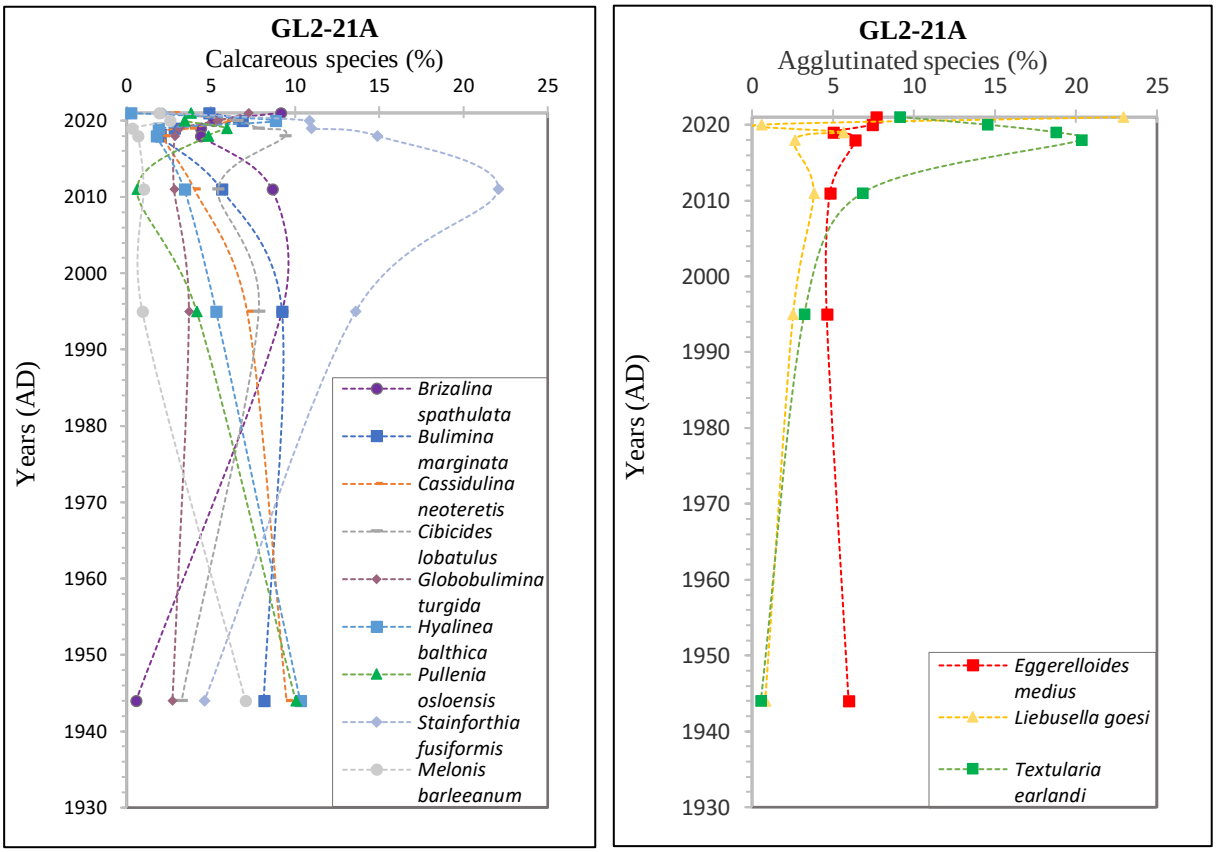

Figure 22: *Relative abundance of selected species in the northern core (GL2). Calcareous species plotted in the left figure and agglutinated species in the right figure.*

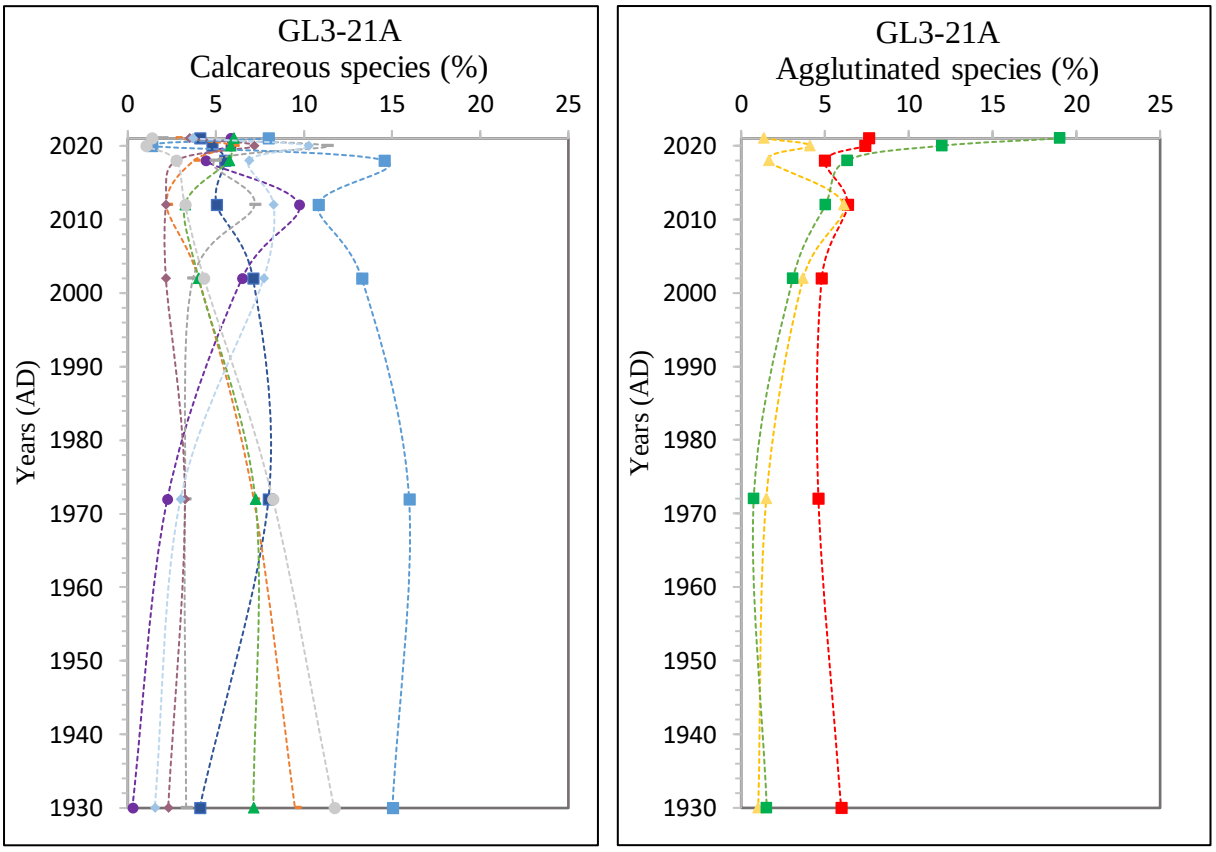

Figure 23: *Relative abundance of selected species in the southern core (GL3). Calcareous species plotted in the left figure and agglutinated species in the right figure.*

3.8.3 Agglutinated vs calcareous foraminifera

The percentage of agglutinated foraminiferal tests increases upwards from 1940-2021 in the northern (GL2) and southern (GL3) sediment cores (Figure 24). Highest relative abundance appears in the surface samples of both cores (51% in the northern and 45% in the southern core), and lowest in the oldest core interval (12%). Values between 12-20% characterize the period between the 1930s to mid-2010s. A drop in agglutinated foraminifera is detected around 2018. Agglutinated tests at the southern core increases towards the surface sediments (Figure 24), ranging from 18% to 45%.

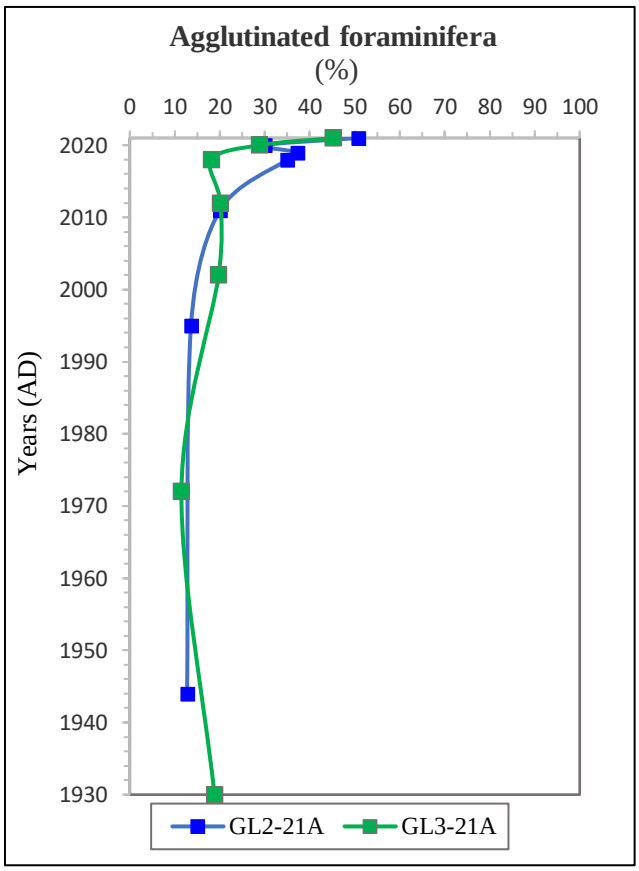

Figure 24: *Percentage of agglutinated foraminifera. Northern (GL2) and southern core (GL3).*

3.8.4 Benthic foraminiferal accumulation rate (BFAR)

In the northern core, the benthic foraminiferal accumulation rate steadily increases up to 2019 and abruptly increases in 2020-2021 (Figure 25). At the southern core (GL3), the BFAR is stable up to ~2018. A drop occurs in 2020 before it reaccelerates up to 2021 (Figure 25). Overall, the BFAR is higher at the northern core (GL2) compared to the southern.

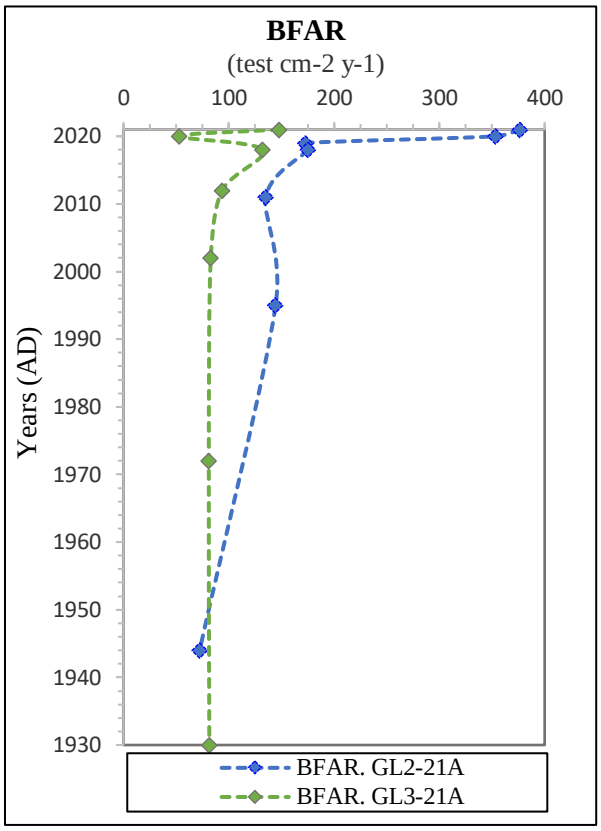

Figure 25*: Benthic foraminifera accumulation rate (test cm-2 y-1). Northern (GL2) and southern (GL3) cores.*

3.8.4 Ecological quality indices, diversity and sensitivity

At the northern station (GL2), the Foram-AMBI increase up to ~2.8 in 2011. It drops down in the consecutive interval and stabilize in 2020 and 2021 (Figure 26). The AMBI ranges from 2.06 in the deepest analyzed core interval to 2.70 in ~2011. At the southern station, the Foram-AMBI elevates upwards in the sediment core. It peaks in 2020 and 2021 as it reaches 2.39 in the surface. The lowest AMBI is found in ~1930 at 1.69 (Figure 26).

The foram-AMBI is derived from selected species that are assigned to different ecological groups (EG) (Appendix: K). Sensitive species belonging to the EG1 decline from the early 1940s up to 2018 at the northern station (GL2). In 2019, EG1 increases up to 2020 as it reaches 28%. The relative abundance decreases down to ~8% in 2021. EG2 shows an inverted pattern from EG1. The EG2 species have a slight increase up to 2018 (~19%), then a decrease to 2020 (~6%) and resurges in 2021 (~35%). EG3 and EG5 shows opposite trend from the mid-1940s to 2021. Up to the early 2010s, the EG3 species decline in relative abundance (~35%). The trend reverses up to 2021 where it reaches 55% relative abundance. EG5 shows an increasing trend up to the early 2010s where it constitutes ~22%. Thereafter it declines towards 2021 where is makes up ~2% of the relative abundance at the northern station (GL2) (Figure 27, Table 9).

The distribution of the different EGs in the southern sediment core (GL3) is relatively stable until the mid-2010s. From then on, a clear increase in EG3 species is observed. EG1, EG2 and EG5 comprise smaller percentages with ~17%, ~15% and ~4% respectively in 2021. EG3 dominates in 2021 with ~64 % relative abundance (figure 28, Appendix: K).

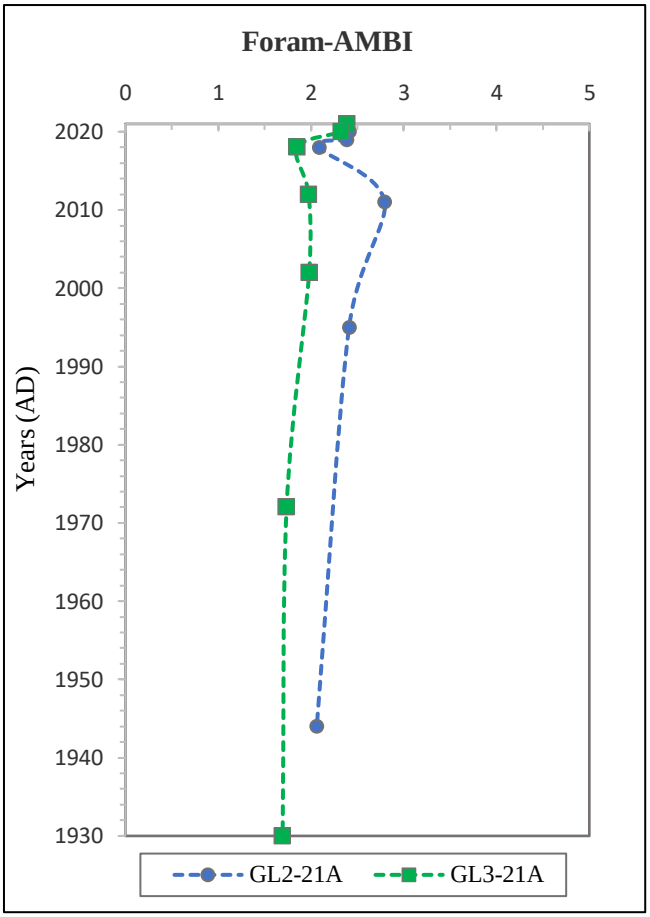

Figure 26*: Foram-AMBI at the northern (GL2) and southern stations (GL3).*

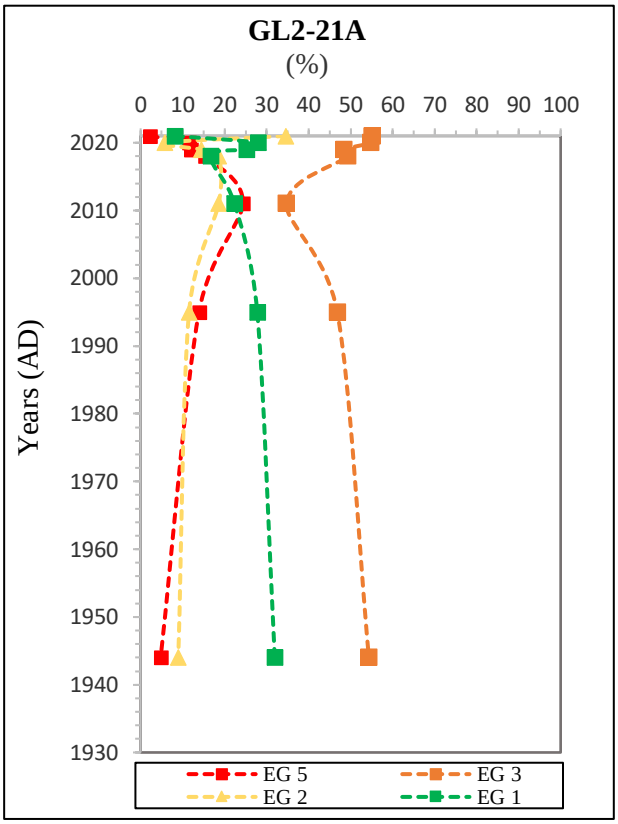

Figure 27: *Relative abundance of ecological groups. Northern core (GL2).*

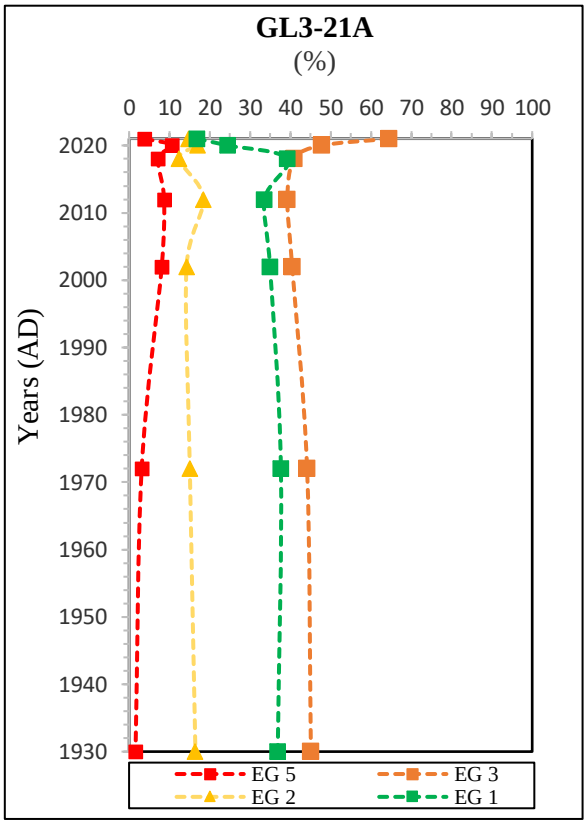

Figure 28: *Relative abundance of ecological groups. Southern core (GL3).*

Diversity indices are fairly stable prior to the early 2010s. H'(log2) is stable throughout the core, except from a small decline in the younger intervals (Figure 29a). ES100 is at its highest at the northern station in ~2011 and in ~2019 at the southern station (Figure 29b). NQI_f is stable throughout the core baring a small decline in the youngest centimeters (Figure 29c). All diversity indices for the northern (GL2) and southern station (GL3) represent high ecological statuses.

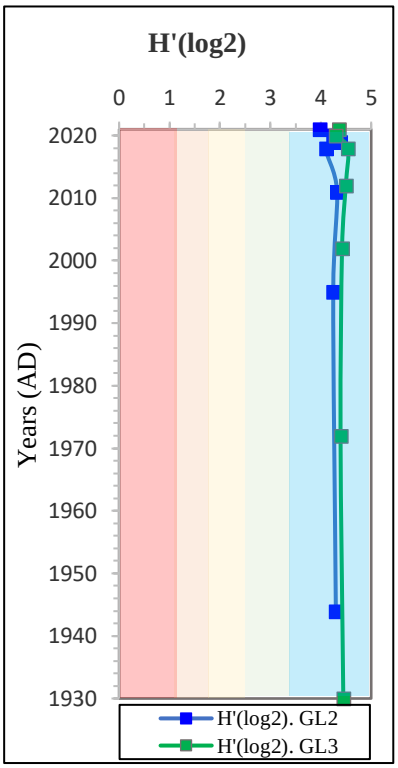

Figure 29A*: H'(log2).*

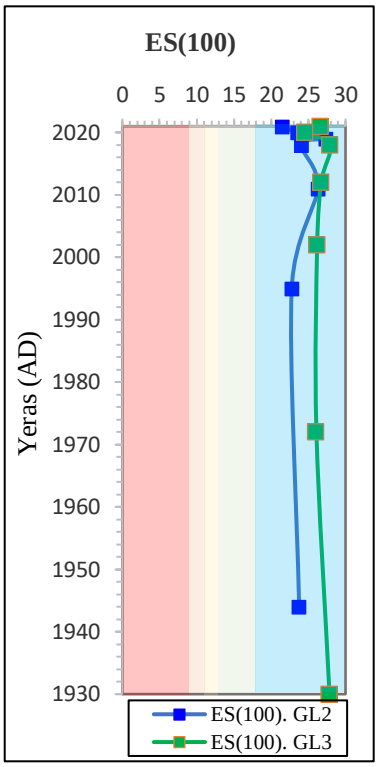

Figure 29B*: ES(100). Colors in Figure 27 (a,b,c), correspond to class boundaries defined by Alve et al., 2019.*

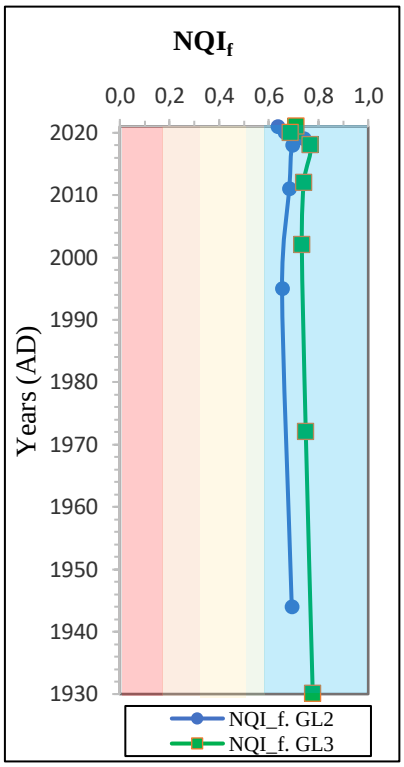

Figure 29C*: NQI$_f$.*

4 Discussion

4.1 Heavy metal pollution history

The development of heavy metal concentration at the northern station (GL2) reflects most of the previously recorded pollution history in the Hvaler estuary (*Helland et al., 2002; Polovodova Asteman et al., 2015*). The discharge from Saugbrugsforeningen to the Hvaler estuary is primarily linked to the heavy metal emissions from the roasting of sulfide ores. This cumulated in 1970-1975 and is detected at the northern station (GL2) as concentrations increase up to the mid-1960s/early 1970s (Figure 8) (*Knutzen, et al., 1978*). The declining trend (post-early 1970s) fits well with the period where restrictions on discharge of industrial waste to the Glomma River was implemented (*Helland, 2001*). The communal sewage treatment plant in Fredrikstad (Figure 1) was established during the late 1980s but did not result in a substantial decline of heavy metal concentrations at the northern station (GL2) (*Berge et al., 1996*). At the southern station (GL3), the initial decline, from the mid-1960s (1963), occurs simultaneous as the declining trend at the northern station (GL2) begins. These declining trends happens ~3 years earlier than most of the previously documented pollution development in the area (*Helland, 2001; Helland et al., 2002; Polovodova Asteman et al., 2015*). However, the premature decline from 1963 coincides with the industrial reform in the early 1960s, from coal and manufactured-gas plants to hydropower and electrical furnaces, in the Hvaler estuary's vicinity (*Arp et al., 2011*). This turnover is not described by Helland and Polovodova which might imply that the reform didn't promote an impactful reduction of heavy metal concentrations in the estuary (*Helland, 2001; Helland et al., 2002; Polovodova Asteman et al., 2015)*. Even though some concentrations are elevated at the stations, especially in the early 1960s, it is important to note that all values from the two locations are in the "high" to "good" status classes (*Veileder, 2018*) (Appendix: G).

Station 5 and 9 surveyed by Helland (2002) are compared to the northern (GL2) and southern station (GL3) as they represent a location inside the Hvaler skerries and the outer basin respectively (Figure 30). Singling out the lead (Pb) concentration; the previously documented values from the central part of the estuary, in the Hvaler skerries, (Station 5, *Helland et al., 2002*), does not match the concentration development measured at the northern (GL2) and southern (GL3) stations. The primary sources of Pb to the estuary are identified as natural lead seeping from terrestrial sediments, local industry, and atmospheric long-range transport of leaded gasoline (*Helland et al., 2002*). The concentration maximum from station 5 was dated to 1955, while it further out in the Hvaler basin (Station 9, *Helland et al., 2002*) was reached in 1980. The inconsistent periods of maxima are hypothesized to be caused by the difference in particle adsorption and distribution, as well as hydrological conditions in the area (*Helland et al., 2002*). However, the analyses of grain sizes (Figure 7B, Figure 7C), TOC_{63} (Figure 13) and $\delta^{13}C$ (Figure 15) do not indicate a particular increase of riverine discharge in 1955 nor in 1980 at the northern (GL2) or southern stations (GL3). This might imply that the Pb-concentrations reflect the strength and flow of the Skagerrak coastal currents, rather than the discharge from the Glomma River.

Copper (Cu) concentrations gradually accumulated to the 1990s until a process adjustment was implemented. This reduced the concentrations in the Hvaler estuary by 90% (*Helland, 2001*). However, the reduction is neither reflected at the northern (GL2) nor at the southern station (GL3) (Figure 8 Figure 9).

The concentrations of zinc (Zn) in the northern (GL2) and southern (GL3) cores correspond to the temporal development from the estuary described by Holtan (1996) and Helland (2001). Zink, used in the Borregaard industries rayon products, reached maxima concentrations in 1968 in their study (*Holtan, 1996*), while the highest concentration of zinc is found in 1963 at the northern (GL2), and southern station (GL3) (Figure 8, Figure 9). Uncertainties for these intervals are ±3 and ±5 years respectively (Appendix: D), which means that the peaks detected from the zinc-results matches the concentration development described by Helland (2002).

Helland (2002) determined that the highest mercury (Hg) concentrations occurred in 1965 and declined towards the present (due to process adjustment). The concentrations increase to 1963 at the northern (GL2) and southern (GL3) station, which agrees with Helland's (2002) observations, but the concentrations do not show a drastic decline from the 1990s as Holtan (1996) describes. Furthermore, the distinct spike in 2015, at the southern station (GL3), do not correspond to any documented leaks from local industries (Figure 9).

The heavy metal concentrations are generally higher at the southern station (GL3) compared to the northern station (GL2) (Table 2). This is unexpected, as the northern station (GL2) is located closer to the prominent heavy metal sources, from industries in vicinity of Fredrikstad, Sarpsborg and Halden (Figure 1). The riverine influence is declining out in the archipelago and should results in lower concentrations at the southern station (GL3). Additionally, during periods of low river discharge, particle sedimentation will primarily happen north of the Hvaler islands *(Walday et al., 2006*). However, the many islands, currents, channels, and narrow straits in the Hvaler skerries can influence the discharge pattern and disturb the transport of heavy metals to the estuary. Normally (excluding larger floods), the estuary is only influenced by the riverine transport in some areas (*Walday et al., 2006*) (Figure 31). Under normal conditions, the particles transported by the Glomma River do not reach the southern station (GL3), while the northern station (GL2) experience some influence. Outside of the Hvaler skerries, the strength and placement of the Baltic and Jylland currents governs most of the surface water circulations in the Hvaler estuary (Figure 2). Consequently, the surface waters in the Hvaler area flows in a northwestern direction (*Berge et al., 1996; Helland et al., 2002*). As such, the coastal currents do initially flow towards the southern station (GL3) and then to the northern (GL2) (Figure 2, Figure 32). The discharge from the Glomma River has seemingly transported less heavy metals to the southern station (GL3) compared to the northern (GL2) and received more elements by the coastal currents (*Walday et al., 1996*). This could also explain the low resemblance between the concentration

development of heavy metals in the southern core (GL3) and the documented pollution history of the area. The simultaneous increase and decreases of elements detected in the sediment cores can represent periods of higher discharge or coastal current forcing at the different stations (Figure 8, Figure 9). The development of heavy metal concentrations at the stations are most likely a result of competing and changing hydrological conditions and emissions from local industry to the estuary.

Table 2: *Difference in average of heavy metal concentrations between the northern (GL2) and southern (GL3) stations. *Hg values are semiquantitative and should be interpreted with caution.*

Average heavy metal concentrations (mg/kg)	Cu	Zn	Cd	Pb	*Hg	Cr	Ni
Northern core (GL2)	16,41	87,97	0,13	43,12	73,79	35,97	24,83
Southern core (GL3)	18,24	95,27	0,15	46,16	73,54	36,24	25,76
Increased/reduced concentration at GL3 (%)	+11,15	+8,3	+15,38	+7,1	-0,34	+0,1	+3,8

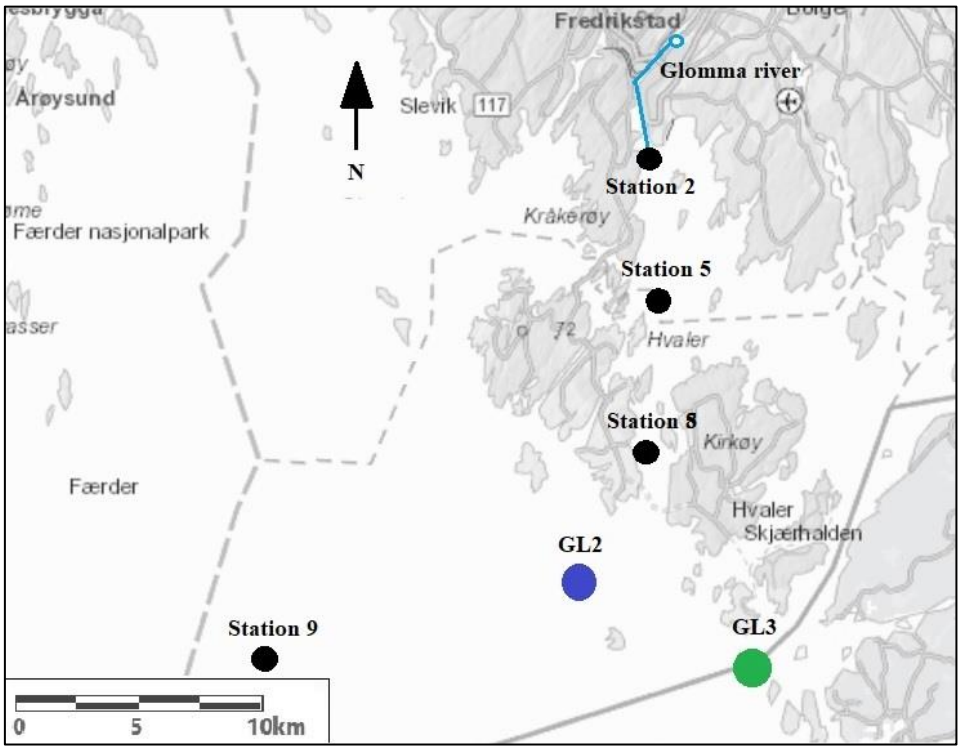

***Figure 30**: Location of station 2,5,8 and 9 studied by Helland et al. (2002) and GL2 and GL3 (Modified from NVE, 2022c).*

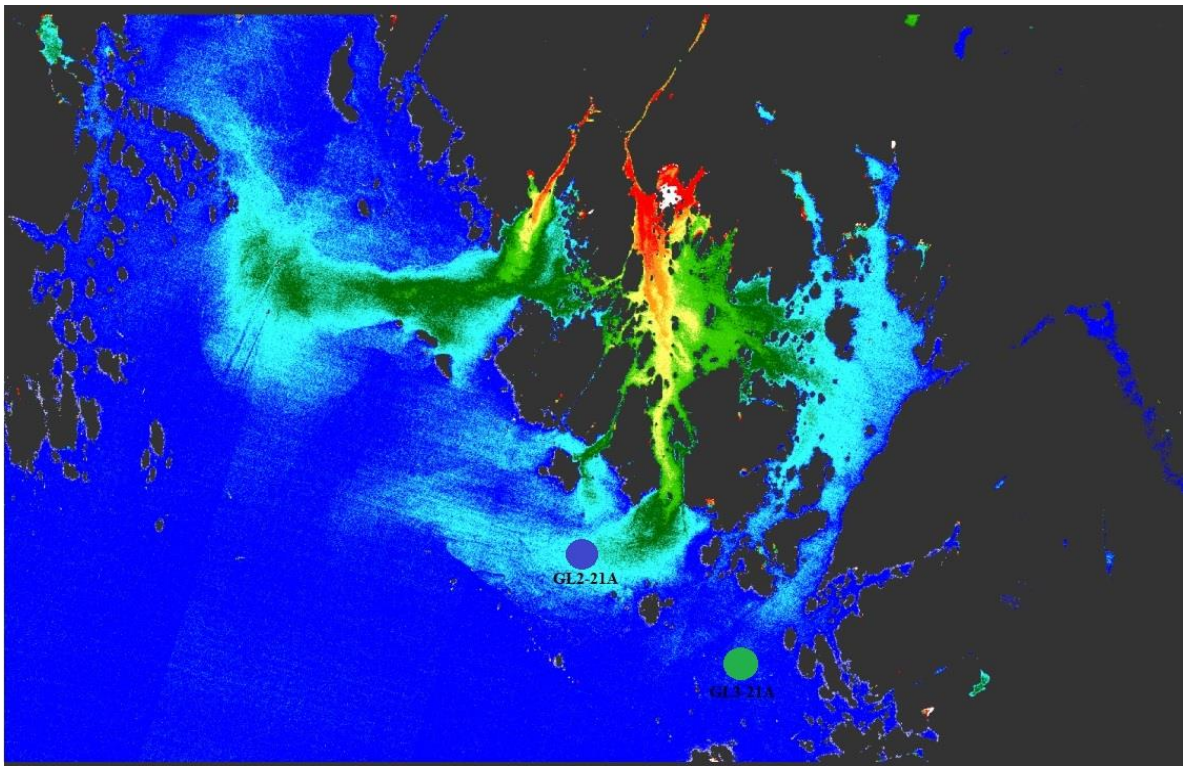

Figure 31*: Relative distribution of particles in surface waters from Glomma River to the Hvaler estuary. The northern station is marked in blue and southern in green. Image is computed from 12. August. 2015 (Modified from Miljødirektoratet et al., 2019). Discharge measured at Solbergfoss was 1100 m^3/s (NVE, 2022a).*

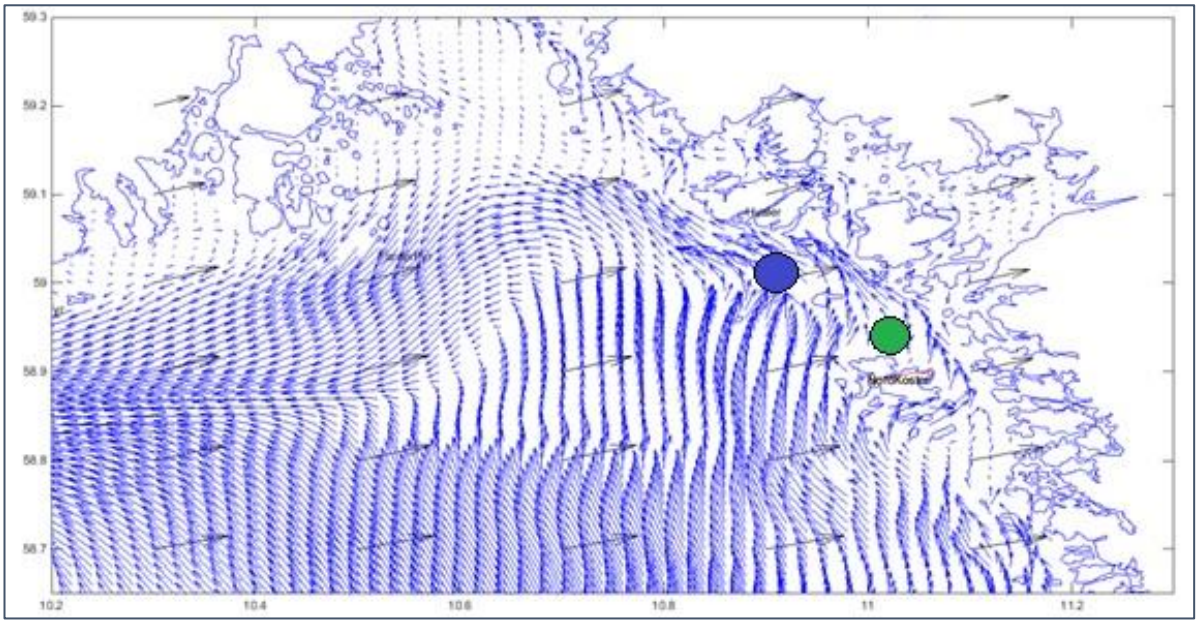

Figure 32*: Surface circulation patterns from 2. January. 2015 in the Hvaler shower a northwestern flow direction (Modified from Ryrfors, 2015). The northern station is marked in blue and southern in green. The northeastern wind direction is marked with black arrows.*

4.2 Heavy metal accumulation rates

The accumulation rates are used to recalculate the concentration profiles to reveal the heavy metal flux to the sediments (Figure 10). The heavy metal accumulation rates are higher at the northern station (GL2) compared to the southern station (GL3). This can indicate that the heavy metals primarily are transported to the northern station by riverine discharge, and less so to the southern station. The highest flux at the northern station is detected around the 1990s, which can be associated with the pollution history of the Hvaler estuary described by Helland et al. (2002) where heavy metal concentrations peaks in the 1980s and reach a minimum in the early 1990s *(Helland et al., 2002*). The reason why the heavy metals concentrations don't reflect the entirety of the pollution history could be explained by the high sediment accumulation at the northern station. High SAR can dilute and obscure the "real" heavy metal concentrations (*Croudace & Cundy, 1995; Costa-Böddeker et al., 2018*). The SAR is on average ~64% higher at the northern station (GL2) than at the southern station (GL3) (Figure 6). Estuarine environments with high SAR are known to show lower than expected heavy metal concentrations (*Costa-Böddeker et al., 2018*), and could explain why the concentrations are lower at the northern (GL2) than at the southern station (GL3).

4.3 Sources and accumulation rates of organic carbon over time

The effects of decomposition and diagenesis

The marine organic matter produced in the photic zone is partially degraded and remineralized as it sinks to the seabed, and it can be laterally transported (*Alcolombri, 2021*). After deposition, it is further degraded in the biologically active zone. Therefore, only a small fraction of the original OM is considered to be stored in the sampled sediment cores (GL2 and GL3). Typically, only a few percent of the original OM become buried and preserved in the sediments of estuarine environments (*Meyers, 1997*). Other studies aiming to determine OM sources, conclude that the C/N-ratio and $\delta^{13}C$ are the most reliable parameters to deduce the origin of OM (*Meyers, 1994*). Thornton and McManus (1994) narrow it down to only using $\delta^{13}C$ in their study. This is because the isotope signature is less affected by biochemical alterations. $\delta^{15}N$-isoptopes on the other hand can be influenced by biochemical alterations through recycling and is therefore by itself not a reliable parameter (*Thornton & McManus, 1994*).

4.4 Determining the sources of organic carbon over time

TOC/TN

The TOC/TN-ratio is used to determine whether the origin of organic material is marine or terrestrial. Organic material originating from marine algae and plants have a lower TOC/TN-ratio than material from terrestrial plants. The ratio for marine algae ranges from 4-10 (*Meyers, 1994; Meyers, 1997; Lamb et al., 2006*), while terrestrial plants have a ratio higher than 12 *(Prahl et al., 1980; Lamb et al., 2006)*. In the present study, the OM seems mainly to be of marine origin as the ratio at the northern station (GL2) range from 6.0 (1974) to ~7.9 (1959), and ~5.4 (2021) to ~7.4 (1997) at the southern (GL3). The TOC/TN-ratio from the northern and southern stations does not indicate a distinct shift of organic matter being more marine or terrestrial in origin (Figure 17). In this study, the TOC/TN-rations are compared to the values of Helland et al. (2002), which depict a TOC/TN-ratio transect from the Glomma River outlet to the Hvaler skerries (*Helland et al., 2002*). The ratios from station 8 (Figure 30) (~4 km north of GL2 and GL3) studied by Helland et al. (2002) have a TOC/TN ratio of ~7.8. Compared to the northern station (GL2), the ratio fits well, but is a bit low (average: 7.03), while the ratio is even lower at the southern station (GL3) (average: 6.98) (Figure 17). The elevated ratios seen at the northern station (GL2) (in 1959 and 1967) could represent flood-layers from increased riverine discharge. The higher ratio observed in 1967 coincides with the elevated discharge detected in 1967 (Figure 3, Figure 17). However, no flood-layer is detected in the grain size analysis during these periods (figure 7A, B, C) which contradicts this presumption.

Stable isotope ratios

Terrestrial and marine plants utilize different sources of carbon during photosynthesis. This difference can be used to distinguish between terrestrial and marine sources of organic carbon deposited in sediments. The terrestrial C3 plants use CO_2 from the atmosphere ($\delta^{13}C \approx -7‰$) and produce organic matter with $\delta^{13}C$ average signature values of -27‰. Lacustrine algae have the same isotopic signature as terrestrial plants, while marine algae have a distinct isotopic signature. They mainly use dissolved bicarbonate ($\delta^{13}C \approx 0‰$) as inorganic carbon source, thus, increasing their produced organic matter average signature values to ~ -20 and -22‰ (*Meyers, 1994; Meyers, 1997*).

Helland et al., (2002) determined the $\delta^{13}C$ from the outer part of the Hvaler skerries (Station 8) (Figure 30). At this station, the $\delta^{13}C$ ranged from -20.5 to -24.8‰. The riverine influence was determined to be of greater magnitude closer to the outlet of Glomma River than at station 8 (*Helland et al., 2002*). The $\delta^{13}C$ ranged from -22.53‰ (2002) to -22.85‰ (1963) at the northern station (GL2) and from -22.61‰ (2016) to -22.69‰ (1936) at the southern (GL3) (Figure 15). Both station's $\delta^{13}C$-signatures are mainly of marine origin. In comparison to station 5 (*Helland et al., 2002*), the northern (GL2) and southern (GL3) stations have a smaller range regarding their $\delta^{13}C$-signatures. The southern station has the smallest range of the two, which agrees with Helland et al. (2002) findings- that the riverine influence diminishes further away from the Glomma River outlet. Both the northern (GL2) and the southern (GL3) stations show a slight trend towards terrestrial $\delta^{13}C$-signatures from the early 1930s to 2021 which could indicate an increase of riverine discharge during this period. This assumption is supported by the increasing SAR at the northern (GL2) and southern (GL3) stations, as it possibly indicates an increase in river runoff. The southern station (GL3) has lower values, compared to the northern (GL2) and has seemingly a stronger affinity to marine origin of its organic carbon sources.

Terrestrial and marine plants use different sources of inorganic nitrogen for photosynthesis. The terrestrial plants use atmospheric N_2, which has $\delta^{15}N$-signature of 0‰, while marine plants use NO_{3-} with $\delta^{15}N$-signature of 7-10‰ (*Meyers, 1997*). Terrestrial plants in coastal areas are determined to have $\delta^{15}N$-signatures of 2‰ (*Thornton & McManus, 1994*). In this thesis, these signatures are used to determine the sources of deposited organic matter in the estuary.

$\delta^{15}N$-signatures presented by Helland et al. (2002) for station 8 results from acid treated samples, while this study used non-acid treated samples, and is therefore not directly comparable. However, the temporal development of $\delta^{15}N$ composition is of use, as the values at station 5 increase from 0.9‰ (late 1800s) to 3.6‰ in recent deposits (Figure 16). Values were higher at station 8 compared to station 5 throughout this period (*Helland et al., 2002,* Figure 30). The elevated signal from the innermost station (station 5) was determined to be caused by increased production of marine algae due to increased amounts of nutrients from riverine discharge. This means that elevated $\delta^{15}N$-signals in lacustrine environments can result from increased terrestrially derived nutrients.

The $\delta^{15}N$-signatures at the northern station are generally higher compared to the southern which corresponds to the evolvement seen from station 5 and 8 in Helland's results (*Helland et al., 2002*). Periods of increasing $\delta^{15}N$ detected in the Hvaler estuary by Helland (2002) is interpreted as algae blooms of *Chrysochromulina polylepsis* and *Prororectum minimum* that happened in 1989-1993 and 1988 respectively. These instances were not detected in this study.

As mentioned, $\delta^{15}N$ values can be affected sediment reworking, recycling, and other biochemical transformations. Thus, it should be applied in conjunction with other parameters such as $\delta^{13}C$ and TOC/TN-ratios to determine the sources of organic matter. The $\delta^{15}N$ values are moderately consistent at the northern (GL2) and southern (GL3) stations up to the mid-2010s where there is a small increase (indirectly more terrestrial values) to the recent (Figure 16). This development is consistent with the $\delta^{13}C$ as these values indicate an increasing terrestrial influence from the early 1930s to 2021.

4.5 Mixing equation

The results from the mixing equation indicate that there has been an increasing supply of terrestrial carbon to the estuary, especially at the northern station (GL2) from the year 2000 to 2021. During these 21 years, the fraction of terrestrial carbon increased by ~ 8 %. At the southern station (GL3) the distinct increase began in 1992 and increased by ~ 8% to 2021 (Figure 18). The fraction is lower at the southern station (GL3) up to the early 2000s. Thereafter, the fractions are more similar to that of the northern station (GL2). The mixing equation is normally just applied to surface sediments collected along a transect from terrestrial, estuarine, and marine areas, where the goal is to determine where the transitional samples belong to in this environmental range (*Thornton & McManus, 1994; Helland et al., 2002*). Both the spatial and the temporal evolution at the northern (GL2) and southern (GL3) stations are considered in this thesis to characterize the change and sources of organic carbon. The higher percentage of terrestrial carbon at northern station (GL2) imply that it has experienced more riverine influence (from the early 1940s to the early 2000s) than the southern station (GL3). The trend is seemingly weakened from the mid-2000 to recent as the fractions are more similar.

The end-members used in this study were selected to represent both extremes of the estuarine environment. The marine end-member selected for TOC/TN and $\delta^{13}C$ was chosen from the deep marine Hvaler basin (Station 9) (Figure 30, *Helland et al., 2002*), while the terrestrial end-member selected for TOC/TN was chosen from an inland location near Sarpsborg (~30 km northeast of the Hvaler skerries). The terrestrial $\delta^{13}C$-values were not given from this location. Values from station 2 (Figure 30) was therefore selected instead as it's the closest to the Glomma River. The reason why terrestrial TOC/TN-ratio used in this study wasn't selected from the same station, (station 2), is due to the undegraded organic matter found in the surface samples which made it unrepresentative for the rest of the core (*Helland et al., 2002*). The results where these end-members are applied (mixing equation and C/N-

ratios) should therefore be viewed with some caution as the end-members are selected from different areas in the Hvaler estuary.

Collectively, these results show an increase of organic material to the estuary, and especially from terrestrial sources. As expected, the northern station (GL2) has seemingly been more influenced by the river discharge and therein nutrient influx to the estuary.

The AR-TIC and AR-TOC_{63} reflects that the northern station (GL2) in particular has experienced increased amounts of organic carbon from the early 1970s to the early 1900s. While having a more modest increasing trend, the southern station (GL3) has the same development (Figure 19). Both $\delta^{13}C$ and the TOC/TN-ratio indicate that the sources of organic carbon predominantly is marine with an increasing terrestrial influence. This development is also supported by the increasing $\delta^{15}N$ values at the northern (GL2), and especially southern station (GL3). The increase of $\delta^{15}N$ can be used as a specific tracer for the effects of exacerbated eutrophication in coastal areas (*Struck et al., 2000*).

4.6 Ecological parameters

4.6.1 The use of foraminifera as environmental proxies

Using foraminifera as an environmental proxy relies on correct species identification. Some challenges are associated with the use of foraminifera; some species are hard to distinguish from one another and taphonomic processes can influence the preservation of the test. For the latter, agglutinated foraminifera can break apart and calcareous species can dissolve. When handling the foraminifera, the sieving process can disintegrate more delicate tests. The organic lining (which adhere the grains in agglutinated test) can degrade due to diagenesis and chemical processes and agglutinated foraminifera can thereby be unidentifiable.

There does not seem to be a prominent process of calcite dissolution at these two locations as many thin-shelled species (*S. fusiformis* and *N. iridea*) are well preserved in the sediment cores. It is therefore valid to determine that the calcite dissolution process haven't led to the increasing percent of agglutinated species. Only minor abraded surfaces and some broken protrusions of the tests were detected. This could either have occurred during the sieving process or by diagenesis. The analyzed benthic foraminifera abundance is therefore regarded as representative and valid in this study.

4.6.2 Foraminifera influenced by heavy metal pollution

The foraminiferal abundances are quite stable from 1944 to 1995 at the northern station (GL2) and from the early 1930s to the early 2000s at the southern station (GL3). Figures 8 and 9 show an overall increasing trend of heavy metal concentrations up to the early 1960s at the northern (GL2) and southern (GL3) stations. The up-core increasing concentrations are still in the high to good status classes. After the early-to mid-1960s/1970s, the heavy metal concentrations are decreasing to the recent. The foraminiferal assemblages do not show any correlation to this fluctuation, and thus the temporal changes in foraminiferal assemblages are most likely not caused by the development of the heavy metal concentration. The changes are most likely a reflection of the spatial and hydrological difference between the two stations and not the development of heavy metal concentrations.

4.6.3 Ecological changes

The trends of relative abundance of the selected species are similar to the patterns described by Polovodova Asteman et al., 2021 in the Kosterfjord (~35 km north of the surveyed stations, Figure 33). Their study reports on an environmental change occurring between 1988 and 2012 in their sediment core (KSK-12-01C/D). Polovodova et al., (2021) calculated foram-AMBI and NQI_f showed a distinct shift around 2002 (Figure 34), while the EcoQS were constantly in the high status class. Calcareous species dominated from 1988 to 2007, until the benthic foraminifera showed a drastic faunal change reflected in a distinct increase of agglutinated species (mainly *Textularia earlandi*) from 2007 to 2012 in the Kosterfjord. The period between 2007-2012 is determined by Polovodova Asteman et al., (2021) to represent the changes of environmental conditions in the area. A high freshwater influence has previously been suggested to result in the increased abundance of agglutinated foraminifera (*Polovodova Asteman et al., 2017*). It is suspected that these faunal changes happened due to the increased riverine discharge, trawling activity, decreased salinity in the surface water, and increased transport of particulate organic matter to the coastal area. This in turn is linked to the darkening of the Skagerrak coastal waters. The increased riverine/freshwater influence detected between 2007-2012 in Polovodova et al., (2021) results can be recognized in $\delta^{13}C$ and TIC and TOC-AR-results from the stations in Hvaler estuary (Figure 15, Figure 19), but not in the C/N nor $\delta^{15}N$ results.

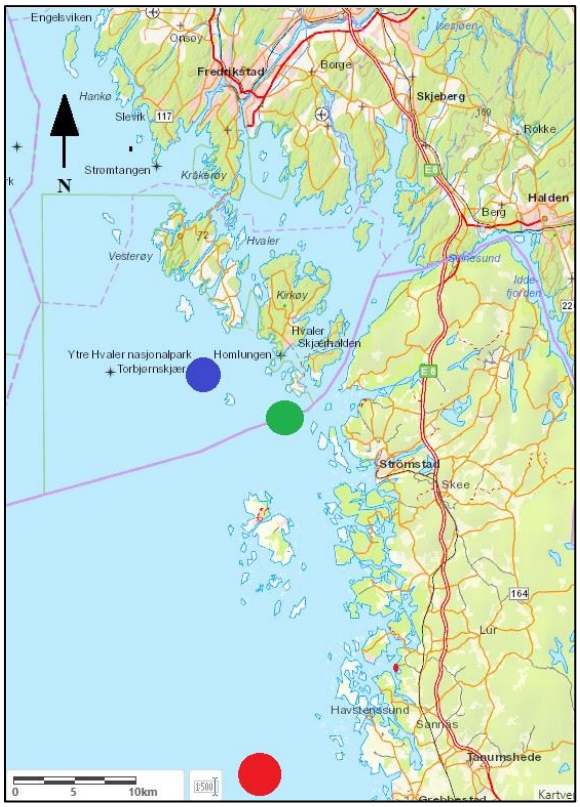

Figure 33: *Red dot shows the location of the analyzed core (KSK-12-01C/D) from the Kosterfjord (approx. 15 km south of the surveyed stations). Blue dot shows location of the northern (GL2) station and southern (GL3) in blue (Modified from NVE, 2022c).*

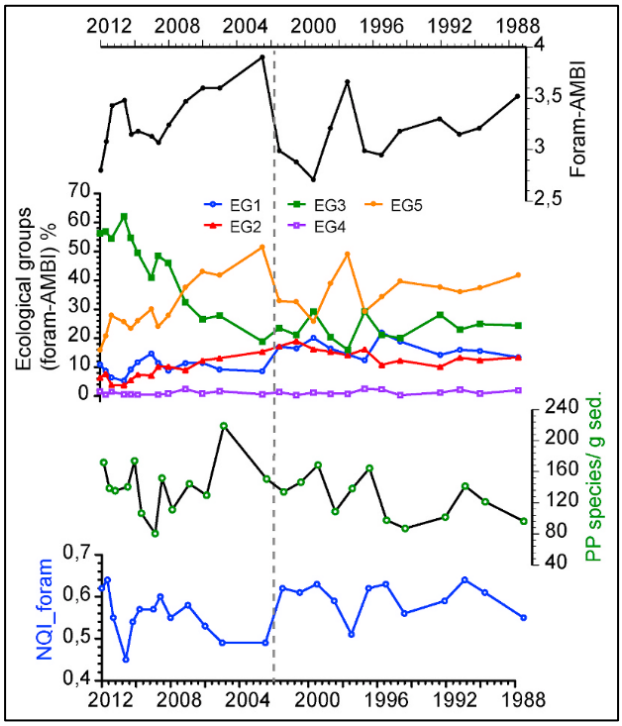

***Figure 34**: Foram-AMBI (top), distribution of ecological groups (EG) 1–5, distribution of primary production (PP) species & NQI_f results (bottom) (Polovodova et al., 2021).*

The calcareous species in the northern (GL2) and southern (GL3) cores makes up ~89% of the total abundance from the earliest recorded deposits to the late 1990s/early-2000s (Figure 24). A distinct change occurs in the late 2000s as the abundance of agglutinated species increase up to ~50% in recent sediments**.** This distinct shift begins to occur about the early 2000s in the Hvaler estuary. Both the northern (GL2) and southern (GL3) stations show an increase of the agglutinated species (*T. earlandi, E. medius, L. goesi*), especially in the younger part of the cores (early-2000s to 2021). This is also illustrated by the increasing BFAR shown in Figure 25. *Textularia earlandi* is the dominating species in the most recent deposits at the southern station (GL3) (15%, 2020-2021), while another agglutinated species, *Liebusella goesi*, dominates with ~23% in the surface sediments of the northern station (GL2).

The results from the northern station (GL2) show that *L. goesi* increase simultaneously as *T. earlandi* decreases in ~2018. *T. earlandi* is a known opportunistic species able to withstand high organic enrichment of the sediments (*Alve et al., 2016*). It is therefore classified to EG III, while *L. goesi* is in EG II (less tolerant to organic enrichment). The change from *T. earlandi* to *L. goesi* dominance in more recent sediments at the northern station (GL2) is, however, likely not a representation of decreasing organic enrichment in the estuary. Overall, EG III species show an increasing trend from 2018 to the recent (Figure 27), and NQI_f -values decrease (Figure 29C) which implies that the organic enrichment continues to increase during this period. Additionally, the TOC_{63}-AR -results indicate stable values from 2018 to the surface (Figure 19, Figure 35). Altogether, this implies a continuation, and not a decrease,

of riverine influence and transport of terrestrially derived matter to the Hvaler estuary from the mid-to late-2010s to the present.

The up-core decrease of species assigned to EG I (*H. balthica, C. lobatulus)* does follow the increasing TOC_{63}-AR up-core as they are sensitive to organic matter enrichment. Polovodova et al., 2021 reported that *S. fusiformis (*EG V) dominated between 2007-2012, which matches the development from the northern station (GL2) where it makes up 22% of the relative abundance (2011). This evolution is also detected at the southern station (GL3), but to a lesser extent (~8%), which could be explained by the lower TOC_{63}-results from the southern station (GL3) (Figure 19).

The northern (GL2) and southern core (GL3) are dominated by EG III (Figure 27, Figure 28). As previously mentioned, the EG III -species are tolerant to organic enrichment. EG5-species at the northern station (GL2) have a distinct increase from 1995-2011 which goes on the expense of EG III -species during this period. This is primarily caused by the increase of *S. fusiformis* during this period. Post 2011, EG III increases and EG V decreases consequently. This is also detected in the foram-AMBI calculations (Figure 26), which shows a general decline from the early-2010s to the late 2010s. The TOC_{63}-AR-results does not mirror the evolvement of EG V as the rate is constant while EG V decreases from the early-2010s (Figure 19, Figure 35).

Trawling of the seafloor is another factor which can be considered, especially regarding the effects of resuspended material on benthic foraminifera. It is suggested that trawling releases nutrients and organic material on which foraminifera can feed on (*Polovodova Asteman et al., 2021*). If there is too much enrichment of organic carbon, then a decline in concentration of total foraminifera could be expected. This is however not the case for the northern station (GL2) in the Hvaler estuary, whereas the concentrations increase up-core from ~250-650 (test/g >63µm). The southern station (GL3) does however show a decline from ~450-370 (test/g >63µm) between the early 1930s to the recent with a fluctuating pattern (Appendix: J). Polovodova Asteman et al., (2021) reports that concentrations in foraminiferal test increased after trawling activity was limited to waters bellow 60 m water depth in the Kosterfjord (2009). Unfortunately, confirming this relationship is not possible from the northern (GL2) or southern (GL3) core-results as the same injunction already was implemented in the Hvaler estuary in 1929 (*Dahl & Grimsrud, 2021*). According to Spezzaferri et al., 2013 trawling can negatively affect the species which are associated with coral reef habitats. *H. balthica*, is known to live in coral reefs, and is a pronounced species in both the northern (GL2) and southern (GL3) cores. This species shows a decrease up-core, which possibly can be because of the destruction from bottom trawling of the coral reefs in the Hvaler estuary (*Thorsnæs & Pharo, 2022*). However, there has not been documented an

increased in bottom trawling from the early 1930s/1940s in the Hvaler estuary (*Fiskeridirektoratet, pers. comm., May 2022).*

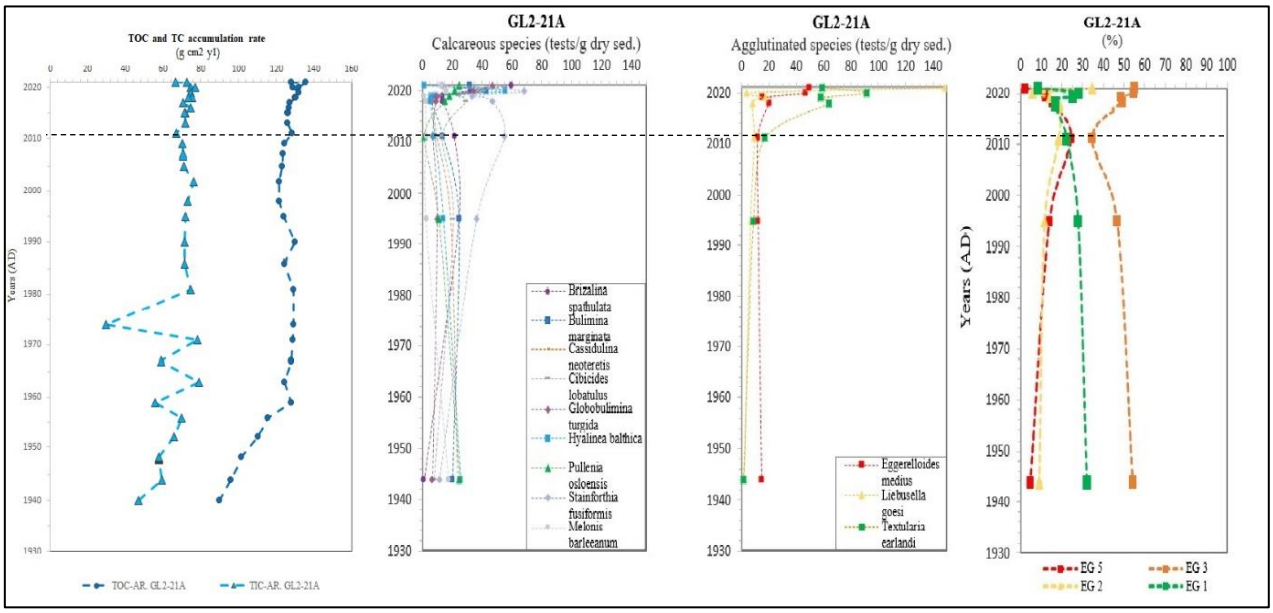

Figure 35: *TOC and TIC-AR (left) compared to the development of absolute abundance of benthic foraminifera (middle) and ecological groups (left) at the northern (GL2) station. The black horizontal dotted line indicates a distinct change occurring in the foraminiferal abundance and distribution of the ecological groups in the early 2010s as the TOC/TIC-AR peaks.*

In conclusion, the benthic foraminifera indicate a shift in the early-to mid-2000s. The timing of the changes coincides with reported activities in the coastal Skagerrak and increased outflow from the Balthica sea between 1998 and 2000 (*Frigstad et al., 2013*). The increased absolute and relative abundance of agglutinated foraminifera (*T. earlandi, E. medius, L. goesi*) in coastal settings further seem to support this increased freshwater influence due to high runoff from land over time. This can altogether be linked to the increasing darkening of the Hvaler estuary from the early-to-mid-2000s. The northern foraminiferal communities are seemingly more affected by this phenomenon that the southern station (GL3).

4.7 Implications and evidence of coastal darkening

The darkening phenomenon in the outer Oslofjord is predominantly linked to the riverine influx of DOM (Frigstad et al., 2020a). There has been detected a generally large transport of organic material in the draining rivers to the Hvaler estuary. This is associated with high density of forests (conifer trees) and peatlands in the river's catchment areas (*Frigstad et al., 2020a*). Additionally, the coastal surface waters are naturally enriched with high DOC (dissolved organic carbon) due to the inflowing Baltic current (*Seidel et al., 2017*), and the southern North Sea (*Painter et al., 2018*).

As mentioned in the introduction, the current circulations in the Hvaler estuary are complex with an extensive exchange of water masses flowing in from the Atlantic Ocean, North Sea and Baltic Sea that mix with the riverine discharge from local sources (*Christensen et al., 2018; Albretsen et al., 2012,* Figure 2). The darkening of Norwegian coastal waters has been interpreted as a response to long-term decrease in salinity in the NCC (Norwegian coastal current) due to increased riverine discharge and precipitation (*Aksnes et al., 2009*). Measured salinity in the surface waters at the northern (GL2) and southern (GL3) stations (Figure 36) reflect an attenuating salinity concentration from the proximal (GL2) to distal (GL3) part of the estuary in the shallowest 30 m. This is expected as the station located closer to the Glomma River (GL2) is more influenced by riverine freshwater (*Frigstad et al, 2020a*). However, it was raining on the day of sediment sampling which might have influenced the measured salinity concentrations and made these results less representative. Nevertheless, the northern station (GL2) has seemingly experienced higher influence from riverine discharge, and consequently coastal darkening, as evidenced by the generally higher TOC/TIC-AR, heavy metal-AR, and its stronger affinity to terrestrially derived organic material (indicated by $\delta^{13}C$, $\delta^{15}N$, and the mixing equation).

Freshwater draining from riverine sources attenuates the light more than oceanic saline waters. As such the Secchi depth is shallower in coastal waters with higher riverine discharge (*Jerlov, 1968*). Secchi depth is the measured depth of which a Secchi disc no longer is visible to the human eye as its lowered down from the water surface. This trend reflects a negative correlation between light attenuation and salinity, which makes salinity in coastal waters a proxy for darkening (*Frigstad et al., 2020b*). Secchi depth measurements have been collected from the North Sea (therein Skagerrak) from 1903-1998 (*Dupont & Aksnes, 2013*). Altogether, the Secchi depth had decreased down in the coastal waters by 3.6 ± 0.25 (-36%) for the shallower areas in the North Sea during this period. After the 1970s, the Secchi depth had elevated in the coastal waters, but not to the same water-levels as before (*Frigstad et al., 2020b*). The sediment accumulation rate (SAR) at the northern station (GL2) has risen by ~80% from the early 1970s (0.3 g cm^{-2} y^{-1}) to the mid-1990s (0.54 g cm^{-2} y^{-1}) (Figure 6), while AR-TOC_{63} and AR-TIC increase by ~5% and ~20% respectively during this period (Figure 19). These rates from the southern station (GL3) are also increasing, but the increasing trend is more consistent throughout the entire core (early 1930s to 2021). The increasing AR-rates (sediment, TOC_{63} and TIC) does reflect an increase of riverine discharge, (therein an increase of particles in the coastal waters)

which could contribute to the darkening phenomenon in the Hvaler estuary. However, these results do not indicate there being a smaller influx of particles from the 1970s as Frigstad et al. (2013) suggested. This could be because of the spatial difference between the cores surveyed in this study and the stations studied by Frigstad et al. (2013), in the general Skagerrak coastal area.

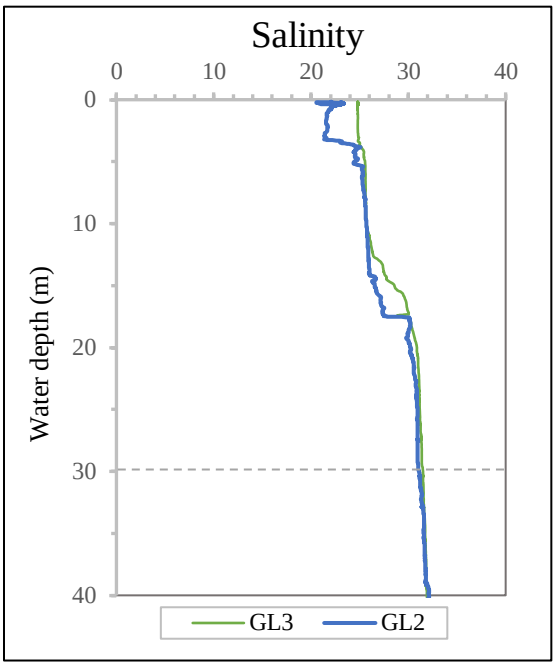

Figure 36*: Salinity result from the northern (GL2) and southern (GL3) station (16.08.2022). The horizontal grey dotted line shows elevated values at the southern (GL3) station.*

Frigstad et al. (2013) studied a 20-year series (1991-2010) of long-term increasing POM (particulate organic matter) in the Skagerrak coastal waters (upper 0-30 m). POM is the organic fraction which retains when seawater is sieved through a filter with pore size ranging from 0.22-0.7µm (*Frigstad et al., 2020b*). In their study, Frigstad et al., (2013) link flocculation to a sharp increase of suspended POM and dissolved nitrogen concentrations detected between 1998-2000. Flocculation ("*a process where dissolved matter aggregates and forms larger particles in an estuarine environment*" (*Frigstad et al., 2020b*) is believed to exacerbate and enhance the concentrations of POM in the coastal waters and add on to the darkening of the Skagerrak coastal waters (*Frigstad et al., 2013*). This phenomenon happens for the most part in coastal areas, such as estuaries, where fresh and saline waters mix (*Asmala et al., 2013*). The distinct increase of suspended POM and dissolved nitrogen (1998-2000), occurs simultaneously as depopulation of sugar kelp and carnivorous fish is detected in the area (*Frigstad et al. 2013*). This event indicates a regime shift of increased riverine discharge taking place in the early 2000s in the Skagerrak coastal waters (*Frigstad et al., 2021b*). This shift is less pronounced but also reflected in the benthic fauna analyzed in the Hvaler estuary (GL2, GL3) were agglutinated foraminifera show a distinct increasing trend from the early 2000s (Figure 20, Figure 21). An increase in nitrogen and DOM (dissolved organic matter) concentrations during the same period as Frigstad et al., (2021)

where detected in Skagerrak coastal waters (Staalstrøm et al., 2021), further implying an increased darkening of coastal waters.

The increase of DOM and POM in the Skagerrak coastal waters (*Frigstad et al., 2021b; Staalstrøm et al., 2022*) can also be a response to the increasing air temperature in Norway from the early 1990s to the recent (Figure 37). Increased air temperatures can lead to longer growth seasons for terrestrial plants and consequently increase the influx of DOM to coastal areas (*Ritson et al., 2013*). The period from the early 1990s to the recent show higher air temperatures than normal (Figure 37), which fits with the regime shift of higher influence from riverine discharge in the Hvaler estuary.

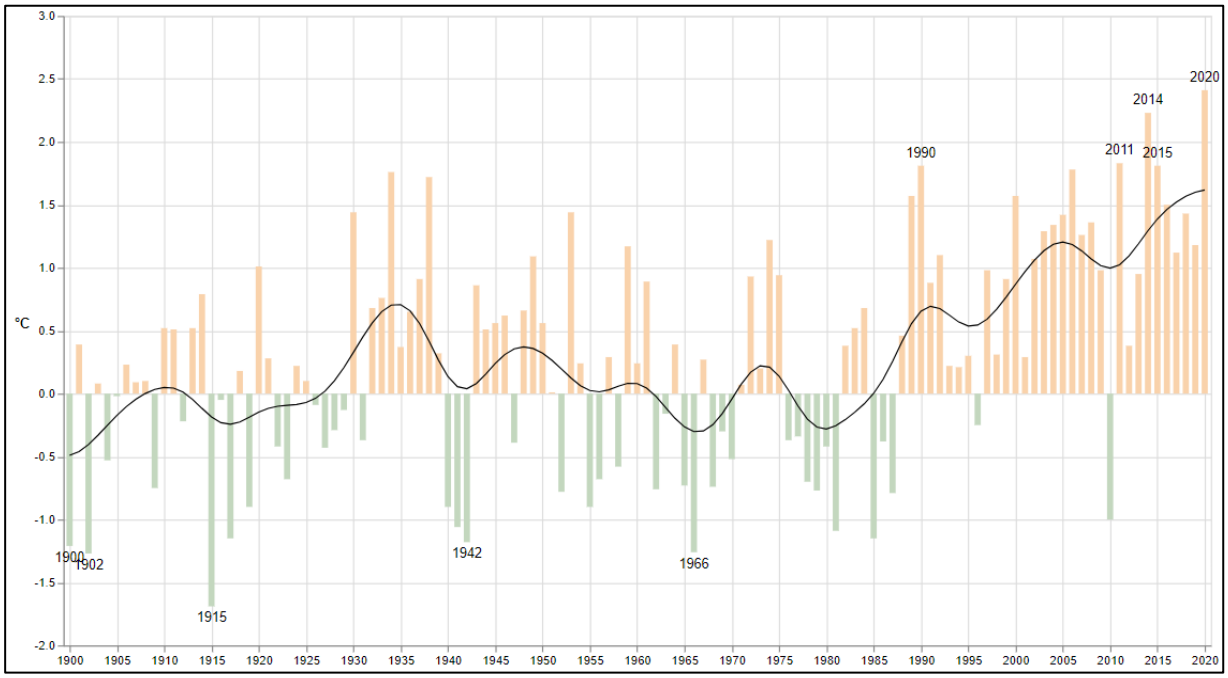

Figure 37*: Annual air temperature deviations from the stable trend between 1961-1990 in Norway. The graph represents the time from 1900-2020 (Meteorologisk institutt, 2021)*

The development of POM in the Hvaler estuary was not specifically analyzed in this thesis, but is partially reflected by the TOC-concentrations and accumulation rate at the northern (GL2) and southern (GL3) stations. Looking at these parameters, the TOC-concentrations (Figure 13) do not show a significant increase from the early 2000s, but the TOC-AR (Figure 19) show an increasing trend during the past 20 years.

The hydrogeographical measurements and geochemical results attained in this thesis show an increased influence of riverine discharge from the early 1930s/1940s to the present. Consequently, higher amounts of organic and inorganic material have been transported out to the Hvaler estuary and exacerbated the darkening of the Skagerrak coastal waters, and Hvaler estuary therein. Several events, such as bottom trawling, floods and costal erosion may also contribute to the amount of total suspended material (TSM) in the Hvaler estuary (*Capuzzo et al., 2015*). Two locations in the Hvaler estuary have been used as dumping sites in the area (Jylterenna and Angroetrenna) and bottom trawling has been performed at the

surveyed stations (Figure 38). This could have led to an increase of TSM at the two stations as particles further are distributed by the coastal currents. The bottom trawling activity in the Hvaler area has however been present since 1897 to the recent (*Hedberg, 2021*), which makes it difficult to determine the impact of this activity.

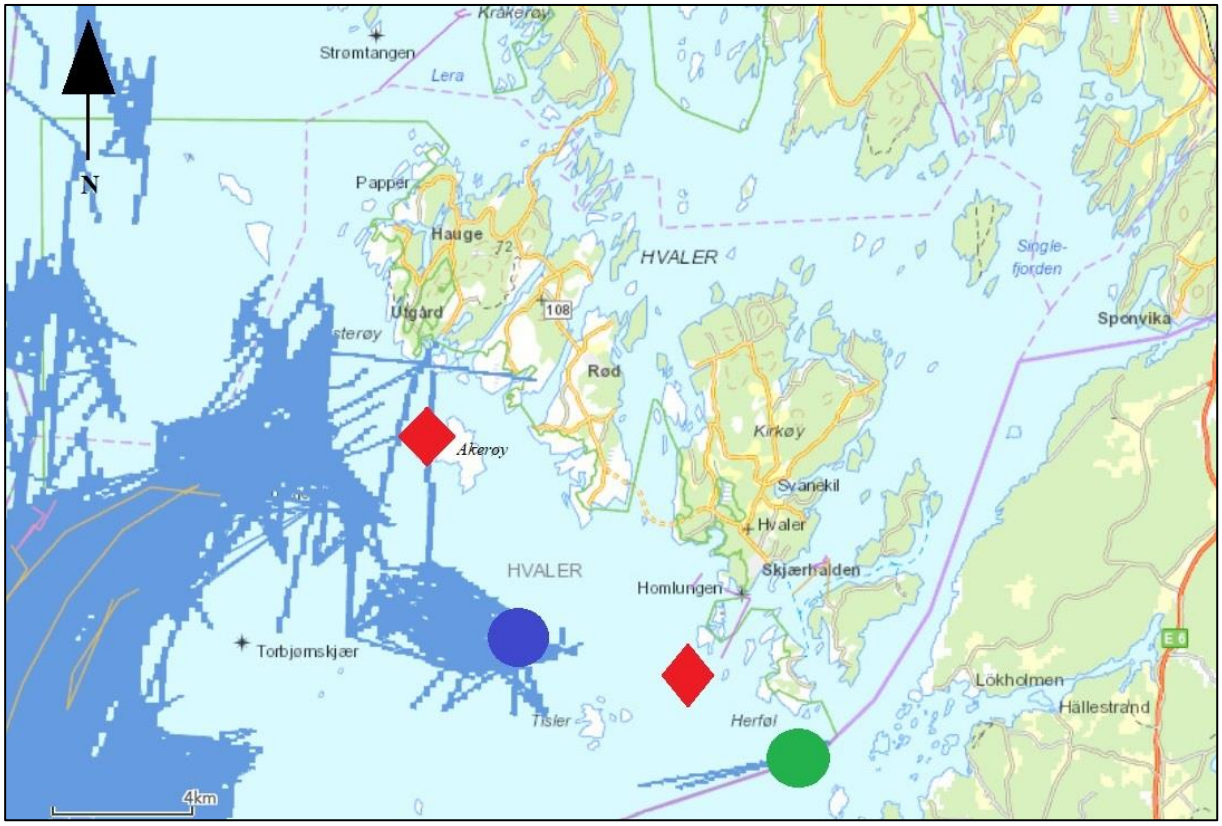

Figure 38: *Red diamonds represents the two dumping sites; Jylterenna (west for Akerøy) and Angroetrenna (west for Herføl). Blue dot represents the northern station (GL2), and the green dot represents the southern station (GL3). Dark blue lines show bottom trawling from the area from 2011 to the present (modified from fiskeridirektoratet, 2022).*

4.8 Reference conditions

The time series documented in the northern (GL2) and southern (GL3) sediment cores, (early 1930s to the recent), might not be old enough to represent reference conditions in the Hvaler estuary. This assessment is determined by the temporal development of the geochemical and biological results attained in this thesis and the accompanying documented pollution history in the area. Most parameters show a changing temporal evolution from the early 1930s to the present, which in this thesis has been linked to the increase of riverine discharge and influx of terrestrial detritus from agricultural practices, industrial activities, and sewage emissions. However, the rising terrestrial organic matter input to the estuary might also be response to climate changes (increased precipitation and flood events) during the last century, and therefore show a natural development in the Hvaler coastal area.

6 Conclusion

- The previously recorded pollution history in the Hvaler estuary is reflected in the sediment cores from the northern (GL2) and southern (GL3) stations. Both stations show a decrease in heavy metal concentrations from the early 1960s to the present. This coincides with the initiation of the industrial reform in the Hvaler area vicinity. The high SAR is believed to dilute the concentrations at the northern station (GL2) and explain why the measured concentrations are higher at the southern station (GL3). Regulations and restrictions to decrease the industrial waste from the Glomma River in the early 1990s has seemingly contributed to a decrease in the heavy metal influx to the northern station (GL2). These measures are not detected at the southern station (GL3) as it is less influenced by the riverine discharge. All values from the two locations were in the "high" to "good" environmental status classes.

- Collectively, the result from the isotope-analysis and the mixing equation show that the source of organic carbon predominantly is marine with an increasing terrestrial influence. Of the two stations analyzed, the northern station (GL2) has seemingly been more influenced by riverine discharge, and therein a nutrient influx, from the early 1940s to the present. The TOC-concentrations in the area are in the "high" to "good" environmental status classes

- The benthic foraminifera assemblage shows a shift in the early-to mid-2000s as the abundance of agglutinated foraminifera increase towards 2021. The increased abundance of agglutinated foraminifera and species tolerant to organic enrichment are associated to the increasing TOC-AR and nutrient influx to the Hvaler estuary during this period.

- The increased riverine discharge from the early 1930s to the recent has transported higher amounts of organic and inorganic particles to the Hvaler estuary and exacerbated the darkening of the Hvaler estuary. This is linked to the increased riverine discharge and temperatures in the estuarial area which are promoted by climate changes during the last century. The geochemical results indicate that the darkening phenomenon continues to increase in the coastal waters. Bottom trawling and dumping are also believed to increase the amount of suspended material in the estuary.

7 References

Aasgaard, S. M. (2020). *Ecological implications of changing sources and accumulation rates of organic carbon during the last 300 years in Hvaler, ytre Oslofjorden*. https://www.duo.uio.no/handle/10852/79600

Akershus energi. (2022). *Oversikt over kraftverk*. Akershus Energi. https://akershusenergi.no/om-akershus-vannkraft/oversikt-kraftverk/

Aksnes, D., Dupont, N., Staby, A., Fiksen, Ø., Kaartvedt, S., & Aure, J. (2009). Coastal water darkening and implications for mesopelagic regime shifts in Norwegian fjords. *Marine Ecology Progress Series*, *387*, 39–49. https://doi.org/10.3354/meps08120

Albretsen, J., Aure, J., Sætre, R., & Danielssen, D. S. (2012). Climatic variability in the Skagerrak and coastal waters of Norway. *ICES Journal of Marine Science*, *69*(5), 758–763. https://doi.org/10.1093/icesjms/fsr187

Alve, E. (1995). Benthic foraminiferal responses to estuarine pollution; a review. *The Journal of Foraminiferal Research*, *25*(3), 190–203. https://doi.org/10.2113/gsjfr.25.3.190

Alve, E., Hess, S., Bouchet, V. M. P., Dolven, J. K., & Rygg, B. (2019). Intercalibration of benthic foraminiferal and macrofaunal biotic indices: An example from the Norwegian Skagerrak coast (NE North Sea). *Ecological Indicators*, *96*, 107–115. https://doi.org/10.1016/j.ecolind.2018.08.037

Alve, E., Korsun, S., Schönfeld, J., Dijkstra, N., Golikova, E., Hess, S., Husum, K., & Panieri, G. (2016). Foram-AMBI: A sensitivity index based on benthic foraminiferal faunas from North-East Atlantic and Arctic fjords, continental shelves and slopes. *Marine Micropaleontology*, *122*, 1–12. https://doi.org/10.1016/j.marmicro.2015.11.001

Anno Norsk skogmuseum. (2020). *Fabrikkanlegget ved treforedlingsbedriften Saugbrugsforeningen i Halden.* https://digitaltmuseum.no/021016588189/fabrikkanlegget-ved-treforedlingsbedriften-saugbrugsforeningen-i-halden

Anon. (1993). *General circulation in Skagerrak and Kattegat.* ResearchGate. https://www.researchgate.net/figure/General-circulation-in-Skagerrak-and-Kattegat-Anon-1993_fig6_282732889

Arias-Ortiz, A., Masqué, P., Garcia-Orellana, J., Serrano, O., Mazarrasa, I., Marbà, N., Lovelock, C. E., Lavery, P. S., & Duarte, C. M. (2018). Reviews and syntheses: 210Pb-derived sediment and carbon accumulation rates in vegetated coastal ecosystems – setting the record straight. *Biogeosciences*, *15*(22), 6791–6818. https://doi.org/10.5194/bg-15-6791-2018

Arnesen, V. (2001). The Pollution and Protection of the Inner Oslofjord: Redefining the Goals of Wastewater Treatment Policy in the 20th Century. *Ambio*, *30*, 282–286. https://doi.org/10.1639/0044-7447(2001)030[0282:TPAPOT]2.0.CO;2

Arp, H. P. H., Villers, F., Lepland, A., Kalaitzidis, S., Christanis, K., Oen, A. M. P., Breedveld, G. D., & Cornelissen, G. (2011). Influence of historical industrial epochs on pore water and partitioning profiles of polycyclic aromatic hydrocarbons and polychlorinated biphenyls in Oslo Harbor, Norway, sediment cores. *Environmental Toxicology and Chemistry*, *30*(4), 843–851. https://doi.org/10.1002/etc.466

Asmala, E., Autio, R., Kaartokallio, H., Pitkänen, L., Stedmon, C., & Thomas, D. (2013). Bioavailability of riverine dissolved organic matter in three Baltic Sea estuaries and the effect of catchment land-use. *Biogeosciences Discussions*, *10*, 9819–9865. https://doi.org/10.5194/bgd-10-9819-2013

Berge, J., Brevik, E., Godal, A., & Berglind, L. (1996). Overvåking av Hvaler—Singlefjorden og munningen av Iddefjorden 1990—1994. Miljøgifter i organismer. (Monitoring of the Hvaler-

Singlefjord and the outer part of the Iddefjord 1990-1994. Contaminants in organisms). I *146*. Norsk institutt for vannforskning. https://niva.brage.unit.no/niva-xmlui/handle/11250/208793

Blain, C. O., Hansen, S. C., & Shears, N. T. (2021). Coastal darkening substantially limits the contribution of kelp to coastal carbon cycles. *Global Change Biology*, *27*(21), 5547–5563. https://doi.org/10.1111/gcb.15837

Bokn, T. L., Moy, F. E., & Walday, M. (1996). Improvement of the shallow water communities following reductions of industrial outlets and sewage discharge in the Hvaler estuary, Norway. *Hydrobiologia*, *326*(1), 297–304. https://doi.org/10.1007/BF00047822

Bouchet, V. M. P., Alve, E., Rygg, B., & Telford, R. J. (2012). Benthic foraminifera provide a promising tool for ecological quality assessment of marine waters. *Ecological Indicators*, *23*, 66–75. https://doi.org/10.1016/j.ecolind.2012.03.011

Brekke, S. (2021). Kronos Titan. I *Store norske leksikon*. http://snl.no/Kronos_Titan

Bækkelund, B. (2021). Tømmerfløting. I *Store norske leksikon*. http://snl.no/t%C3%B8mmerfl%C3%B8ting

Capuzzo, E., Stephens, D., Silva, T., Barry, J., & Forster, R. M. (2015). *Decrease in water clarity of the southern and central North Sea during the 20th century—Capuzzo—2015—Global Change Biology—Wiley Online Library*. https://onlinelibrary.wiley.com/doi/full/10.1111/gcb.12854

Christensen, K. H., Sperrevik, A. K., & Broström, G. (2018). On the Variability in the Onset of the Norwegian Coastal Current. *Journal of Physical Oceanography*, *48*(3), 723–738. https://doi.org/10.1175/JPO-D-17-0117.1

Clarke, K., & Gorley, R. N. (2006). Primer v6: User Manual/Tutorial. I *PRIMER-E*.

Costa-Böddeker, S., Thuyên, L. X., Hoelzmann, P., de Stigter, H. C., van Gaever, P., Huy, H. Đ., & Schwalb, A. (2018). The hidden threat of heavy metal pollution in high sedimentation and highly dynamic environment: Assessment of metal accumulation rates in the Thi Vai Estuary, Southern Vietnam. *Environmental Pollution*, *242*, 348–356. https://doi.org/10.1016/j.envpol.2018.05.096

Croudace, I. W., & Cundy, A. B. (1995). *Heavy Metal and Hydrocarbon Pollution in Recent Sediments from Southampton Water, Southern England: A Geochemical and Isotopic Study | Environmental Science & Technology*. https://pubs.acs.org/doi/10.1021/es00005a021

Dahl, E., & Naustvoll, L. (2018). *Utredning av prioriterte områder for tiltak mot stillehavsøsters i Vestfold*. Havforskningsinstituttet. https://www.hi.no/hi/nettrapporter/rapport-fra-havforskningen/2018/22-2018_rapport_fra_havforskningen

Dahl, N. J., & Grimsrud, E. (2021, mars 26). *Feil om reketråling i Oslofjorden*. https://www.budstikka.no/article/633376!/

De Wit, H. A., Valinia, S., Weyhenmeyer, G. A., Futter, M. N., Kortelainen, P., Austnes, K., Hessen, D. O., Räike, A., Laudon, H., & Vuorenmaa, J. (2016). Current browning of surface waters will be further promoted by wetter climate. *Environmental Science & Technology Letters*, *3*(12), 430–435. https://doi.org/10.1021/acs.estlett.6b00396

Deininger, A., Faithfull, C. L., Lange, K., Bayer, T., Vidussi, F., & Liess, A. (2016). Simulated terrestrial runoff triggered a phytoplankton succession and changed seston stoichiometry in coastal lagoon mesocosms. *Marine Environmental Research*, *119*, 40–50. https://doi.org/10.1016/j.marenvres.2016.05.001

Deininger, A., & Frigstad, H. (2019). Reevaluating the Role of Organic Matter Sources for Coastal Eutrophication, Oligotrophication, and Ecosystem Health. *Frontiers in Marine Science*, *6*. https://doi.org/10.3389/fmars.2019.00210

Diaz, R., & Rosenberg, R. (1995). Marine benthic hypoxia: A review of its ecological effects and the behavioural response of benthic macrofauna. *Oceanography and marine biology. An annual review [Oceanogr. Mar. Biol. Annu. Rev.]*, *33*, 245–303.

Dolven, J. K., Alve, E., Rygg, B., & Magnusson, J. (2013). Defining past ecological status and in situ reference conditions using benthic foraminifera: A case study from the Oslofjord, Norway. *Ecological Indicators*, *29*, 219–233. https://doi.org/10.1016/j.ecolind.2012.12.031

Dupont, N., & Aksnes, D. L. (2013). *Centennial changes in water clarity of the Baltic Sea and the North Sea | Elsevier Enhanced Reader*. https://doi.org/10.1016/j.ecss.2013.08.010

Einsele, G. (1992). Sedimentation Rates and Organic Matter in Various Depositional Environments. I G. Einsele (Red.), *Sedimentary Basins: Evolution, Facies, and Sediment Budget* (s. 385–408). Springer. https://doi.org/10.1007/978-3-642-77055-5_10

Engesmo, A., Staalstrøm, A., Gran-Stadniczeñko, S., Borgersen, G., Beylich, B., Kaste, Ø., & Walday, M. G. (2021). Overvåking av Ytre Oslofjord 2019-2023—Årsrapport 2020. I *58*. Norsk institutt for vannforskning. https://niva.brage.unit.no/niva-xmlui/handle/11250/2837864

European Environmental Agency. (2021). *Ecological status of surface waters in Europe*. https://www.eea.europa.eu/ims/ecological-status-of-surface-waters

Faugli, P. E. (2022). *Elektrisitetens forvaltningshistorie 1877-1921* (Norges vassdrags- og energidirektora Nr. 12/2020; s. 292).

Fiskeridirektoratet. (2022). *Fiskeri*. Directorate of fisheries. https://portal.fiskeridir.no/portal/apps/webappviewer/index.html?id=ea6c536f760548fe9f56e6edcc4825d8&extent=204865.3155%2C6513760.717%2C419241.7443%2C6606047.5683%2C25833

Fosseng. (2000). *TUNE HISTORIELAG | Greåker—Som jeg husker det*. TUNE HISTORIELAG. https://www.tunehistorielag.com/artikler/bygda-var/greaker-som-jeg-husker-det/

Frigstad, H., Andersen, G. S., Trannum, H. C., Naustvoll, L. J., Kaste, Ø., & Hjermann, D. Ø. (2018). *Synthesis of climate relevant results from selected monitoring programs in the coastal zone. Part 2: Quantitative analyses*. https://niva.brage.unit.no/niva-xmlui/handle/11250/2595792

Frigstad, H., Andersen, T., Hessen, D. O., Jeansson, E., Skogen, M., Naustvoll, L.-J., Miles, M. W., Johannessen, T., & Bellerby, R. G. J. (2013). Long-term trends in carbon, nutrients and stoichiometry in Norwegian coastal waters: Evidence of a regime shift. *Progress in Oceanography*, *111*, 113–124. https://doi.org/10.1016/j.pocean.2013.01.006

Frigstad, H., Kaste, Ø., Deininger, A., Kvalsund, K., Christensen, G., Bellerby, R. G. J., Sørensen, K., Norli, M., & King, A. L. (2020a). Influence of Riverine Input on Norwegian Coastal Systems. *Frontiers in Marine Science*, *7*. https://doi.org/10.3389/fmars.2020.00332

Frigstad, H., Harvey, T., Deininger, A., & Rose, A. (2020b). *Increased light attenuation in Norwegian coastal waters—A literature review* (Nr. 200200; s. 58).

Gade, H. G. (1968). Horizontal and vertical exchanges and diffusion in the water masses of the oslo fjord. *Helgoländer Wissenschaftliche Meeresuntersuchungen*, *17*(1), 462–475. https://doi.org/10.1007/BF01611247

Guerrero, J.-L., & Sample, J. E. (2021). *Kildefordelte tilførsler av nitrogen og fosfor til norske kystområder i 2019—Tabeller, figurer og kart (Teotil)—Miljødirektoratet*. Miljødirektoratet/Norwegian Environment Agency. https://www.miljodirektoratet.no/publikasjoner/2021/mars-2021/kildefordelte-tilforsler-av-nitrogen-og-fosfor-til-norske-kystomrader-i-2019---tabeller-figurer-og-kart/

Hambro, E. (2021). *Vi slipper ut altfor mye nitrogen i Ytre Oslofjord | Miljødirektoratet*. https://kommunikasjon.ntb.no/pressemelding/vi-slipper-ut-altfor-mye-nitrogen-i-ytre-oslofjord-?publisherId=17847187&releaseId=17910430

Hanssen-Bauer, I., Førland, E. J., Haddeland, I., Hisdal, H., Mayer, S., Nesje, A., Nilsen, J. E. Ø., Sandven, S., Sandø, A. B., Sorteberg, A., & Ådlandsvik, B. (2017). *Climate in Norway 2100 – a knowledge base for climate adaptation—Miljødirektoratet*. Miljødirektoratet/Norwegian Environment Agency. https://www.miljodirektoratet.no/publikasjoner/2017/mai-2017/climate-in-norway-2100--a-knowledge-base-for-climate-adaptation/

Hedberg, G. (2021). *Rekefisket er historisk*. Dagsavisen. https://www.dagsavisen.no/demokraten/debatt/2021/11/15/rekefisket-er-historisk/

Heldal, H. E., Helvik, L., Appleby, P., Haanes, H., Volynkin, A., Jensen, H., & Lepland, A. (2021). Geochronology of sediment cores from the Vefsnfjord, Norway. *Marine Pollution Bulletin*, *170*, 112683. https://doi.org/10.1016/j.marpolbul.2021.112683

Helland, A. (1995). Vurdering av faste dumpeplasser langs Østfoldkysten. I *85*. Norsk institutt for vannforskning. https://niva.brage.unit.no/niva-xmlui/handle/11250/208212

Helland, A. (2001). The Importance of Selective Transport and Sedimentation in Trend Monitoring of Metals in Sediments. An Example from the Glomma Estuary, East Norway. *Water, Air, and Soil Pollution*, *126*(3), 339–361. https://doi.org/10.1023/A:1005243728540

Helland, A., Åberg, G., & Skei, J. (2002). Source dependent behaviour of lead and organic matter in the Glomma estuary, SE Norway: Evidence from isotope ratios. *Marine Chemistry*, *78*(2), 149–169. https://doi.org/10.1016/S0304-4203(02)00016-6

Hess, S., Alve, E., & Reuss, N. S. (2014). Benthic foraminiferal recovery in the Oslofjord (Norway): Responses to capping and re-oxygenation. *Estuarine, Coastal and Shelf Science*, *147*, 87–102. https://doi.org/10.1016/j.ecss.2014.05.012

Holtan, G. (1996). *Overvåking av Hvaler-Singlefjorden og munningen av Iddefjorden 1989-19-94: Forurensningstilførsler 1970-1993—Depotbiblioteket*. https://depotbiblioteket.no/cgi-bin/m2?tnr=143212

Hurlbert, S. H. (1971). The Nonconcept of Species Diversity: A Critique and Alternative Parameters. *Ecology*, *52*(4), 577–586. https://doi.org/10.2307/1934145

Jerlov, N. G. (1968). *Optical Oceanography*. Elsevier.

Knutzen, J., Skei, J., & Baalsrud, K. (1978). Nasjonalt program for overvåking av vannressurser. Pilotprosjekt. Iddefjorden 1977. I *74*. Norsk institutt for vannforskning. https://niva.brage.unit.no/niva-xmlui/handle/11250/202263

Lamb, A. L., Wilson, G. P., & Leng, M. J. (2006). A review of coastal palaeoclimate and relative sea-level reconstructions using δ13C and C/N ratios in organic material. *Earth-Science Reviews*, *75*(1), 29–57. https://doi.org/10.1016/j.earscirev.2005.10.003

Lapierre, J.-F., Guillemette, F., Berggren, M., & del Giorgio, P. A. (2013). Increases in terrestrially derived carbon stimulate organic carbon processing and CO2 emissions in boreal aquatic ecosystems. *Nature Communications*, *4*(1), 2972. https://doi.org/10.1038/ncomms3972

Malone, T. C., & Newton, A. (2020). The Globalization of Cultural Eutrophication in the Coastal Ocean: Causes and Consequences. *Frontiers in Marine Science*, *7*. https://doi.org/10.3389/fmars.2020.00670

Martins, M. V. A., Yamashita, C., Sousa, S. H. de M. e, Koutsoukos, E. A. M., Disaró, S. T., Debenay, J.-P., & Duleba, W. (2019). Response of Benthic Foraminifera to Environmental Variability: Importance of Benthic Foraminifera in Monitoring Studies. I *Monitoring of Marine Pollution*. IntechOpen. https://doi.org/10.5772/intechopen.81658

Meteorologisk institutt. (2021). *Østlandet siden 1900*. Meteorologisk institutt. https://www.met.no/vaer-og-klima/klima-siste-150-ar/regionale-kurver/ostlandet-siden-1900

Meyers, P. A. (1994). Preservation of elemental and isotopic source identification of sedimentary organic matter. *Chemical Geology*, *114*(3–4), 289–302. https://doi.org/10.1016/0009-2541(94)90059-0

Meyers, P. A. (1997). Organic geochemical proxies of paleoceanographic, paleolimnologic, and paleoclimatic processes. *Organic Geochemistry*, *27*(5), 213–250. https://doi.org/10.1016/S0146-6380(97)00049-1

Miljødirektoratet. (2021). *Mudre dumpe utfylling i sjø og vassdrag—Miljødirektoratet*. Miljødirektoratet/Norwegian Environment Agency. https://www.miljodirektoratet.no/ansvarsomrader/vann-hav-og-kyst/mudre-dumpe-utfylling/

Miljødirektoratet, Fiskeridirektoratet, Landbruksdirektoratet, Statens vegvesen, Sjøfartsdirektoratet, Kystverket, Riksantikvaren, Forsvarsbygg, Kulturdepartementet, & fylkesmenn og fylkeskommuner. (2019). *Forslag til helhetlig plan for Oslofjorden—Miljødirektoratet*. Miljødirektoratet/Norwegian Environment Agency. https://www.miljodirektoratet.no/publikasjoner/2019/desember-2019/forslag-til-helhetlig-plan-for-oslofjorden/

Monteith, D. T., Stoddard, J. L., Evans, C. D., de Wit, H. A., Forsius, M., Høgåsen, T., Wilander, A., Skjelkvåle, B. L., Jeffries, D. S., Vuorenmaa, J., Keller, B., Kopácek, J., & Vesely, J. (2007). Dissolved organic carbon trends resulting from changes in atmospheric deposition chemistry. *Nature*, *450*(7169), 537–540. https://doi.org/10.1038/nature06316

Naustvoll, L. J., Norli, M., Selvik, J. R., & Walday, M. G. (2017). *Overvåking av Ytre Oslofjord 2014-2018. Tilførsler og undersøkelser i vannmassene i 2016. Fagrapport.* Norsk institutt for vannforskning. https://imr.brage.unit.no/imr-xmlui/handle/11250/2476899

NOAA. (2021). *Classifying Estuaries: By Water Circulation—Estuaries Tutorial*. https://oceanservice.noaa.gov/education/tutorial_estuaries/est05_circulation.html

NVE. (2022a). *Solbergfoss | Sildre*. https://sildre.nve.no/station/2.605.0

NVE. (2022b). *Kart | Sildre*. https://sildre.nve.no/map?x=380400&y=7228000&zoom=4

NVE. (2022c). *NVE Temakart*. https://temakart.nve.no/

Opdal, A. F., Lindemann, C., & Aksnes, D. L. (2019). Centennial decline in North Sea water clarity causes strong delay in phytoplankton bloom timing. *Global Change Biology*, *25*(11), 3946–3953. https://doi.org/10.1111/gcb.14810

Painter, S. C., Lapworth, D. J., Woodward, E. M. S., Kroeger, S., Evans, C. D., Mayor, D. J., & Sanders, R. J. (2018). Terrestrial dissolved organic matter distribution in the North Sea. *Science of The Total Environment*, *630*, 630–647. https://doi.org/10.1016/j.scitotenv.2018.02.237

Polovodova Asteman, I., Hanslik, D., & Nordberg, K. (2015). An almost completed pollution-recovery cycle reflected by sediment geochemistry and benthic foraminiferal assemblages in a Swedish–Norwegian Skagerrak fjord. *Marine Pollution Bulletin*, *95*(1), 126–140. https://doi.org/10.1016/j.marpolbul.2015.04.031

Polovodova Asteman, I., Risebrobakken, B., Moros, M., Binczewska, A., Dobosz, S., Jansen, E., Sławińska, J., & Bąk, M. (2017). Late Holocene palaeoproductivity changes: A multi-proxy study in the Norwegian Trench and the Skagerrak, North Sea. *Boreas*, *47*. https://doi.org/10.1111/bor.12264

Polovodova Asteman, I., Van Nieuwenhove, N., Andersen, T. J., Linders, T., & Nordberg, K. (2021). Recent environmental change in the Kosterhavet National Park marine protected area as reflected by hydrography and sediment proxy data. *Marine Environmental Research*, *166*, 105265. https://doi.org/10.1016/j.marenvres.2021.105265

Prahl, F. G., Bennett, J. T., & Carpenter, R. (1980). The early diagenesis of aliphatic hydrocarbons and organic matter in sedimentary particulates from Dabob Bay, Washington. *Geochimica et Cosmochimica Acta*, *44*(12), 1967–1976. https://doi.org/10.1016/0016-7037(80)90196-9

Ritson, J. P., Graham, N. . J. D., Templeton, M. R., Clark, J. M., Gough, R., & Freeman, C. (2013). *The impact of climate change on the treatability of dissolved organic matter (DOM) in upland*

water supplies: A UK perspective—ScienceDirect. https://www.sciencedirect.com/science/article/pii/S0048969713015787

Ryrfors, T. (2015). *Surface circulation in the North-Eastern Skagerrak and the spreading of Glomma water along the Swedish coast*. https://doi.org/10.13140/RG.2.1.1829.9602

Seidel, M., Manecki, M., Herlemann, D. P. R., Deutsch, B., Schulz-Bull, D., Jürgens, K., & Dittmar, T. (2017). Composition and transformation of dissolved organic matter in the baltic sea. *Frontiers in Earth Science*, *5*. https://doi.org/10.3389/feart.2017.00031

Shultz, D. J., & Calder, J. A. (1976). Organic carbon 13C12C variations in estuarine sediments. *Geochimica et Cosmochimica Acta*, *40*(4), 381–385. https://doi.org/10.1016/0016-7037(76)90002-8

Spellerberg, I. F. (2008). Shannon–Wiener Index. I *Reference Module in Earth Systems and Environmental Sciences* (s. 3249–3252). https://doi.org/10.1016/B978-008045405-4.00132-4

Spezzaferri, S., Rüggeberg, A., Stalder, C., & Margreth, S. (2013). Benthic Foraminifer Assemblages from Norwegian Cold-Water Coral Reefs. *Journal of Foraminiferal Research*, *43*(1), 21–39. https://doi.org/10.2113/gsjfr.43.1.21

SSB. (2020). *Tømmerfløting 1871-1999—Siste slep for «Axel»*. Statistics Norway. https://www.ssb.no/a/histstat/artikler/art-2000-09-27-01.html

SSB. (2022). *Tabell—Topp 10 kommuner etter antall hytter*. Statistics Norway. https://www.ssb.no/303773/topp-10-kommuner-etter-antall-hytter

Stenseth, N. Chr., Moland, E., Vermaat, J., Harman, C., Knutsen, J. A., Chirstensen, K. H., Knutsen, H., & Mikalsen, B. (2019). *Skagerrak-Kattegat-Oslofjorden – Kunnskapsutvikling for et friskt og produktivt havområde—Det matematisk-naturvitenskapelige fakultet*. https://www.mn.uio.no/om/aktuelt/arrangementer/arendalsuka/rapport-skagerrak-kattegat-oslofjorden.html

Sterner, C. (2013). *Top Five Things You Should Know About Algae*. Energy.Gov. https://www.energy.gov/eere/articles/top-five-things-you-should-know-about-algae

Struck, U., Emeis, K., Voss, M., Christiansen, C., & Kunzendorf, H. (2000). Records of southern and central Baltic Sea eutrophication in δ13C and δ15N of sedimentary organic matter. *Marine Geology*, *164*, 157–171. https://doi.org/10.1016/S0025-3227(99)00135-8

Staalstrøm, A., Walday, M., Vogelsang, C., Frigstad, H., Borgersen, G., Albretsen, J., & Naustvoll, L.-J. (2022). *Utredning av behovet for å redusere tilførslene av nitrogen til Ytre Oslofjord—Miljødirektoratet*. Miljødirektoratet/Norwegian Environment Agency. https://www.miljodirektoratet.no/publikasjoner/2021/juni-2021/utredning-av-behovet-for-a-redusere-tilforslene-av-nitrogen-til-ytre-oslofjord/

Szmytkiewicz, A., & Zalewska, T. (2014). Sediment deposition and accumulation rates determined by sediment trap and 210Pb isotope methods in the Outer Puck Bay (Baltic Sea). *Oceanologia*, *56*(1), 85–106. https://doi.org/10.5697/oc.56-1.085

The research council of Norway. (2019). *A green-blue link made browner: How terrestrial climate change affects marine ecology - Prosjektbanken*. Prosjektbanken - Forskningsrådet. https://prosjektbanken.forskningsradet.no/project/FORISS/287490

Thornton, S. F., & McManus, J. (1994). Application of Organic Carbon and Nitrogen Stable Isotope and C/N Ratios as Source Indicators of Organic Matter Provenance in Estuarine Systems: Evidence from the Tay Estuary, Scotland. *Estuarine, Coastal and Shelf Science*, *38*(3), 219–233. https://doi.org/10.1006/ecss.1994.1015

Thorsnæs, G., & Pharo, J. T. (2022). Hvaler. I *Store norske leksikon*. http://snl.no/Hvaler

Veileder. (2018). *Klassifiseringsveileder 02:2018 Klassifisering av miljøtilstand i vann. Økologisk og kjemisk klassifiseringssystem for kystvann, grunnvann, innsjøer og elver*. Vannportalen. https://www.vannportalen.no/veiledere/klassifiseringsveileder/

Vermont Water Quality Standards. (2014). *Vermont Water Quality Standards | Department of Environmental Conservation*. https://dec.vermont.gov/content/vermont-water-quality-standards

Walday, M., Berge, J., Helland, A., & Rinde, E. (2006). Konsekvensutredning for Ytre Hvaler, Østfold. Deltema naturmiljø i sjøen. I *68*. Norsk institutt for vannforskning. https://niva.brage.unit.no/niva-xmlui/handle/11250/213383

Walday, M., Borgersen, G., Beylich, B., Eikrem, W., Gitemark, J., Naustvoll, L. J., Selvik, J. R., & Staalstrøm, A. (2019). Overvåking av Ytre Oslofjord i 2014-2018. 5-årsrapport. I *99*. Norsk institutt for vannforskning. https://niva.brage.unit.no/niva-xmlui/handle/11250/2628649

Walday, M., & Moy, F. E. (1996). Improvement of the shallow water communities following reductions of industrial outlets and sewage discharge in the Hvaler estuary, Norway. *Hydrobiologia*, *327*, 297–304.

Walday, M., Selvik, J. R., & Norli, M. (2014). *Overvåking av Ytre Oslofjord—Tilførsler og undersøkelser i vannmassene i 2013. Fagrapport*. Norsk institutt for vannforskning. https://niva.brage.unit.no/niva-xmlui/handle/11250/218717

Water Framework Directive. (2022). NatureScot. https://www.nature.scot/professional-advice/protected-areas-and-species/safeguards-beyond-protected-areas/water-framework-directive

Wentworth, C. K. (1922). *Wentworth (1922) grain size classification*. The Planetary Society. https://www.planetary.org/space-images/wentworth-1922-grain-size

WoRMS. (2022). *WoRMS - World Register of Marine Species—Foraminifera*. https://www.marinespecies.org/aphia.php?p=taxdetails&id=1410

Zalesny, E. R. (1959). Foraminiferal ecology of Santa Monica Bay, California. *Micropaleontology*, *5*(1), 101–126. https://doi.org/10.2307/1484158

8 Appendix

A Ecological status classification

Table 3: Ecological Status classification for heavy metals, TOC_{63} and oxygen concentrations from Veileder, 2018, and H'log2_f, ES100_f and NQI_f from Alve et al., 2019.

Parameter	Unit	Status				
		High I	Good II	Moderate III	Poor IV	Bad V
Cadmium (Cd)	mg/kg	0.2	2.5	16	157	> 157
Lead (Pb)	mg/kg	25	150	1480	2000	2000-2500
Nickel (Ni)	mg/kg	30	42	271	533	> 533
Copper (Cu)	mg/kg	20	84	84	147	> 147
Zinc (Zn)	mg/kg	90	139	750	6690	> 6690
Chromium (Cr)	mg/kg	60	660	6000	15500	15500-25000
Mercury (Hg)	mg/kg	0.05	0.52	0.75	1.45	> 1.45
TOC63	mg/g	0-20	20-27	27-34	34-41	41-200
Oxygen	ml/l	>4.5	4.5-3.5	3.5-2.5	2.5-1.5	<1.5
H'log2_f		5.0-3.4	3.4-2.4	2.4-1.8	1.8-1.2	1.2-0
ES100		35-18	18-13	13-11	11-9	9-0
NQI_f		1-0.54	0.54-0.45	0.45-0.31	0.31-0.13	0.13-0

B Mean annual discharge measured at Solbergfoss

Table 4: Mean annual discharge of the river Glomma from 1964 to 2021 measured at Solbergfoss: Norwegian Water Resources and Energy Directorate station 2.605.0 (*NVE, 2022c*).

Year	Mean annual discharge (m^3/s)	Year	Mean annual discharge (m^3/s)
1964	678.06	1993	742.78
1965	728.32	1994	651.44
1966	696.34	1995	719.85
1967	891.57	1996	506.63
1968	647.55	1997	660.45
1969	538.49	1998	740.48
1970	577.15	1999	750.99
1971	624.12	2000	972.13
1972	639.66	2001	737.01
1973	594.55	2002	662.03
1974	614.97	2003	582.76
1975	611.32	2004	626.78
1976	499.1	2005	674.08
1977	622.8	2006	725.67
1978	552.55	2007	710.45
1979	687.3	2008	792.79
1980	644	2009	750.78
1981	647.01	2010	706.08
1982	607.37	2011	900.44
1983	679	2012	843.75
1984	732.03	2013	742.39
1985	862.72	2014	85.,3
1986	616.28	2015	778.63
1987	898.21	2016	637.74
1988	863.93	2017	743.22
1989	705.18	2018	682.45
1990	726.72	2019	781.3
1991	546.27	2020	857.56
1992	619.61	2021	757.38

C Overview of selected intervals for subsampling

Table 5: Selected core intervals for subsampling (GL2).

Core intervals selected for sub-sampling
MSc Hvaler June 2021
Amund Bråten Rian
Sediment core: GL2-21A

Core	Core interval (cm)	Core depth (cm)	Dating	TC, TN	Heavy metals	Foraminifera	Isotopes	Grain size
GL2-21 A	0-1	0.5	x	x	x	x	x	x*2
GL2-21 A	1 -2	1.5		x	x	x	x	x*2
GL2-21 A	2 - 3	2.5	x	x	x		x	x*2
GL2-21 A	3 - 4	3.5		x	x	x	x	x*2
GL2-21 A	4 - 5	4.5	x	x	x	x	x	x*2
GL2-21 A	5 - 6	5.5		x	x		x	x*2
GL2-21 A	6 - 7	6.5		x	x		x	x*2
GL2-21 A	7 - 8	7.5		x	x		x	x*2
GL2-21 A	8 - 9	8.5	x	x	x	x	x	x*2
GL2-21 A	9- 10	9.5		x	x		x	x*2
GL2-21 A	10 - 11	10.5		x	x		x	x*2
GL2-21 A	11 - 12	11.5						
GL2-21 A	12 - 13	12.5	x	x	x		x	x*2
GL2-21 A	13 - 14	13.5						
GL2-21 A	14 - 15	14.5		x	x	x	x	x*2
GL2-21 A	15 - 16	15.5						
GL2-21 A	16 - 17	16.5	x	x	x		x	x*2
GL2-21 A	17 - 18	17.5						
GL2-21 A	18 - 19	18.5		x	x		x	x*3
GL2-21 A	19 - 20	19.5						
GL2-21 A	20 - 22	21	x	x	x	x	x	x*2
GL2-21 A	22 - 24	23						
GL2-21 A	24 - 26	25	x	x	x		x	x*2
GL2-21 A	26 - 28	27						
GL2-21 A	28 - 30	29	x	x	x		x	x*2
GL2-21 A	30 - 32	31						
GL2-21 A	32 - 34	33	x	x	x	x	x	x*2
GL2-21 A	34-36	35						
GL2-21 A	36-38	37	x	x	x			x*2
GL2-21 A	38-40	39	x					
GL2-21 A	40-42	41	x	x	x		x	x*2
GL2-21 A	42-44	43	x					
GL2-21 A	44-46	45	x	x	x	x	x	x*2
GL2-21 A	46-48	47	x					
GL2-21 A	48-50	49	x	x	x		x	x*2
GL2-21 A	50-52	51	x	x	x		x	x*2
GL2-21 A	52-54	53	x	x	x		x	x*2
GL2-21 A	54-56	55		x	x		x	x*2
GL2-21 A	56-58	57	x	x	x	x	x	x*2
GL2-21 A	58-60	59		x	x		x	x*3
GL2-21 A	60-62	61	x	x	x		x	x*2
GL2-21 A	62-64	63		x	x		x	x*2
GL2-21 A	64-66	65	x	x	x		x	x*2
GL2-21 A	66-67	67		x	x	x	x	x*2

Table 6: Selected core intervals for subsampling (GL3).

Core intervals selected for sub-sampling
MSc Hvaler June 2021
Amund Bråten Rian
Sedimentary core GL3-21A

Core	Core interval (cm)	Core depth (cm)	Dating	TC, TN	Heavy metals	Foraminifera	Isotopes	Grain size
GL3-21 A	0-1	0.5	x	x	x	x	x	x*2
GL3-21 A	1 -2	1.5		x	x	x	x	x*2
GL3-21 A	2 - 3	2.5	x	x	x		x	x*2
GL3-21 A	3 - 4	3.5		x	x	x	x	x*2
GL3-21 A	4 - 5	4.5	x	x	x	x	x	x*2
GL3-21 A	5 - 6	5.5		x	x		x	x*2
GL3-21 A	6 - 7	6.5		x	x		x	x*2
GL3-21 A	7 - 8	7.5		x	x		x	x*2
GL3-21 A	8 - 9	8.5	x	x	x	x	x	x*2
GL3-21 A	9- 10	9.5		x	x		x	x*2
GL3-21 A	10 - 11	10.5		x	x		x	x*2
GL3-21 A	11 - 12	11.5						
GL3-21 A	12 - 13	12.5	x	x	x		x	x*2
GL3-21 A	13 - 14	13.5						
GL3-21 A	14 - 15	14.5		x	x		x	x*2
GL3-21 A	15 - 16	15.5				x		
GL3-21 A	16 - 17	16.5	x	x	x		x	x*2
GL3-21 A	17 - 18	17.5						
GL3-21 A	18 - 19	18.5		x	x		x	x*2
GL3-21 A	19 - 20	19.5	x					
GL3-21 A	20 - 22	21	x	x	x		x	x*2
GL3-21 A	22 - 24	23	x			x		
GL3-21 A	24 - 26	25	x	x	x		x	x*3
GL3-21 A	26 - 28	27	x					
GL3-21 A	28 - 30	29	x	x	x			x*2
GL3-21 A	30 - 32	31	x	x	x	x	x	x*2
GL3-21 A	32 - 34	33	x	x	x		x	x*2
GL3-21 A	34-36	35	x	x	x		x	x*2
GL3-21 A	36-38	37	x	x	x		x	x*2
GL3-21 A	38-40	39	x	x	x	x	x	x*2
GL3-21 A	40-42	41	x	x	x		x	x*2
GL3-21 A	42-44	43	x	x	x		x	x*2
GL3-21 A	44-46	45		x	x	x	x	x*2

D Radiometric dating and SAR report

Samples from four different sediment cores in the Outer Oslofjord was sent to the Environmental Radioactivity Research Center (ERRC) for radiometric dating and to determine SAR. The presented report is edited to only include the results from the sediment cores which are considered and discussed in this thesis (GL2 and GL3).

Radiometric dating of four marine sediment cores from the Glomma Estuary, Outer Oslofjord and Skagerrak, Norway

(Revised 13.05.2022)

P.G.Appleby and G.T.Piliposian

Environmental Radioactivity Research Centre

University of Liverpool

Methods

Dating by ^{210}Pb and ^{137}Cs was carried out on four marine sediment cores from the Glomma Estuary (GL1-21F, water depth 73 m), Outer Oslofjord (OF2-21D, water depth 355 m) and Skagerrak (GL2-21A and GL3-21A, water depths 209 m, 212 m). Sub-samples from each core were analysed for ^{210}Pb, $^{2\mathbf{a}}$Ra, and ^{137}Cs by direct gamma assay in the Liverpool University Environmental Radioactivity Laboratory using Ortec HPGe GWL series well-type coaxial low background intrinsic germanium detectors (Appleby *et al.* 1986). ^{210}Pb was determined via its gamma emissions at 46.5 keV, and ^{226}Ra by the 295 keV and 352 keV γ-rays emitted by its daughter radionuclide ^{214}Pb following 3 weeks storage in sealed containers to allow radioactive equilibration. ^{137}Cs was measured by its emissions at 662 keV. The absolute efficiencies of the detectors were determined using calibrated sources and sediment samples of known activity. Corrections were made for the effect of self-absorption of low energy γ-rays within the sample (Appleby *et al.* 1992).

Results

Results of the radiometric analyses carried out on each core are given in Tables 1–4 and shown graphically in Figures 1.i–4.i. Supported ^{210}Pb activity was assumed to be equal to the measured ^{226}Ra activity, and unsupported ^{210}Pb activity calculated by subtracting supported ^{210}Pb from the measured total ^{210}Pb activity. Since all four cores had ^{210}Pb inventories well in excess of values supported by the direct atmospheric flux, they all appear to be from sites dominated by high levels of sediment focusing. This process was most intense at the site of core GL2-21A. In consequence, ^{210}Pb supply rates are likely to have varied in response to variations in the sedimentation rate. It follows that neither of the simple (CRS and CIC) ^{210}Pb dating models (Appleby & Oldfield 1978) are likely to be applicable to the ^{210}Pb

records as a whole, though they can still be applied in a piecewise way where there are reliable chronostratigraphic dates as reference points. In the present case these are likely to include the 1986 and 1963 ^{137}Cs dates determined from records of fallout from the Chernobyl accident and the atmospheric testing of nuclear weapons. Best chronologies for each core were determined following an assessment of all the data using the methods outlined in Appleby (2001). The results are shown in Figures 1.ii–4.ii and given in detail in Tables 5–8.

Skagerrak core GL2-21A

Lead-210 Activity

Total ^{210}Pb activity at the base of the core (66 cm) remains significantly above that of the supporting ^{226}Ra (Figure 3.i(a)). Unsupported ^{210}Pb concentrations (Figure 3.i(b)) decline more or less exponentially with depth though there are significant irregular departures from the general trend. The overall decline, from 138 Bq kg^{-1} in the near surface sediments to 19 Bq kg^{-1} at the base, corresponds to around 3 ^{210}Pb half-lives and suggests that the core spans around 70 years.

Artificial Fallout Radionuclides

The ^{137}Cs activity versus depth record (Figure 3.i(c)) has a broad peak between 36-52 cm in which concentrations consistently exceed 26 Bq kg^{-1}. Within this feature there are two small peaks, between 38-44 cm and 44-50 cm that may record fallout from the 1986 Chernobyl accident, and the early 1960s fallout maximum from the atmospheric testing of nuclear weapons.

Core Chronology

^{210}Pb dates calculated using the CRS model place 1986 and 1963 both within broad ^{137}Cs peak, 1986 within the 36-38 cm section and 1963 within the 50-52 cm section, reasonably close to the depths suggested by the ^{137}Cs peaks. Although the indistinct nature of the ^{137}Cs record makes precise attribution not possible it is reasonable to suppose that the ^{137}Cs peak at 38-44 cm dates from around 1986. This implies a mean post-1986 sedimentation rate of around 0.54 g cm^{-2} y^{-1} (1.2 cm y^{-1}), twice as high as at the site of the Outer Oslofjord core. It is also twice as high as in the pre-1986 part of the record. The raw ^{210}Pb results suggest that during the period spanned by sediments below 47 cm there was a relatively uniform sedimentation rate of around 0.29 g cm^{-2} y^{-1} (0.54 cm y^{-1}). Estimates of the time spanned by sediments between 41-47 cm range from 6 to 10 years depending on the assumptions made. The chronology shown in Figure 3.ii and given in detail in Table 7 assumes an intermediate value of 8 years. On these calculations the base of the core is dated to the mid-1940s.

Skagerrak core GL3-21A

Lead-210 Activity

Total ^{210}Pb (Figure 4.i(a)) appears to reach equilibrium with ^{226}Ra at a depth of around 45 cm. Unsupported ^{210}Pb concentrations (Figure 4.i(b)) decline more or less exponentially with depth in the uppermost 20 cm. A more irregular record in sediments below that depth may indicate some instability during this earlier period.

Artificial Fallout Radionuclides

The ^{137}Cs record (Figure 3.i(c)) has two distinct peaks, at 25 cm and 35 cm. Although they may indicate the 1986 and 1963 depths, it is possible that these features, most particularly the 35 cm peak, have been affected by the same events as those causing the instabilities in the ^{210}Pb record.

Core Chronology

^{210}Pb dates calculated using the CRS model place 1986 and 1963 at depths of 20 cm and 29 cm, significantly above the depths of the ^{137}Cs peaks. Revised dates calculated using the ^{137}Cs dates as reference points suggest that the discrepancy is due to variations in the ^{210}Pb supply rates in response to changes in the intensity of sediment focussing. The results of these calculations are shown in Figure 4.ii and given in detail in Table 8. The post-1963 dates should be fairly reliable. They suggest that sedimentation rates increased from around 0.20 g cm^{-2} y^{-1} (0.36 cm y^{-1}) in the early 1960s to 0.30 g cm^{-2} y^{-1} (0.63 cm y^{-1}) by the year 2000. The present value is estimated to be 0.40 g cm^{-2} y^{-1} (1.12 cm y^{-1}). Pre-1963 dates are much more problematic. Making reasonable assumptions (continuity of sedimentation rate or continuity of the ^{210}Pb supply rate), estimates of the date of the base of the core range from 1931 to 1938, with a mean value in the mid-1930s. Assuming this value, calculations of the pre-1963 dates suggest a relatively uniform sedimentation rate for this period of 0.18 g cm^{-2} y^{-1} (0.31 cm y^{-1}).

References

Appleby P.G., 2001. Chronostratigraphic techniques in recent sediments, in *Tracking Environmental Change Using Lake Sediments Volume 1: Basin Analysis, Coring, and Chronological Techniques*, (eds W M Last & J P Smol), Kluwer Academic, pp171-203.

Appleby,P.G., P.J.Nolan, D.W.Gifford, M.J.Godfrey, F.Oldfield, N.J.Anderson & R.W.Battarbee, 1986. ^{210}Pb dating by low background gamma counting. *Hydrobiologia*, **141**:21-27.

Appleby,P.G. & F.Oldfield, 1978. The calculation of ^{210}Pb dates assuming a constant rate of supply of unsupported ^{210}Pb to the sediment. *Catena*, **5**:1-8

Appleby,P.G., N.Richardson, & P.J.Nolan, 1992. Self-absorption corrections for well-type germaniun detectors. *Nucl. Inst.& Methods B,* **71**: 228-233.

Table 3. Fallout radionuclide concentrations in the Skagerrak sediment core GL2-21A

Depth		^{210}Pb Total		^{210}Pb Unsupported		^{210}Pb Supported		^{137}Cs	
cm	g cm^{-2}	Bq kg^{-1}	±	Bq kg^{-1}	±	Bq kg^{-1}	±	Bq kg^{-1}	±
0.5	0.1	167.3	9.9	138.1	10.1	29.3	2.2	3.8	1.3
2.5	0.7	154.4	10.1	133.5	10.3	21.0	2.0	1.3	1.4
4.5	1.4	160.2	9.8	135.4	10.1	24.8	2.2	4.3	1.4
8.5	3.0	147.9	9.8	120.5	10.0	27.4	2.0	9.4	1.3
12.5	4.8	136.3	9.4	106.5	9.5	29.8	1.8	6.4	1.3
16.5	6.5	149.5	10.2	121.2	10.5	28.4	2.3	6.9	1.5
21.0	8.6	121.6	8.9	98.1	9.0	23.5	1.6	7.6	1.0
25.0	10.6	94.8	9.5	71.3	9.7	23.4	2.1	6.6	1.1
29.0	12.6	89.9	8.8	64.6	9.0	25.4	2.2	12.4	1.4
33.0	14.7	98.0	9.0	70.0	9.2	28.0	2.0	13.0	1.3
37.0	16.7	103.5	8.2	76.1	8.4	27.4	1.6	26.1	1.5
39.0	17.8	84.8	6.6	59.0	6.8	25.8	1.5	28.1	1.2
41.0	18.8	82.2	8.6	54.6	8.8	27.6	2.1	30.4	1.7
43.0	19.9	75.5	7.7	46.5	7.9	29.0	1.9	28.7	1.5
45.0	20.9	67.2	6.8	39.7	6.9	27.5	1.5	26.5	1.3
47.0	21.9	77.0	7.7	47.8	7.9	29.2	1.8	28.9	1.4
49.0	22.9	75.5	7.0	52.1	7.2	23.4	1.8	26.9	1.4
51.0	24.0	69.8	7.8	44.8	8.0	25.0	1.7	26.2	1.4
53.0	25.1	58.4	6.0	35.0	6.1	23.4	1.1	13.9	1.0
57.0	27.3	53.9	5.2	29.8	5.3	24.1	1.2	11.3	1.4
61.0	29.4	50.1	7.9	22.7	8.0	27.4	1.6	7.1	0.9
65.0	31.6	47.0	5.8	19.4	6.7	27.6	3.4	3.8	1.0

Table 4. Fallout radionuclide concentrations in the Skagerrak sediment core GL3-21A

Depth		^{210}Pb Total		^{210}Pb Unsupported		^{210}Pb Supported		^{137}Cs	
cm	g cm^{-2}	Bq kg^{-1}	±	Bq kg^{-1}	±	Bq kg^{-1}	±	Bq kg^{-1}	±
0.5	0.1	166.6	10.1	134.8	10.4	31.8	2.3	7.5	1.5
2.5	0.8	132.0	8.9	102.4	9.1	29.6	1.7	9.1	1.3
4.5	1.6	123.5	9.9	94.5	10.2	29.0	2.2	10.7	1.4
8.5	3.4	143.6	10.0	111.3	10.3	32.3	2.4	8.7	1.7
12.5	5.2	116.7	8.7	95.6	8.9	21.0	1.7	8.7	1.1
16.5	7.0	116.4	10.1	84.7	10.4	31.7	2.3	12.2	1.7
19.5	8.5	97.1	10.3	74.2	10.4	22.9	2.0	5.4	1.2
21.0	9.3	95.8	9.5	67.0	9.7	28.9	2.1	16.9	1.4
23.0	10.4	77.6	8.6	46.4	8.8	31.2	2.1	21.5	1.5
25.0	11.4	72.8	7.6	44.7	7.8	28.1	1.8	26.1	1.4
27.0	12.5	78.8	8.0	48.8	8.2	30.0	1.6	16.5	1.1
29.0	13.6	51.8	6.2	25.0	6.4	26.8	1.6	12.2	1.2
31.0	14.7	57.3	6.3	32.3	6.5	24.9	1.4	11.6	1.2
33.0	15.8	41.4	7.2	10.6	7.4	30.8	1.8	14.0	1.2
35.0	16.9	72.4	8.6	48.5	8.8	23.9	1.9	19.9	1.5
37.0	18.0	59.1	6.4	31.3	6.5	27.8	1.3	16.1	1.1
39.0	19.2	50.3	7.1	21.4	7.2	28.9	1.6	10.7	1.0
41.0	20.4	54.5	6.3	28.2	6.5	26.3	1.5	5.8	1.0
43.0	21.6	35.4	5.5	8.2	5.7	27.2	1.4	2.6	0.8
45.0	22.9	30.4	5.9	0.9	6.1	29.6	1.6	1.8	1.0

Table 7. ^{210}Pb chronology of the Skagerrak sediment core GL2-21A

Depth		Chronology			Sedimentation Rate		
		Date	Age				
cm	g cm^{-2}	AD	y	±	g cm^{-2} y^{-1}	cm y^{-1}	± (%)
0.0	0.0	2021	0	0			
0.5	0.1	2021	0	1	0.58	1.85	8.5
2.5	0.7	2020	1	1	0.58	1.62	8.9
4.5	1.4	2019	2	2	0.58	1.50	8.7
8.5	3.0	2016	5	2	0.56	1.36	9.7
12.5	4.8	2013	8	2	0.54	1.24	10.4
16.5	6.5	2009	12	2	0.54	1.17	10.4
21.0	8.6	2005	16	2	0.55	1.15	11.3
25.0	10.6	2002	19	2	0.56	1.13	15.4
29.0	12.6	1998	23	2	0.55	1.08	16.0
33.0	14.7	1995	26	2	0.54	1.05	15.7
37.0	16.7	1990	31	3	0.50	0.96	14.8
39.0	17.8	1988	33	3	0.46	0.88	15.8
41.0	18.8	1986	35	3	0.43	0.83	19.9
43.0	19.9	1984	37		0.40	0.77	
45.0	20.9	1981	40		0.36	0.70	
47.0	21.9	1978	43		0.32	0.62	
49.0	22.9	1974	47		0.30	0.57	
51.0	24.0	1971	50		0.29	0.54	
53.0	25.1	1967	54		0.29	0.53	
57.0	27.3	1959	62		0.29	0.54	
61.0	29.4	1952	69		0.29	0.54	
65.0	31.6	1944	77		0.29	0.54	

Table 8. ^{210}Pb chronology of the Skagerrak sediment core GL3-21A

Depth		Chronology			Sedimentation Rate		
		Date	Age				
cm	g cm^{-2}	AD	y	±	g cm^{-2} y^{-1}	cm y^{-1}	± (%)
0.0	0.0	2021	0	0			
0.5	0.1	2021	0	2	0.40	1.12	9.1
2.5	0.8	2019	2	2	0.38	0.95	10.2
4.5	1.6	2017	4	2	0.36	0.84	12.0
8.5	3.4	2012	9	2	0.33	0.75	10.9
12.5	5.2	2006	15	2	0.31	0.68	11.4
16.5	7.0	2000	21	2	0.30	0.63	14.4
19.5	8.5	1995	26	3	0.30	0.62	16.6
21.0	9.3	1992	29	3	0.31	0.60	17.3
23.0	10.4	1989	32	3	0.29	0.55	21.7
25.0	11.4	1986	35	4	0.26	0.50	20.8
27.0	12.5	1981	40	4	0.24	0.45	
29.0	13.6	1976	45	4	0.24	0.44	
31.0	14.7	1972	49	4	0.24	0.43	
33.0	15.8	1968	53	5	0.21	0.38	
35.0	16.9	1963	58	5	0.21	0.36	
37.0	18.0	1955	66		0.18	0.31	
39.0	19.2	1950	71		0.18	0.31	
41.0	20.4	1942	79		0.18	0.30	
43.0	21.6	1936	85		0.18	0.30	

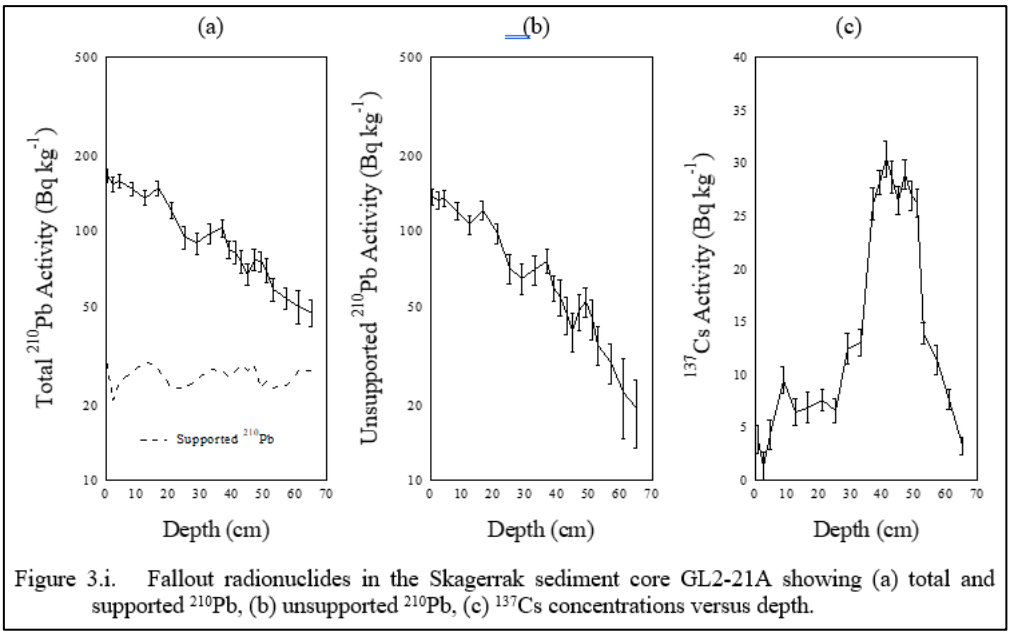

Figure 3.i. Fallout radionuclides in the Skagerrak sediment core GL2-21A showing (a) total and supported ^{210}Pb, (b) unsupported ^{210}Pb, (c) ^{137}Cs concentrations versus depth.

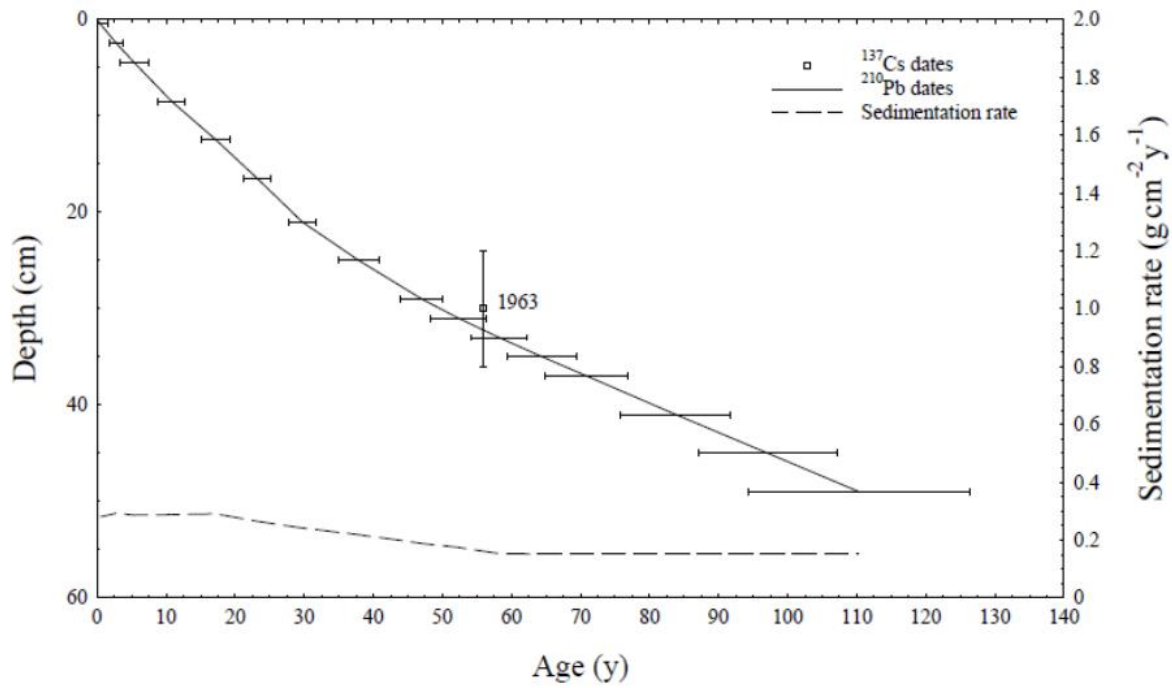

Figure 3.ii. Radiometric chronology of the Glomma Estuary sediment core SMA-19 showing the CRS model ^{210}Pb dates and sedimentation rates and the 1963 depth determined from the ^{137}Cs record.

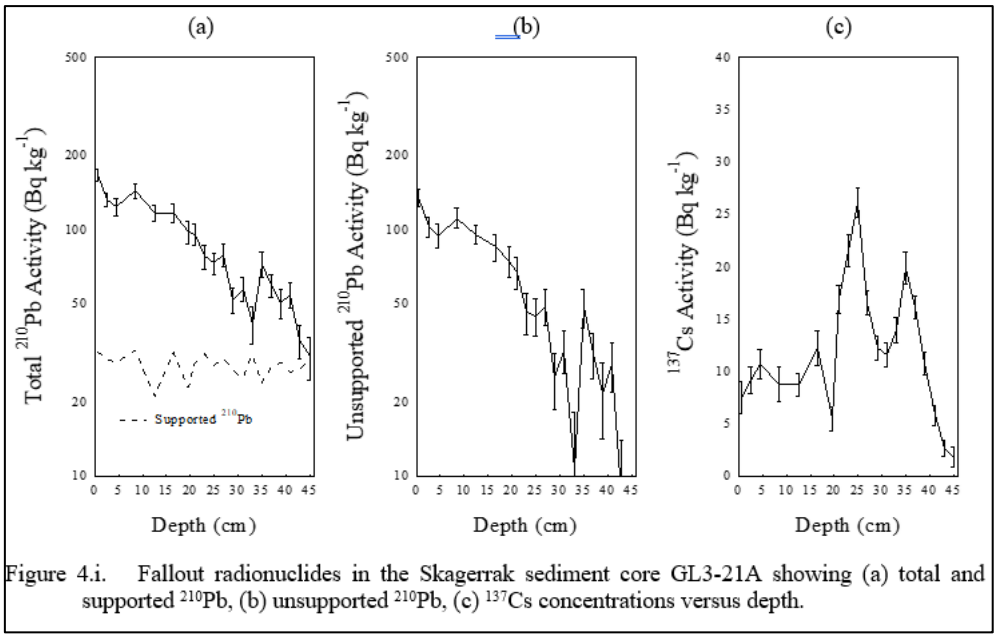

Figure 4.i. Fallout radionuclides in the Skagerrak sediment core GL3-21A showing (a) total and supported ^{210}Pb, (b) unsupported ^{210}Pb, (c) ^{137}Cs concentrations versus depth.

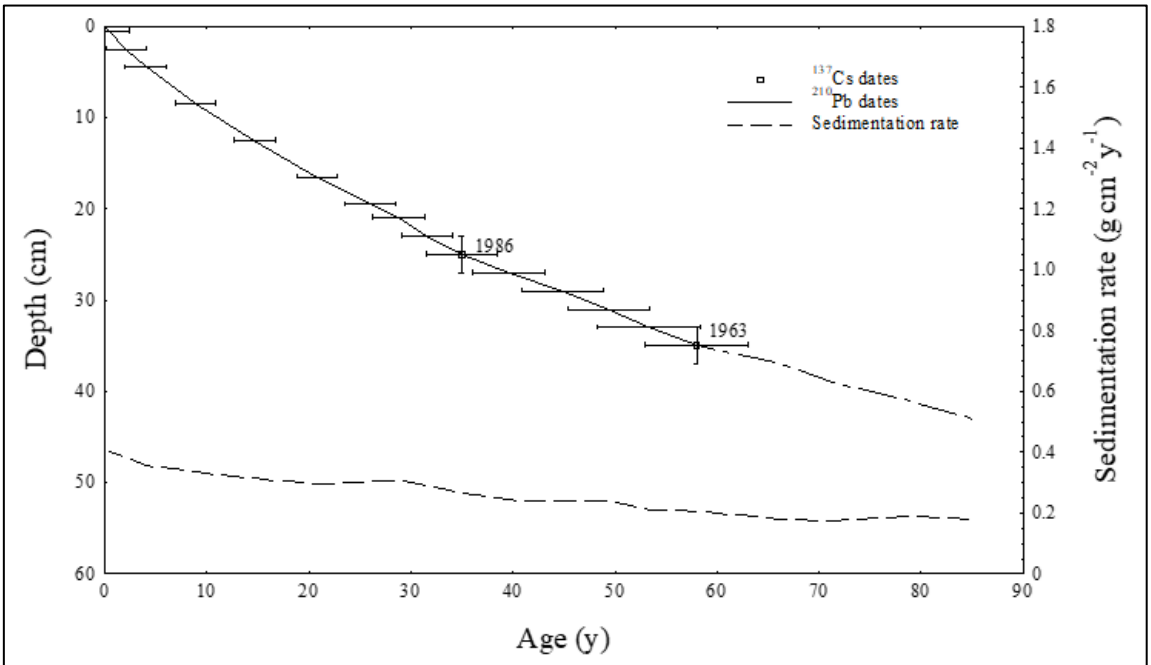

Figure 4.ii. Radiometric chronology of the Skagerrak Estuary sediment core GL3-21A showing the 1986 and 1963 ^{137}Cs dates and the ^{210}Pb dates and sedimentation rates calculated by applying the CRS model in a piecewise way using the ^{137}Cs dates as reference points. In the lower part of the depth versus age curve it was not possible to assign uncertainties to the ^{210}Pb dates.

E Water content

Table 7: Water content (%) in the northern (GL2) and southern (GL3) sediment cores.

Core	Core interval (cm)	Core depth (cm)	Water content (%)
GL2-21A	0-1	0.5	79.77
GL2-21A	1 -2	1.5	73.38
GL2-21A	2 - 3	2.5	71.80
GL2-21A	3 - 4	3.5	71.30
GL2-21A	4 - 5	4.5	70.46
GL2-21A	5 - 6	5.5	68.79
GL2-21A	6 - 7	6.5	67.35
GL2-21A	7 - 8	7.5	67.06
GL2-21A	8 - 9	8.5	65.91
GL2-21A	9- 10	9.5	65.14
GL2-21A	10 - 11	10.5	66.11
GL2-21A	11 - 12	11.5	66.01
GL2-21A	12 - 13	12.5	65.83
GL2-21A	13 - 14	13.5	65.39
GL2-21A	14 - 15	14.5	65.68
GL2-21A	15 - 16	15.5	65.80
GL2-21A	16 - 17	16.5	64.84
GL2-21A	17 - 18	17.5	64.62
GL2-21A	18 - 19	18.5	63.68
GL2-21A	19 - 20	19.5	63.42
GL2-21A	20 - 22	21	62.98
GL2-21A	22 - 24	23	61.21
GL2-21A	24 - 26	25	61.43
GL2-21A	26 - 28	27	61.95
GL2-21A	28 - 30	29	61.93
GL2-21A	30 - 32	31	60.60
GL2-21A	32 - 34	33	60.85
GL2-21A	34-36	35	60.76
GL2-21A	36-38	37	60.08
GL2-21A	38-40	39	60.13
GL2-21A	40-42	41	60.75
GL2-21A	42-44	43	60.50
GL2-21A	44-46	45	61.31
GL2-21A	46-48	47	61.42
GL2-21A	48-50	49	60.48
GL2-21A	50-52	51	60.09
GL2-21A	52-54	53	58.00
GL2-21A	54-56	55	59.40
GL2-21A	56-58	57	59.76
GL2-21A	58-60	59	59.16
GL2-21A	60-62	61	59.70
GL2-21A	62-64	63	59.39
GL2-21A	64-66	65	58.21
GL2-21A	66-67	67	56.96

Core	Core interval (cm)	Core depth (cm)	Water content (%)
GL3-21 A	0-1	0.5	76.32
GL3-21 A	1 -2	1.5	73.12
GL3-21 A	2 - 3	2.5	70.23
GL3-21 A	3 - 4	3.5	66.57
GL3-21 A	4 - 5	4.5	65.54
GL3-21 A	5 - 6	5.5	64.21
GL3-21 A	6 - 7	6.5	64.04
GL3-21 A	7 - 8	7.5	64.14
GL3-21 A	8 - 9	8.5	64.96
GL3-21 A	9- 10	9.5	64.26
GL3-21 A	10 - 11	10.5	64.43
GL3-21 A	11 - 12	11.5	65.81
GL3-21 A	12 - 13	12.5	65.63
GL3-21 A	13 - 14	13.5	64.48
GL3-21 A	14 - 15	14.5	64.12
GL3-21 A	15 - 16	15.5	63.99
GL3-21 A	16 - 17	16.5	63.55
GL3-21 A	17 - 18	17.5	63.15
GL3-21 A	18 - 19	18.5	62.60
GL3-21 A	19 - 20	19.5	60.86
GL3-21 A	20 - 22	21	59.77
GL3-21 A	22 - 24	23	59.91
GL3-21 A	24 - 26	25	60.38
GL3-21 A	26 - 28	27	59.85
GL3-21 A	28 - 30	29	58.45
GL3-21 A	30 - 32	31	58.52
GL3-21 A	32 - 34	33	58.19
GL3-21 A	34-36	35	58.25
GL3-21 A	36-38	37	58.79
GL3-21 A	38-40	39	56.10
GL3-21 A	40-42	41	55.84
GL3-21 A	42-44	43	54.94
GL3-21 A	44-46	45	53.89

F Grain size distribution

Table 8: Table of grain size distribution at GL2-21A using Wentworth, 1922 classification.

Core	Core interval (cm)	Core depth (cm)	Clay (%)	Fine silt (%)	Medium silt (%)	Coarse silt (%)	Fine sand (%)	Medium sand (%)	Clay & Silt (%)	Sand (%)
			≤ 4 µm	4- 16 µm	16-32 µm	32-63 µm	63-125 µm	125-500 µm	2- 63 µm	63 µm -2 mm
GL2	0-1	0,5	12.42	43.26	21.72	17.10	3.82	1.68	94.50	5.50
GL2	1 -2	1,5	16.65	52.04	17.21	9.06	2.80	2.24	94.96	5.04
GL2	2 - 3	2,5	14.41	51.32	20.03	9.57	2.73	1.94	95.33	4.67
GL2	3 - 4	3,5	15.41	53.29	18.46	8.53	2.49	1.82	95.69	4.31
GL2	4 - 5	4,5	17.52	49.54	17.87	10.53	2.70	1.84	95.46	4.54
GL2	5 - 6	5,5	17.04	54.33	16.48	7.80	2.40	1.95	95.65	4.35
GL2	6 - 7	6,5	12.53	50.65	22.89	10.64	2.20	1.09	96.71	3.29
GL2	7 - 8	7,5	14.56	52.39	19.90	9.28	2.30	1.58	96.13	3.87
GL2	8 - 9	8,5	13.88	52.50	20.51	8.71	2.29	2.11	95.60	4.40
GL2	9- 10	9,5	13.88	50.58	20.77	10.33	2.50	1.95	95.56	4.44
GL2	10 -11	10,5	17.23	53.32	17.80	8.12	1.92	1.60	96.47	3.53
GL2	12 -13	12,5	16.97	52.55	17.26	8.78	2.33	2.10	95.57	4.43
GL2	14 - 15	14,5	14.23	50.48	20.01	10.47	2.65	2.17	95.19	4.81
GL2	16 - 17	16,5	13.48	51.74	21.54	9.73	2.10	1.40	96.49	3.51
GL2	18 - 19	18,5	19.20	53.34	15.11	7.85	2.34	2.16	95.49	4.51
GL2	20 - 22	21	16.76	52.66	17.85	8.59	2.28	1.86	95.87	4.13
GL2	24 - 26	25	14.31	52.87	19.61	9.35	2.03	1.84	96.14	3.86
GL2	28 - 30	29	13.89	52.78	20.80	8.45	2.00	2.08	95.92	4.08
GL2	32 - 34	33	15.62	53.59	18.26	8.35	2.01	2.17	95.82	4.18
GL2	36-38	37	16.60	54.19	17.08	7.14	2.32	2.67	95.00	5.00
GL2	40-42	41	16.79	53.19	17.68	7.95	2.05	2.34	95.61	4.39
GL2	44-46	45	14.50	50.90	19.67	10.18	2.47	2.28	95.24	4.76
GL2	48-50	49	13.10	49.48	20.90	11.24	2.80	2.49	94.71	5.29
GL2	50-52	51	13.87	49.69	18.99	11.70	3.12	2.63	94.26	5.74
GL2	52-54	53	13.19	47.53	20.34	14.77	3.56	0.61	95.83	4.17
GL2	54-56	55	16.13	54.10	18.60	9.19	1.85	0.14	98.01	1.99
GL2	56-58	57	14.11	50.57	20.47	10.52	2.04	2.29	95.67	4.33
GL2	58-60	59	13.09	47.63	22.64	12.89	2.09	1.66	96.25	3.75
GL2	60-62	61	15.83	53.66	19.15	7.99	1.69	1.68	96,63	3,37
GL2	62-64	63	17.77	53.83	16.52	7.93	1.84	2.10	96,06	3,94
GL2	64-66	65	16.35	51.63	18.75	9.46	2.07	1.74	96,18	3,82
GL2	66-67	67	18.60	53.65	16.06	7.66	1.78	2.25	95,97	4,03

Table 9: Table of grain size distribution at GL3-21A using Wenworth (1922) classification.

Core	Core interval (cm)	Core depth (cm)	Clay (%)	Fine silt (%)	Medium silt (%)	Coarse silt (%)	Fine sand (%)	Medium sand (%)	Clay & Silt (%)	Sand (%)
			≤ 4 μm	4- 16 μm	16-32 μm	32-63 μm	63-125 μm	125-500 μm	2- 63 μm	63 μm -2 mm
GL3	0-1	0.5	17.35	49.75	15.35	8.84	3.66	5.06	91.28	8.72
GL3	1 -2	1.5	18.36	53.30	14.99	8.10	2.85	2.40	94.75	5.25
GL3	2 - 3	2.5	17.19	52.01	15.65	8.66	3.21	3.27	93.52	6.48
GL3	3 - 4	3.5	20.10	51.67	13.48	7.75	3.16	3.84	93.00	7.00
GL3	4 - 5	4.5	14.78	54.04	18.29	7.77	2.42	2.71	94.87	5.13
GL3	5 - 6	5.5	21.84	50.95	12.52	7.56	2.98	4.14	92.87	713
GL3	6 - 7	6.5	13.73	50.34	21.15	11.02	2.35	1.42	96.24	3.76
GL3	7 - 8	7.5	14.25	53.83	20.21	9.01	2.10	0.61	97.29	2.71
GL3	8 - 9	8.5	14.24	49.65	19.44	11.66	3.11	1.90	94.99	5.01
GL3	9- 10	9.5	16.40	54.61	16.78	7.89	2.28	2.04	95.68	4.32
GL3	10 - 11	10.5	16.23	52.54	18.30	9.06	2.31	1.56	96.13	3.87
GL3	12 - 13	12.5	17.95	53.13	15.21	8.07	2.67	2.98	94.35	5.65
GL3	14 - 15	14.5	12.70	49.55	21.62	12.06	2.48	1.58	95.93	4.07
GL3	16 - 17	16.5	13.86	53.42	19.91	9.03	2.03	1.74	96.22	3.78
GL3	18 - 19	18.5	17.28	54.45	15.96	7.79	2.24	2.29	95.48	4.52
GL3	20 - 22	21.0	13.03	47.95	19.77	13.16	3.59	2.50	93.91	6.09
GL3	24 - 26	25.0	16.18	54.10	17.33	8.16	2.18	2.05	95.77	4.23
GL3	26-28	27.0	11.96	43.48	19.92	17.20	5.55	1.89	92.56	7.44
GL3	28 - 30	29.0	15.80	51.40	17.17	9.96	3.00	2.67	94.33	5.67
GL3	30 - 32	31.0	16.36	51.73	16.70	9.90	2.87	2.44	94.68	5.32
GL3	32 - 34	33.0	17.88	54.29	15.38	7.50	2.18	2.77	95.05	4.95
GL3	34-36	35.0	14.76	53.33	19.04	8.40	1.98	2.50	95.52	4.48
GL3	36-38	37.0	17.43	54.08	16.09	7.49	2.19	2.71	95.10	4.90
GL3	38-40	39.0	16.42	55.11	16.71	7.44	1.91	2.41	95.68	4.32
GL3	40-42	41.0	17.19	54.84	15.97	7.34	2.08	2.59	95.34	4.66
GL3	42-44	43.0	19.06	54.99	14.77	6.82	2.02	2.34	95.64	4.36
GL3	44-46	45.0	20.88	54.40	13.51	6.62	1.94	2.65	95.41	4.59

G Heavy metal concentrations

Table 10: Heavy metal concentrations and environmental status in the northern sediment core (GL2-21A) in accordance with the Norwegian guidelines for classification in sediments (*Veileder, 2018*). Year presented in bold are original results from the ERRC-report while non-bold ages are interpolated values.

Core	Core depth (cm)	Date	Cu (mg/kg)	Zn (mg/kg)	Cd (mg/kg)	Pb (mg/kg)	Cr (mg/kg)	Ni (mg/kg)
GL2-21 A	0.5	**2021**	13.86	70.62	0.04	30.27	30.92	22.26
GL2-21 A	1.5	2021	14.50	75.33	0.06	33.16	33.80	23.75
GL2-21 A	2.5	**2020**	14.23	73.32	0.10	31.87	32.79	22.89
GL2-21 A	3.5	2020	15.13	74.10	0.05	32.83	34.50	23.78
GL2-21 A	4.5	**2019**	14.89	76.25	0.13	34.23	33.80	23.54
GL2-21 A	5.5	2018	15.23	77.98	0.15	35.23	34.67	24.38
GL2-21 A	6.5	2018	15.24	76.73	0.09	33.88	33.78	23.88
GL2-21 A	7.5	2017	14.23	73.02	0.09	32.81	33.01	23.12
GL2-21 A	8.5	**2016**	15.60	78.71	0.12	35.80	34.52	24.35
GL2-21 A	9.5	2015	15.81	80.12	0.09	36.48	35.01	24.45
GL2-21 A	10.5	2015	17.02	85.67	0.16	39.59	38.02	26.20
GL2-21 A	12.5	2013	17.65	83.26	0.14	38.94	35.33	24.38
GL2-21 A	14.5	**2011**	14.94	76.04	0.15	36.16	33.41	23.27
GL2-21 A	16.5	2009	16.23	81.17	0.14	37.76	35.99	25.33
GL2-21 A	18.5	2007	16.00	83.19	0.05	38.59	35.34	24.32
GL2-21 A	21	2005	15.31	80.44	0.23	38.84	35.11	24.18
GL2-21 A	25	**2002**	16.05	85.09	0.14	40.46	35.82	25.05
GL2-21 A	29	**1998**	16.52	89.20	0.22	44.30	36.55	25.29
GL2-21 A	33	**1995**	17.05	92.27	0.23	44.94	36.73	25.14
GL2-21 A	37	**1990**	19.74	101.45	0.11	49.89	41.42	27..57
GL2-21 A	41	**1986**	17.91	91.49	0.15	45.78	36.20	24.53
GL2-21 A	45	1981	18.04	100.49	0.23	52.09	38.70	25.71
GL2-21 A	49	**1974**	17.83	98.85	0.14	54.57	37.71	25.15
GL2-21 A	51	**1971**	18.64	105.75	0.14	56.51	39.71	26.46
GL2-21 A	53	**1967**	17.27	99.09	0.14	52.83	36.35	24.15
GL2-21 A	55	1963	18.65	107.85	0.18	56.73	38.32	26.31
GL2-21 A	57	**1959**	17.47	102.39	0.22	52.62	36.36	25.10
GL2-21 A	59	1956	16.83	99.35	0.14	52.82	37.02	25.49
GL2-21 A	61	**1952**	16.98	98.84	0.10	52.92	36.29	25.40
GL2-21 A	63	1948	17.39	102.31	0.10	53.87	38.46	26.67
GL2-21 A	65	**1944**	16.33	98.16	0.06	52.54	38.85	27.10
GL2-21 A	66,5	1940	16.53	96.45	0.12	50.38	36.47	25.49

Table 11: Heavy metal environmental classification of the southern sediment core (GL3-21A) in accordance with the Norwegian guidelines for classification in sediments (*Veileder, 2018*). Year presented in bold are original results from the ERRC-report while non-bold ages are interpolated values.

Core	Core depth (cm)	Date	Cu (mg/kg)	Zn (mg/kg)	Cd (mg/kg)	Pb (mg/kg)	Cr (mg/kg)	Ni (mg/kg)
GL3-21A	0.5	**2021**	14.76	75.00	0.07	32.31	30.48	22.58
GL3-21A	1.5	2020	15.59	78.49	0.08	34.82	32.54	23.33
GL3-21A	2.5	**2019**	16.17	82.63	0.11	38.17	33.77	24.13
GL3-21A	3.5	2018	16.05	81.60	0.16	39.61	33.74	23.93
GL3-21A	4.5	**2017**	18.40	94.15	0.25	44.35	38.82	28.13
GL3-21A	5.5	2016	18.39	93.24	0.04	43.55	37.63	27.07
GL3-21A	6.5	2015	17.82	90.32	0.23	42.83	36.76	26.27
GL3-21A	7.5	2014	17.23	87.66	0.17	40.02	35.32	25.07
GL3-21A	8.5	**2012**	29.72	105.45	0.13	44.71	38.29	27.30
GL3-21A	9.5	2011	16.46	83.50	0.07	39.02	33.53	23.91
GL3-21A	10.5	2009	18.22	93.13	0.07	43.70	37.55	26.53
GL3-21A	12.5	**2006**	16.91	86.61	0.15	39.17	34.04	24.46
GL3-21A	14.5	2003	16.97	87.98	0.12	41.53	34.22	24.34
GL3-21A	16.5	**2000**	17.89	93.86	0.14	46.06	36.78	26.05
GL3-21A	18.5	1997	18.88	98.85	0.24	47.81	37.97	26.49
GL3-21A	21	**1992**	18.32	96.34	0.12	47.55	36.52	25.68
GL3-21A	25	**1986**	19.12	104.47	0.15	51.24	37.23	26.19
GL3-21A	27	**1981**	18.62	102.65	0.16	51.29	35.86	24.97
GL3-21A	29	**1976**	18.41	105.06	0.18	54.83	35.79	25.54
GL3-21A	31	**1972**	18.64	105.77	0.25	53.97	36.80	26.61
GL3-21 A	33	**1968**	18.68	108.92	0.20	55.45	37.17	26.44
GL3-21A	35	**1963**	21.16	120.48	0.28	62.73	42.12	29.20
GL3-21A	37	**1955**	20.87	115.84	0.16	59.98	39.74	27.48
GL3-21A	39	**1950**	19.59	109.64	0.15	56.45	38.37	26.79
GL3-21A	41	**1942**	17.92	101.34	0.09	50.74	35.96	25.52
GL3-21A	43	**1936**	15.78	84.19	0.12	41.53	35.23	25.44
GL3-21A	45	1930	15.80	85.15	0.16	42.83	36.16	26.07

H TC, TOC and TN results.

Table 12: TC, TOC and TN results for GL2.

Core	Core interval (cm)	Core depth (cm)	TC (mg/g)	TOC (mg/g)	TIC (mg/g)	TN (mg/g)
GL2-21A	0-1	0.5	32.61	21.13	11.49	3.21
GL2-21A	1-2	1.5	34.97	22.42	12.55	3.25
GL2-21A	2-3	2.5	34.81	21.95	12.86	3.20
GL2-21A	3-4	3.5	34.75	21.45	13.29	3.24
GL2-21A	4-5	4.5	34.80	21.95	12.85	3.22
GL2-21A	5-6	5.5	35.27	22.02	13.24	3.25
GL2-21A	6-7	6.5	35.16	22.31	12.85	3.20
GL2-21A	7-8	7.5	34.57	21.98	12.59	3.13
GL2-21A	8-9	8.5	35.17	21.85	13.32	3.20
GL2-21A	9-10	9.5	35.17	22.15	13.02	3.20
GL2-21A	10-11	10.5	35.22	22.27	12.96	3.18
GL2-21A	12-13	12.5	35.17	22.11	13.06	3.18
GL2-21A	14-15	14.5	35.32	22.91	12.41	3.19
GL2-21A	16-17	16.5	35.39	22.41	12.98	3.16
GL2-21A	18-19	18.5	35.19	22.11	13.08	3.16
GL2-21A	20-22	21	35.25	22.06	13.18	3.15
GL2-21A	24-26	25	35.89	21.79	14.10	3.19
GL2-21A	28-30	29	35.27	21.78	13.49	3.11
GL2-21A	32-34	33	34.89	21.82	13.07	3.06
GL2-21A	36-38	37	35.71	22.74	12.97	3.13
GL2-21A	40-42	41	34.81	21.83	12.97	3.07
GL2-21A	44-46	45	35.54	22.19	13.35	3.13
GL2-21A	48-50	49	27.47	22.15	5.32	3.67
GL2-21A	50-52	51	35.89	21.94	13.96	3.12
GL2-21A	52-54	53	33.23	22.53	10.69	2.89
GL2-21A	54-56	55	36.64	22.27	14.36	3.14
GL2-21A	56-58	57	33.25	22.91	10.34	2.89
GL2-21A	58-60	59	34.93	21.52	13.41	3.00
GL2-21A	60-62	61	34.60	21.44	13.16	2.98
GL2-21A	62-64	63	33.90	21.31	12.59	2.91
GL2-21A	64-66	65	35.35	21.57	13.78	3.04
GL2-21A	66-67	66,5	33.45	21.73	11.72	2.89

Table 13: TC, TOC and TN results for GL3.

Core	Core interval (cm)	Core depth (cm)	TC (mg/g)	TOC (mg/g)	TIC (mg/g)	TN (mg/g)
GL3-21A	0-1	0.5	37.06	20.42	16.64	3.77
GL3-21A	1-2	1.5	35.03	23.89	11.14	3.43
GL3-21A	2-3	2.5	36.49	23.82	12.67	3.57
GL3-21A	3-4	3.5	35.59	23.26	12.32	3.37
GL3-21A	4-5	4.5	35.52	23.29	12.23	3.34
GL3-21A	5-6	5.5	35.97	24.44	11.52	3.34
GL3-21A	6-7	6.5	35.71	23.54	12.17	3.33
GL3-21A	7-8	7.5	35.78	23.56	12.22	3.35
GL3-21A	8-9	8.5	35.78	22.78	13.01	3.33
GL3-21A	9-10	9.5	36.11	23.57	12.54	3.47
GL3-21A	10-11	10.5	35.80	23.09	12.71	3.33
GL3-21A	12-13	12.5	35.46	22.59	12.87	3.31
GL3-21A	14-15	14.5	35.48	23.04	12.44	3.28
GL3-21A	16-17	16.5	35.94	23.04	12.90	3.31
GL3-21A	18-19	18.5	35.67	24.35	11.32	3.29
GL3-21A	20-22	21	35.54	23.18	12.36	3.28
GL3-21A	24-26	25	35.67	23.73	11.95	3.26
GL3-21A	26-28	27	34.55	22.90	11.65	3.18
GL3-21A	28-30	29	34.49	22.55	11.94	3.16
GL3-21A	30-32	31	34.25	22.83	11.42	3.11
GL3-21A	32-34	33	34.07	22.28	11.78	3.10
GL3-21A	34-36	35	34.88	22.88	12.00	3.21
GL3-21A	36-38	37	34.79	22.13	12.66	3.19
GL3-21A	38-40	39	33.26	21.53	11.73	3.03
GL3-21A	40-42	41	33.29	21.89	11.40	3.05
GL3-21A	42-44	43	31.95	20.44	11.51	2.94
GL3-21A	44-46	45	32.48	20,.3	12.45	2.98

I Isotope values

Table 14: Carbon-isotope results for GL2 and GL3.

Core depth	Core interval	Core	$\delta^{13}C_{VPDB}$ (‰)	%C	Core depth	Core interval	Core	$\delta^{13}C_{VPDB}$ (‰)	%C
0-1	0.5	GL2-21A	-22.92	2.83	0-1	0.5	GL3-21A	-22.74	2.83
1-2	1.5	GL2-21A	-23.02	2.81	1-2	1.5	GL3-21A	-22.68	3.06
2-3	2.5	GL2-21A	-23.01	2.51	2-3	2.5	GL3-21A	-22.75	3.19
3-4	3.5	GL2-21A	-22.97	2.82	3-4	3.5	GL3-21A	-22.78	3.00
4-5	4.5	GL2-21A	-22.94	2.72	4-5	4.5	GL3-21A	-22.61	2.91
5-6	5.5	GL2-21A	-22.92	2.61	5-6	5.5	GL3-21A	-22.96	2.96
6-7	6.5	GL2-21A	-22.87	2.66	6-7	6.5	GL3-21A	-22.92	3.06
7-8	7.5	GL2-21A	-22.84	2.61	7-8	7.5	GL3-21A	-22.76	3.00
8-9	8.5	GL2-21A	-22.90	2.74	8-9	8.5	GL3-21A	-22.73	2.81
9-10	9.5	GL2-21A	-22.82	2.68	9-10	9.5	GL3-21A	-22.66	2.82
10-11	10.5	GL2-21A	-22.82	2.58	10-11	10.5	GL3-21A	-22.66	2.84
12-13	12.5	GL2-21A	-22.83	2.66	12-13	12.5	GL3-21A	-22.57	2.80
14-15	14.5	GL2-21A	-22.74	2.49	14-15	14.5	GL3-21A	-22.56	2.86
16-17	16.5	GL2-21A	-22.74	2.53	16-17	16.5	GL3-21A	-22.47	2.82
18-19	18.5	GL2-21A	-22.75	2.58	18-19	18.5	GL3-21A	-22.41	2.66
20-22	21	GL2-21A	-22.62	2.58	20-22	21	GL3-21A	-22.37	2.74
24-26	25	GL2-21A	-22.53	2.61	24-26	25	GL3-21A	-22.45	2.86
28-30	29	GL2-21A	-22.60	2.74	26-28	27	GL3-21A	-22.44	2.70
32-34	33	GL2-21A	-22.65	2.74	30-32	31	GL3-21A	-22.55	2.69
40-42	41	GL2-21A	-22.59	2.69	32-34	33	GL3-21A	-22.50	2.69
44-46	45	GL2-21A	-22.78	2.92	34-36	35	GL3-21A	-22.46	2.73
48-50	49	GL2-21A	-22.66	2.74	36-38	37	GL3-21A	-22.42	2.69
50-52	51	GL2-21A	-22.71	2.61	38-40	39	GL3-21A	-22.49	2.64
52-54	53	GL2-21A	-22.76	2.67	40-42	41	GL3-21A	-22.47	2.61
54-56	55	GL2-21A	-22.85	2.55	42-44	43	GL3-21A	-22.34	2.28
56-58	57	GL2-21A	-22.66	2.27	44-46	45	GL3-21A	-22.35	2.36
58-60	59	GL2-21A	-22.76	2.53					
60-62	61	GL2-21A	-22.71	2.47					
62-64	63	GL2-21A	-22.74	2.53					
64-66	65	GL2-21A	-22.75	2.56					
66-67	66,5	GL2-21A	-22.70	2.56					

Table 15: Nitrogen-isotope results for GL2 and GL3.

Core depth	Core interval	Core	$\delta^{15}N_{AIR}$ (‰)	%N	Core depth	Core interval	Core	$\delta^{15}N_{AIR}$ (‰)	%N
0-1	0.5	GL2-21A	6.99	0.28	0-1	0.5	GL3-21A	6.73	0.33
1-2	1.5	GL2-21A	6.80	0.30	1-2	1.5	GL3-21A	6.68	0.32
2-3	2.5	GL2-21A	6.76	0.28	2-3	2.5	GL3-21A	6.80	0.33
3-4	3.5	GL2-21A	6.76	0.29	3-4	3.5	GL3-21A	6.68	0.31
4-5	4.5	GL2-21A	6.74	0.29	4-5	4.5	GL3-21A	6.78	0.31
5-6	5.5	GL2-21A	6.70	0.29	5-6	5.5	GL3-21A	6.62	0.31
6-7	6.5	GL2-21A	6.79	0.28	6-7	6.5	GL3-21A	6.53	0.31
7-8	7.5	GL2-21A	6.80	0.28	7-8	7.5	GL3-21A	6.63	0.31
8-9	8.5	GL2-21A	6.75	0.29	8-9	8.5	GL3-21A	6.58	0.31
9-10	9.5	GL2-21A	6.78	0.28	9-10	9.5	GL3-21A	6.59	0.31
10-11	10.5	GL2-21A	6.74	0.28	10-11	10.5	GL3-21A	6.63	0.31
12-13	12.5	GL2-21A	6.76	0.28	12-13	12.5	GL3-21A	6.61	0.31
14-15	14.5	GL2-21A	6.79	0.28	14-15	14.5	GL3-21A	6.67	0.31
16-17	16.5	GL2-21A	6.79	0.28	16-17	16.5	GL3-21A	6.65	0.31
18-19	18.5	GL2-21A	6.79	0.28	18-19	18.5	GL3-21A	6.69	0.31
20-22	21	GL2-21A	6.84	0.28	20-22	21	GL3-21A	6.67	0.30
24-26	25	GL2-21A	6.85	0.28	24-26	25	GL3-21A	6.64	0.30
28-30	29	GL2-21A	6.85	0.27	26-28	27	GL3-21A	6.65	0.29
32-34	33	GL2-21A	6.85	0.27	28-30	29	GL3-21A	6.58	0.28
36-38	37	GL2-21A	6.79	0.28	30-32	31	GL3-21A	6.58	0.28
40-42	41	GL2-21A	6.84	0.28	32-34	33	GL3-21A	6.59	0.28
44-46	45	GL2-21A	6.83	0.27	34-36	35	GL3-21A	6.61	0.29
48-50	49	GL2-21A	6.79	0.27	36-38	37	GL3-21A	6.60	0.29
50-52	51	GL2-21A	6.82	0.27	38-40	39	GL3-21A	6.59	0.28
52-54	53	GL2-21A	7.07	0.30	40-42	41	GL3-21A	6.58	0.27
54-56	55	GL2-21A	6.82	0.26	42-44	43	GL3-21A	6.38	0.26
56-58	57	GL2-21A	6.86	0.26	44-46	45	GL3-21A	6.41	0.27
58-60	59	GL2-21A	6.84	0.26					
60-62	61	GL2-21A	6.95	0.25					
62-64	63	GL2-21A	6.83	0.26					
64-66	65	GL2-21A	6.78	0.25					
66-67	66,5	GL2-21A	6.89	0.24					

J Foraminifera counts

Table 16: foraminifera count (500-63µm) of GL2 and GL3.

Foram count.	GL2							GL3						
Core depth (cm)	0.5	1.5	3.5	4.5	14.5	33	65	0.5	1.5	3.5	8.5	15.5	31	45
Adercotryma glomeratum/wrighti	9	9	6	4	6	5	12	28	6	11	5	7	12	24
Ammodiscus catinus	1			2	1		2	1					1	
Cribrostomoides crassimargo					2									
Cribrostomoides jeffreysi			2		1									
Cribrostomoides nitidus		3												2
Cribrostomoides wiesneri								1	3			1		1
Eggerella europea			1						1					
Eggerella sp.		1												
Eggerelloides medius	36	26	16	29	24	20	22	56	16	15	14	32	23	20
Eggerelloides scaber				1										
Haplophragmoides bradyi	29		7	12	2		3	6	7	2	3			6
Haplophragmoides sphaeriloculum								3						
Hyperammina laevigata	4													
Hippocrepinella alba	1													
Liebusella goesi	108	2	18	12	19	11	3	7	12	6	17	12	6	4
Recurvoides trochamminiforme	8	10	3	5	4	3	2	29	3	4				6
Recurvoides contortus														1
Reophax subfusiformis			1		3	1	1						1	
Textularia earlandi	43	51	60	93	34	14	2	98	35	23	14	10	3	6
Textularia sagittula		2	2		4	5			1	5	2	2		2
Textularia skagerrakensis				2										
Trochammina "skrumpa"			1											
Trochamminopsis quadriloba		1	1					1			1			
Trochammina sp.			1					3						2
Aggl. unidentified														
Ammonia sp.		1	1							1			1	
Amphicoryna scalaris								1			1			
Astrononion gallowayi	7	7	7	7	7	19	21	12	3	12	8	15	26	16
Astrononion sp.		3												
Biloculinella inflata														1
Bolivina pseudoplicata	1		1	2			2		1					2
Bolivinellina pseudopunctata		1	1	2	3	1		2	1	2		1	3	3
Brizalina skagerrakensis						5	29	4		7		3	6	15
Brizalina spathulata	43	18	14	20	43	40	2	30	17	16	27	21	9	1
Bulimina marginata	23	24	9	9	28	40	30	21	14	20	14	23	32	16
Buliminella elegantissima						1								
Cassidulina laevigata			7	4	9			9		13	8	17	15	9
Cassidulina neoteretis	13	21	12	10	20	31	35	15	17	35	15	22	32	40

Cassidulina obtusa		1	4	3	2				1	2	2	3	3	2
Cibicides lobatulus	11	23	25	43	27	34	12	10	33	18	20	12	13	13
Cibicides mundulus								2					1	2
Cibicides sp.							2							
Cornuspira sp.													1	
Discorbinella bertheloti	4	1	2		6		6	2	1	4	2	2	4	4
Elphidium albiumbilicatum	3	3		2		3	2	3	2	3	2			
Elphidium excavatum	8	11	11	7	20	28	21	4	8	10	11	8	10	8
Elphidium sp.		1		2		1		2	1	1				
Epistominella vitrea	9	6	9	26	27	24	8	9	17	6	6	3	5	4
Fissurina sp. 1			1	1	1	1	1		3	1	4	2	1	1
Gavelinopsis praegeri		2	4		1	1			5	1		1		1
Globobulimina turgida	34	19	10	13	14	16	10	18	21	10	6	7	13	9
Hyalinea balthica	1	31	6	8	17	23	38	41	4	53	30	43	64	59
Islandiella norcrossi		1	2	1	5	2		2			1	3		1
Lagena laevis							2							
Lagena striata												2	1	
Lagena sp. 1			1							1		2	1	
Lagena sp. 2													1	
Lagenosolena distoma		1												
Lagenosolena gracillima														2
Lenticulina sp.	1			1					1		1			
Melonis barleeanum	9	9	1	3	5	4	26	7	3	10	9	14	33	46
Miliolinella subrotunda					2	1		3		1	3	1	1	1
Nonionella iridea			7		13	12	9	6	3	8	3	2	7	14
Nonionella turgida	4		7	23	17	5	1	4		3	7			
Nonionellina labradorica	9	3	3	8	5	1	1	6	2	2	6	5	12	5
Nonionella cf. stella		7						5						
Nonionellina sp.	1						1							
Pullenia bulloides														1
Pullenia osloensis	18	12	19	22	3	18	37	31	17	21	9	13	29	28
Pyrgo williamsoni					1					2	1	2	2	
Pyrgo sp.												1		
Pyrgoella sphaera							1							
Quinqueloculina seminula							2	2	1	1	1	3	5	2
Quinqueloculina sp.					2					4				
Rosalina sp.				2										
Stainforthia fusiformis	10	38	35	68	110	59	17	19	30	25	23	25	12	6
Stainforthia skagerakensis		2		4	2	1	5	2		2	2	2	6	2
Trifarina angulosa						1							3	1
Uvigerina peregrina	23		2	6	8	3	1	10	2	3		2	3	3
Calc. unidetified					1									1

K AMBI-groups

Table 17: Foraminifera species assigned to ecological groups and AMBI (*Alve et al., 2016*).

Foraminifera species	**Eco-Group**	**AMBI-factor**
Stainforthia fusiformis	5	6
Eggerelloides medius	3	3
Recurvoides trochamminiforme	3	3
Textularia earlandi	3	3
Brizalina skagerrakensis	3	3
Brizalina spathulata	3	3
Bulimina marginata	3	3
Eggerelloides scaber	3	3
Buliminella elegantissima	3	3
Elphidium albiumbilicatum	3	3
Melonis barleeanum	3	3
Nonionella iridea	3	3
Nonionellina labradorica	3	3
Pullenia osloensis	3	3
Uvigerina peregrina	3	3
Astrononion gallowayi	3	3
Globobulimina turgida	3	3
Haplophragmoides bradyi	2	1.5
Cribrostomoides crassimargo	2	1.5
Reophax subfusiformis	2	1.5
Liebusella goesi	2	1.5
Textularia kattegatensis	2	1.5
Bolivina pseudoplicata	2	1.5
Bolivinellina pseudopunctata	2	1.5
Epistominella vitrea	2	1.5
Islandiella norcrossi	2	1.5
Nonionella turgida	2	1.5
Quinqueloculina seminula	2	1.5
Adercotryma glomeratum	2	1.5
Ammodiscus catinus	1	0
Cribrostomoides nitidum	1	0
Trochamminopsis quadriloba	1	0
Cassidulina laevigata	1	0
Cibicides lobatulus	1	0
Cassidulina neoteretis	1	0
Discorbinella bertheloti	1	0
Elphidium excavatum	1	0
Gavelinopsis praegeri	1	0
Hyalinea balthica	1	0
Trifarina angulosa	1	0

L Taxonomic reference list

The foraminiferal species in this thesis are listed in alphabetical order by their genus name. These species are not included in the reference list. The services used to collect the information were: marinespecies.org, foraminifera.eu and artsdatabanken.no

Adercotryma glomerata (Brady) = *Lituola glomerata* Brady, 1878
Adercotryma wrighti (Brönnimann and Whittaker, 1987). *Adercotryma glomerata*/*wrighti* were merged in this thesis
Astrononion gallowayi (Loeblich and Tappan, 1953)
Amphicoryna scalaris (Batsch, 1791)
Biloculinella inflata (Wright, 1902)
Bolivina pseudoplicata (Heron-Allen and Earland, 1930)
Bolivinellina pseudopunctata (Höglund) = *Bolivina pseudopunctata* Höglund, 1947
Brizalina skagerrakensis (Qvale and Nigam) = *Bolivina skagerrakensis* Qvale and Nigam, 1985
Brizalina spathulata (Williamson) = *Bolivina spathulata* Williamson = *Textularia varibilis* Williamson var. *spathulata* Williamson 1858
Bulimina marginata (d'Orbigny, 1826)
Buliminella elegantissima (d'Orbigny, 1839)
Cassidulina laevigata (d'Orbigny, 1826)
Cassidulina neoteretis (Seidenkrantz, 1995)
Cassidulina obtusa (Williamson, 1858)
Cibicides lobatulus (Walker and Jacob) = *Echinus lobatulus* Walker and Jacob, 1798
Cibicides mundulus (Brady, Parker and Jones, 1888)
Cribrostomoides crassimargo (Norman) = *Haplophragmium crassimargo* Norman, 1892
Cribrostomoides jeffreysii (Williamson) = *Nonionina jeffreysii* Williamson, 1858
Cribrostomoides nitidus (Goës, 1896)
Cribrostomoides wiesneri (Parr, 1950)
Discorbinella bertheloti (d'Orbigny) = *Rosalina bertheloti* d'Orbigny, 1839
Eggerella europea (Christiansen) = *Verneuilina europeum* Christiansen, 1958
Eggerelloides medius (Höglund) = *Verneuilina media* Höglund, 1947
Eggerelloides scaber (Williamson) = *Bulimina scabra* Williamson, 1858
Elphidium albiumbilicatum (Weiss) = *Nonion pauciloculum* (Cushman) subsp. *albiumbilicatum* Weiss, 1954
Elphidium excavatum (Cushman) = *Polystomella excavata* Terquem, 1875
Epistominella vitrea (Parker, 1953)
Gavelinopsis praegeri (Heron-Allen and Earland, 1913)
Globulimina turgida (Bailey) = *Bulimina turgida* Bailey, 1851
Haplophragmoides bradyi (Robertson) = *Trochammina bradyi* Robertson, 1891
Haplophragmoides sphaeriloculum (Cushman, 1910)
Hyalinea balthica (Schröter) = *Nautilus balthicus* Schröter, 1783
Hyperammina laevigata (Wright, 1891) = *Hyperammina elongate* var. *laevigata* Wright 1891
Hippocrepinella alba (Heron-Allen and Earland, 1932)
Islandiella norcrossi (Cushman, 1933) = *Cassidulina norcrossi* Cushman, 1933
Lagena laevis (Montagu) = *Vermiculum laeve* Montagu, 1803
Lagena striata (d'Orbigny) = *Oolina striata* d'Orbigny, 1839
Lagena distoma (*Parker and Jones, 1864*)

Liebusella goësi (Höglund, 1947)
Melonis berleeanus (Williamson) = *Nonionina berleeana* Williamson 1858
Miliolinella subrotunda (Montagu) = *Vermiculum subrotundum* Montagu, 1803
Nonionella iridea (Heron-Allen and Earland, 1932)
Nonionella turgida (Williamson) = *Rotalina turgida* Williamson, 1858
Nonionellina labradorica (Dawson) = *Nonionina scapha* var. *labradorica* Dawson, 1860
Nonionella cf. stella (Cushman and Moyer, 1930) = *Nonionella miocenica* var. *stella* Cushman and Moyer, 1930
Pullenia bulloides (d'Orbigny, 1846)
Pullenia osloensis (Feyling-Hanssen, 1954)
Pyrgo williamsoni (Silvestri, 1923) = *Biloculina williamsoni* Silvestri, 1923
Pyrgoella sphaera (d'Orbigny, 1839) = *Biloculina sphaera* d'Orbigny, 1839
Quinqueloculina seminula (Linné) = *Serpula seminulum* Linnaeus, 1758
Recurvoides contortus (Earland, 1934)
Reophax subfusiformis (Earland, 1933)
Stainforthia fusiformis (Williamson) = *Bulimina pupoides* d'Orbigny var. *fusiformis* Williamson, 1858
Stainforthia skagerakensis (Höglund, 1947) = *Virgulina skagerakensis* Höglund, 1947
Textularia earlandi (Parker 1952) = new name for *Textularia tenuissima* Earland, 1933
Textularia sagittula (Defrance, 1824)
Textularia skagerrakensis (Höglund, 1947)
Trifarina angulosa (Williamson) = *Uvigerina angulosa* Williamson, 1858
Trochamminopsis quadriloba (Höglund) = *Trochammina quadriloba* Höglund 1948 = new name for *Trochammina pusilla* Höglund, 1947
Uvigerina peregrina (Cushman, 1923)